

MM FILE COPY

4

AFGL-TR-88-0133

AD-A199 181

NEW CONCEPTS IN IONOSPHERIC MODIFICATION

P. M. Banks  
A. C. Fraser-Smith  
B. E. Gilchrist  
K. J. Harker  
L. R. O. Storey  
P. R. Williamson

Stanford University  
Star Laboratory  
Stanford, CA 94305

April 1987

Final Report  
15 April 1986-30 September 1987

DTIC  
ELECTE  
SEP 07 1988  
S E D

APPROVED FOR PUBLIC RELEASE; DISTRIBUTION UNLIMITED

AIR FORCE GEOPHYSICS LABORATORY  
AIR FORCE SYSTEMS COMMAND  
UNITED STATES AIR FORCE  
HANSCOM AIR FORCE BASE, MASSACHUSETTS 01731-5000

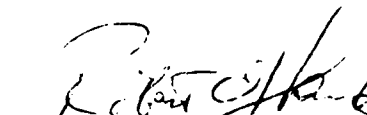
88 9 6 150

This technical report has been reviewed and is approved for publication.

FOR THE COMMANDER



JOHN E. RASMUSSEN, Chief  
Ionospheric Interactions Branch



ROBERT A. SKRIVANEK, Director  
Ionospheric Physics Division

This document has been reviewed by the ESD Public Affairs Office (PA) and is releasable to the National Technical Information Service (NTIS).

Qualified requestors may obtain additional copies from the Defense Technical Information Center. All others should apply to the National Technical Information Service.

If your address has changed, or if you wish to be removed from the mailing list, or if the addressee is no longer employed by your organization, please notify AFGL/DAA, Hanscom AFB, MA 01731. This will assist us in maintaining a current mailing list.

UNCLASSIFIED

SECURITY CLASSIFICATION OF THIS PAGE

ADA199181

## REPORT DOCUMENTATION PAGE

|  |       |  |   |   |
|--|-------|--|---|---|
| 1a. REPORT SECURITY CLASSIFICATION<br>UNCLASSIFIED   |       |  | 1b. RESTRICTIVE MARKINGS<br>N/A   |   |
| 2a. SECURITY CLASSIFICATION AUTHORITY<br>N/A   |       |  | 3. DISTRIBUTION/AVAILABILITY OF REPORT<br>Approved for public release; distribution unlimited |   |
| 2b. DECLASSIFICATION/DOWNGRADING SCHEDULE<br>N/A   |       |  |   |   |
| 4. PERFORMING ORGANIZATION REPORT NUMBER(S)<br>D131-1  |       |  | 5. MONITORING ORGANIZATION REPORT NUMBER(S)<br>AFGL-TR-88-0133                                |   |
| 6a. NAME OF PERFORMING ORGANIZATION<br>Star Laboratory   |       | 6b. OFFICE SYMBOL<br>(If applicable)                                 |   | 7a. NAME OF MONITORING ORGANIZATION<br>Air Force Geophysics Laboratory      |
| 6c. ADDRESS (City, State and ZIP Code)<br>Stanford University<br>Stanford, CA 94305  |       | 7b. ADDRESS (City, State and ZIP Code)<br>Hanscom AFB, MA 01731-5000 |   |   |
| 8a. NAME OF FUNDING/SPONSORING ORGANIZATION<br>AFOSR   |       | 8b. OFFICE SYMBOL<br>(If applicable)<br>NC                           |   | 9. PROCUREMENT INSTRUMENT IDENTIFICATION NUMBER<br>Project Order GLH-6-6015 |
| 8c. ADDRESS (City, State and ZIP Code)<br>Bolling AFB<br>Washington, DC 20332  |       | 10. SOURCE OF FUNDING NOS.   |   |   |
|  |       | PROGRAM ELEMENT NO.<br>61102F  | PROJECT NO.<br>2310   | TASK NO.<br>2310G3  |
|  |       |  |   | WORK UNIT NO.<br>2310G3BK   |
| 11. TITLE (Include Security Classification) New Concepts in Ionospheric Modification (U)   |       |  |   |   |
| 12. PERSONAL AUTHOR(S) P.M. Banks, A.C. Fraser-Smith, B.E. Gilchrist, K.J. Harker, L.R.O. Storey and P.R. Williamson   |       |  |   |   |
| 13a. TYPE OF REPORT<br>FINAL   |       | 13b. TIME COVERED<br>FROM 4/15/86 TO 9/30/87                         |   | 14. DATE OF REPORT (Yr., Mo., Day)<br>1987 April                            |
| 15. PAGE COUNT<br>188  |       |  |   |   |
| 16. SUPPLEMENTARY NOTATION<br>from 19  |       |  |   |   |
| 17. COSATI CODES   |       |  | 18. SUBJECT TERMS (Continue on reverse if necessary and identify by block number)             |   |
| FIELD  | GROUP | SUB. GR.   |   |   |
| 04   | 01    |  | IONOSPHERIC MODIFICATION; PARTICLE BEAMS; ELECTRON BEAMS;                                     |   |
| 20   | 09    |  | PHOTON BEAMS; PLASMA BEAMS. (106) ←   |   |
| 19. ABSTRACT (Continue on reverse if necessary and identify by block number)<br>This report considers the ionospheric modification that can be produced by energetic charged particle and photon beams, which <del>we assume</del> are emitted from a platform or vehicle (spacecraft or rockets) located in the ionosphere. The various beams considered include (1) charged particle beams composed of low, moderate, and high-energy electrons, (2) beams of ions and plasma, and (3) photon beams of soft X-rays and extreme ultraviolet radiation. Briefly considered, in addition to the beam topics, is the ionospheric modification produced by the release of neutral gas of high molecular weight from a rapidly moving vehicle such as the Space Shuttle Orbiter. When a ranking is made in terms of the new information that may be obtained, the scale of the modification that may be produced, and the availability of beam sources, ionospheric modification by means of relativistic electron beams appears particularly promising. However, all the methods have their own distinctive features which could make their use desirable under particular circumstances. The modification produced by means of beams of soft X-rays, for example, is not strongly dependent on the beam's direction relative to the earth's magnetic field, and thus modification can be produced in |       |  |   |   |
| 20. DISTRIBUTION/AVAILABILITY OF ABSTRACT<br>UNCLASSIFIED/UNLIMITED <input checked="" type="checkbox"/> SAME AS RPT. <input type="checkbox"/> DTIC USERS <input type="checkbox"/>  |       |  | 21. ABSTRACT SECURITY CLASSIFICATION<br>UNCLASSIFIED  |   |
| 22a. NAME OF RESPONSIBLE INDIVIDUAL<br>PAUL A. KOSSEY  |       |  | 22b. TELEPHONE NUMBER<br>(Include Area Code)<br>377-3083                                      | 22c. OFFICE SYMBOL<br>AFGL/LID  |

DD FORM 1473, 83 APR

EDITION OF 1 JAN 73 IS OBSOLETE.

UNCLASSIFIED

SECURITY CLASSIFICATION OF THIS PAGE

Block 19 Cont'd

regions inaccessible to a charged particle beam from the same vehicle.



## Acknowledgements

We thank Professors S. E. Harris and J. F. Young, of Stanford's Ginzton Laboratory, Dr. P. A. Kossey, of the Air Force Geophysics Laboratory, Dr. J. Haimson, of Haimson Research Corporation, and Dr. T. E. Moore, of NASA's Marshall Space Flight Center, for their information, advice, and encouragement during the course of this work.

Support for the work was provided by the Air Force Geophysics Laboratory through an augmentation of NASA Grant NAGW 235.

|                    |  |  |
|--------------------|--|--|
| Accession For      |  |  |
| NTIS GRA&I         | <input checked="checked" type="checkbox"/> |  |
| DTIC TAB           | <input type="checkbox"/>                   |  |
| Unannounced        | <input type="checkbox"/>                   |  |
| Justification      |  |  |
| By                 |  |  |
| Distribution/      |  |  |
| Availability Codes |  |  |
| Avail and/or       |  |  |
| Dist               | Special                                    |  |
| A-1                |  |  |



## TABLE OF CONTENTS

|   |    |
|---|----|
| 1. Introduction and Summary . . . . .   | 1  |
| 1.1. Introduction . . . . .   | 1  |
| 1.2. Summary . . . . .  | 2  |
| 1.3. References . . . . .   | 7  |
| 2. Low Energy Electron Beams . . . . .  | 9  |
| 2.1. Ionization Process . . . . .   | 9  |
| 2.2. Electromagnetic Scattering . . . . .                                       | 14 |
| 2.3. Generation of Electromagnetic Waves . . . . .                              | 20 |
| 2.4. Recommendations for Further Work . . . . .                                 | 25 |
| 2.5. Summary . . . . .  | 27 |
| 2.6. References . . . . .   | 28 |
| 3. Moderately Energetic Electron Beams . . . . .                                | 33 |
| 3.1. Previous Space Experiments . . . . .                                       | 33 |
| 3.2. Electron Beam Sources . . . . .  | 34 |
| 3.3. Ionospheric Effects of Electron Beams . . . . .                            | 35 |
| 3.4. Possible Future Experiments . . . . .                                      | 39 |
| 3.5. Summary of Proposed Experiments . . . . .                                  | 41 |
| 3.6. References . . . . .   | 41 |
| 4. Relativistic Electron Beams . . . . .  | 45 |
| 4.1. Introduction . . . . .   | 45 |
| 4.2. Ionization Column Dynamics . . . . .                                       | 46 |
| 4.3. Electrodynamics of an Ionization Column in the Middle Atmosphere . . . . . | 59 |
| 4.4. A Proposed Experiment . . . . .  | 70 |
| 4.5. Closing Remarks . . . . .  | 71 |
| 4.6. References . . . . .   | 72 |
| 4.7. Appendix A . . . . .   | 75 |
| 4.8. Appendix B: Relocation of Ionized Column to Uniform Potential . . . . .    | 85 |
| 5. Ion and Plasma Beams . . . . .   | 91 |
| 5.1. Previous Space Experiments . . . . .                                       | 91 |

|   |     |
|---|-----|
| 5.2. Ion and Plasma Beam Sources . . . . .                        | 96  |
| 5.3. Ionospheric Effects of Ion and Plasma Beams . . . . .        | 107 |
| 5.4. Possible Future Experiments . . . . .                        | 118 |
| 5.5. Summary of Proposed Experiments . . . . .                    | 129 |
| 5.6. References . . . . .   | 131 |
| 6. Ionospheric Modification by X-Rays and EUV Radiation . . . . . | 143 |
| 6.1. Introduction . . . . .                                       | 143 |
| 6.2. Absorption of X-Rays . . . . .                               | 145 |
| 6.3. Absorption Cross Sections . . . . .                          | 148 |
| 6.4. X-Ray Beam Generation by Infrared Lasers . . . . .           | 149 |
| 6.5. X-Ray Generation by Energetic Electron Beams . . . . .       | 163 |
| 6.6. Discussion . . . . .   | 163 |
| 6.7. Suggestions for Further Work . . . . .                       | 166 |
| 6.8. References . . . . .   | 167 |
| 7. Neutral Gas Releases . . . . .                                 | 169 |
| 7.1. Introduction . . . . .                                       | 169 |
| 7.2. Basic Processes . . . . .                                    | 170 |
| 7.3. Discussion . . . . .   | 176 |
| 7.4. Future Work . . . . .  | 178 |
| 7.5. References . . . . .   | 180 |
| 8. Summary . . . . .  | 181 |

## 1. INTRODUCTION AND SUMMARY

### 1.1. Introduction

In 1986, our group (the Space Plasma Group in Stanford University's Space, Telecommunications and Radioscience, or STAR, Laboratory) undertook a short but intensive study of ionospheric modification for the Air Force Geophysics Laboratory (AFGL). The study was an outgrowth of the experimental and theoretical research we are conducting for NASA and for Rome Air Development Center (RADC). This research is largely directed toward the utilization of electron beams in space for vehicle charge control and for electromagnetic wave generation, and it has included experiments on flights of Space Shuttle Orbiters (STS-3 and Spacelab-2) and rockets (CHARGE-1, -2). Our interest and involvement in ionospheric modification arose out of a particular experiment we scheduled during the Spacelab-2 and CHARGE-2 flights, which was first described by *Banks and Gilchrist* [1985]. By directing repetitive pulses of the electron beam downwards along the magnetic field, *Banks and Gilchrist* [1985] predicted that a structure consisting of a regularly-spaced series of ionized columns would be produced that could be observed from the ground by suitably-located radars. Observations of the striated plasma screen, or "picket fence," would provide information about some of the properties of the local ionospheric plasma as well as the ionization produced by the electron gun. It could also conceivably be used as a diffraction screen for HF/VHF radio transmissions.

The picket fence produced in the ionosphere is a form of ionospheric modification, and our work on the topic led us to consider what further forms of ionospheric modification might be produced by energetic particle or photon beams. Support for a study of these concepts in ionospheric modification was provided early in 1986 by AFGL and the research portion of the study concluded at the end of September 1986. We should point out that the study was one of new concepts in ionospheric modification, based on our electron beam work, and thus no effort was directed toward work on ionospheric modification by means of high-powered ground-based incoherent scatter radars, or by other well-established methods such as barium or other similar chemical releases in the ionosphere.

The study naturally divided itself into a limited number of efforts involving topics that looked particularly promising. These topics, together with the members of our group that took the lead on their investigation, are as follows:

- (1) Ionospheric modification by low energy electron beams ( $E_e < 10$  keV) (K. J. Harker and B. E. Gilchrist).
- (2) Ionospheric modification by medium energy electron beams ( $10 \text{ keV} < E_e < 500$  keV) (L. R. O. Storey).
- (3) Ionospheric modification by relativistic electron beams ( $E_e > 500$  keV) (P. M. Banks and B. E. Gilchrist).
- (4) Ionospheric modification by ion and plasma beams (L. R. O. Storey).
- (5) Ionospheric modification by X-ray and extreme ultra-violet (EUV) beams (A. C. Fraser-Smith).
- (6) Ionospheric modification by neutral gas releases from an orbiting vehicle (P. M. Banks).

The chapters of this report follow the above listing of topics. Since there is little overlap between the references cited for each topic, a list of the pertinent references is appended at the end of each chapter instead of in a unified list at the end of the report. Each chapter includes a brief summary section of results and/or recommendations for further work, and these summaries are combined in the following unified summary section.

## 1.2. Summary

### *1.2.1. Ionospheric modification by low energy electron beams*

Present research on ionospheric modification by means of low energy electron beams ( $E_e < 10$  keV) already constitutes a new direction and the available theoretical and experimental results of this research suggest that it is possible to create significant and comparatively persistent ionization enhancements in the E and lower F regions of the ionosphere. Our suggestions for further work are therefore largely directed toward obtaining a better understanding of the modification produced by the beams.

Additional theoretical studies are recommended primarily in two areas: (1) determination of the optimum conditions for beam launching and propagation, and (2) computations of the electromagnetic scattering produced by electron beam induced ionization. Recommendations of experimental work center on the upcoming CHARGE-3 rocket experiment, in which our Laboratory is already actively involved. The primary goal of the CHARGE-3 mission is electromagnetic wave generation using the modulated electron beam from a new high current ( $\sim 4$  A) and higher power (10–15 kW) beam generator. Our suggestions here for additional work mostly involve supplementary ground observations that would provide new information covering the characteristics of the ionospheric modification produced by the beam.

### *1.2.2. Ionospheric modification by medium energy electron beams*

Moderately energetic electron beams ( $10 \text{ keV} < E_e < 500 \text{ keV}$ ) can be used for ionospheric modification in the same way as low energy beams, but without appearing to offer any distinct advantages at the present time. If directed downwards from a rocket or other space vehicle, they can produce ionization at lower altitudes than low energy beams, which could be an advantage under some circumstances. It is also possible that it may be easier for a moderately energetic beam to escape from its source in the presence of vehicle charging. On the other hand, the more energetic electron beams may be more susceptible to beam plasma discharge effects in the vicinity of the vehicle, and, for a given current, they require a larger power source. Our one major recommendation here is for a stronger theoretical and experimental effort to investigate the conditions for escape of low and medium energy electron beams from their sources in the presence of space plasma.

### *1.2.3. Ionospheric modification by relativistic electron beams*

Because of their deep penetration down into the lowest regions of the ionosphere, and even into the comparatively un-ionized middle atmosphere, highly energetic (relativistic) electron beams ( $E_e > 500 \text{ keV}$ ) offer a new ionospheric modification capability. For this reason, we have carried out a thorough initial study of the modification that might be achieved with a moderately powerful ( $\sim 5 \text{ MW}$ ), relativistic ( $\sim 5 \text{ MeV}$ ) electron accelerator from a rocket or satellite platform. It is shown that a single pulse

of electrons from such an accelerator can penetrate to the lower mesosphere and upper stratosphere, creating a dense column of free electrons and positive ions as it does so. At high altitudes the ionized column remains relatively static, decaying only slowly under the influence of recombination, whereas at lower altitudes the electrons are lost rapidly via attachment to neutral molecular oxygen. The ionized column can scatter electromagnetic radiation, and our computations indicate that it may also have a most unusual property: it may initiate an intense upward traveling electrical discharge similar to lightning. This latter property would make possible a whole new class of innovative experiments. However, even if the initiation of discharges proved infeasible, the creation of ionization in the middle atmosphere would enable important measurements to be made in a region where they are currently very difficult or impossible due to vehicle limitations. In particular, it would be possible to obtain information about the ambient electric field, without concern for the vehicle effects that have proven to be a major problem in the interpretation of rocket measurements.

Our study has shown that a rocket-borne relativistic electron beam experiment is feasible with current technology, and an experiment is proposed and discussed in some detail in this report. Because of its feasibility, innovation, and the many new measurements that would be possible in the upper atmosphere with a relativistic electron beam, we highly recommend a relativistic electron beam experiment and a continuation of the theoretical studies that are required to support the experimental effort.

#### *1.2.4. Ionospheric modification by ion and plasma beams*

Our report reviews the experiments that have been conducted in space with plasma beams (no experiments have been conducted with non-neutral ion beams) and it details a number of opportunities for original research in the ionosphere, including ionospheric modification, using both high and low  $\beta$  plasma beams. It is pointed out that a plasma beam can be used to produce artificial plasma density structures in the ionosphere in the same manner as electron beams, but with the difference that the plasma beam structures can be created at higher altitudes. Development of a plasma source of higher power than those currently available in the

U.S. is recommended for use in high  $\beta$  plasma beam generators, which would have application in ionospheric modification. Finally, a high  $\beta$  plasmoid experiment is suggested in which a high-powered laser is used to irradiate a pellet of ionizable material ejected from the Space Shuttle, or other vehicle, thus converting it suddenly into a fully-ionized plasma cloud.

#### *1.2.5. Ionospheric modification by X-ray and extreme ultra-violet (EUV) beams*

This study includes an initial investigation of the possibility of using beams of soft X-rays and extreme ultraviolet radiation for ionospheric modification. It was prompted partly by the following two general advantages of photon beams for modification experiments: (1) Unlike beams of charged particles, photon beams propagate through the ionosphere with little or no dependence on the geomagnetic field. Further, (2) their use for ionospheric modification avoids the potential difficulties with vehicle charging that the use of charged particle beams normally entail. More importantly, in the present instance, the investigation was prompted by new developments in the production and beam formation of soft X-rays/EUV that are currently the subject of research in Stanford University's Ginzton Laboratory and which suggest the feasibility of space experiments.

Our investigation has shown that an X-ray/EUV beam generator with similar characteristics to one already in use in the laboratory can produce columns of substantially enhanced ionization in the ionosphere, and that, as a result of (1) above, the columns do not have to be field aligned. Although the enhancement of ionization decays rapidly under most conditions, it may be detectable for times of the order of minutes during the night at some altitudes. It should be noted that the soft X-ray/EUV beam will not penetrate as deeply down through the lower ionosphere as will a beam of relativistic electrons: the beam is absorbed, and its ionization is produced, predominantly in the altitude range 90-140 km. Penetration below 80 km would require X-rays with energies substantially greater than those that can be produced at present by the technology we have studied.

Because the X-ray/EUV beam technique of ionospheric modification appears to be feasible without any further technical advances, but may be very greatly enhanced



by further development, and because of the other desirable features of X-ray/EUV beams for ionospheric modification that are detailed above, additional research on the technique, leading up to a 'proof-of-concept' rocket experiment, appears to be desirable and is recommended.

#### *1.2.6. Ionospheric modification by neutral gas releases from a rapidly moving space vehicle*

Our study of neutral gas releases in the ionosphere draws attention to a new process which is independent of the better known Critical Ionization Velocity (CIV) effect and which could lead both to the generation of ELF/VLF waves and to electron density fluctuations that could disturb the local ionosphere. The key to the initiation of the process, which involves charge exchange, is release of the neutral gas from a rapidly moving vehicle such as the Space Shuttle. It is also important that the neutral particles should be relatively heavy (compared with  $O^+$ ). Several recommendations of additional theoretical and experimental work are made. First, and perhaps most important at this stage, we recommend that basic calculations be carried out in support of the proposed charge exchange process. These calculations need to cover typical gas releases and to take into account the various possible charge exchange rates for different gases and the effects of cloud expansion. A second recommendation is for a plasma simulation study of the process, preferably using one of the 3-dimensional computer codes that are now available. Experimental recommendations include a study of existing data obtained during thruster firings on STS-3 and Spacelab-2. Considerable optical and plasma data are immediately available for study and rapid progress might be possible simply by analyzing these data. Finally, a Shuttle experiment to test the concepts involved in the new process would be comparatively simple and is recommended.

#### *1.2.7. Conclusion*

This study of new concepts in ionospheric modification has resulted in several detailed suggestions for new experiments in addition to the suggestions we have made for applications of the current low energy electron beam experiments to ionospheric modification. Most of the recommendations involve particle or photon beams, but

an experiment to investigate a new charge exchange mechanism in a cloud of neutral gas released from a rapidly moving vehicle in the ionosphere is also described and is recommended. Two of the suggested new experiments, one involving relativistic electron beams and the another beams of soft X-rays/EUV radiation, utilize new technologies that have only been developed very recently and which have a potentially very large payoff in terms of new effects that can be produced in the ionosphere and in the new knowledge that will be gained.

### 1.3. References

Banks, P.M., and B.E. Gilchrist, Artificial plasma density structures produced by energetic electron beams from rockets and spacecraft, *Geophys. Res. Letts.*, **12**, 175-178, 1985.

## 2. LOW ENERGY ELECTRON BEAMS

Recent rocket and space shuttle experiments have shown that it is possible to launch low energy ( $E_e \leq 10$  keV) electron beams of moderate power into the earth's ionosphere and magnetosphere. Such beams can create significant ionization in the E and low F regions of the ionosphere. Through proper selection of beam related parameters, a variety of plasma density structures can be created, and studied over a period of minutes [Banks and Gilchrist, 1985]. For example, as the spacecraft moves along its path, it should be possible to create a sheet-like density structure by operating the electron gun continuously, or, by pulsing the gun, periodic structures within the sheet could be created. In the following sections we consider the ionospheric modification, electromagnetic wave scattering, and electromagnetic wave generation that can be produced by a low energy electron beam in the ionosphere. The two final sections contain recommendations for future work and a list of references.

### 2.1. Ionization Process

#### 2.1.1. Generation of Ionization

When an electron beam is launched, the number density of the beam,  $n_a$ , is typically several times larger than that of the surrounding ambient plasma. As a consequence, electrostatic forces cause the beam to expand. Intense electrostatic waves resulting from beam-plasma interaction scatter the primary electrons as well as the secondary electrons created by impact ionization. The result of all this is a cylindrically symmetric beam with a broad range of pitch angles. The beam diameter is typically assumed to be twice the electron Larmor radius set by the electron energy and the magnetic field:

$$D \simeq \frac{2v_b}{\omega_{ce}} \quad (2.1)$$

where  $v_b$  is the primary beam velocity and  $\omega_{ce}$  is the electron gyrofrequency.

If the spacecraft has a speed,  $v_s$ , then the volume carved out by the beam is occupied for a time  $D/v_s$ . If the kinetic energy in the beam flows at a rate  $P$ , then the energy deposited in the carved out volume is

$$E = P \frac{D}{v_s} \quad (2.2)$$

and the corresponding total number of collisions is given by  $E/\gamma$  where  $\gamma$  is the energy per collision (35.5 eV). If the length of the volume carved out by the beam is  $L$ , then the volume is  $\pi D^2 L/4$ , and the number of collisions per unit volume is

$$n = \frac{E/\gamma}{\pi D^2 L/4} \cong \frac{P}{D\gamma L v_s} \quad (2.3)$$

The duration of these ionization enhancements depends on the recombination time. The initial ions undergo rapid reactions with the constituent of the neutral upper atmosphere to give mostly  $NO^+$ . This ion is then lost via a dissociative recombination of the form



The recombination rate  $\alpha_D$  gives rise to a decay time

$$\tau_D = \frac{1}{\alpha_D n_e} \cong \frac{7.7 \times 10^6}{n_e} \quad (2.5)$$

where  $n_e$  is in units of electrons/cm<sup>3</sup>.

Equation (2.3) is only approximate, since it does not account for the variation of  $n$  with distance along the beam. A more accurate theory can be built on the result of *Grum* [1957], who showed that the energy lost per electron per unit length (kg/m<sup>2</sup>),  $z$ , is given by

$$\alpha = \frac{E_o}{R} \lambda\left(\frac{z}{R}\right) \quad (2.6)$$

where  $E_o$  is the ionizing electron's initial energy,  $R$  is the range measured in units of kg/m<sup>2</sup>, and  $\lambda$  is a universal function of  $z/R$ . *Grum* showed that

$$R = 4.57 \times 10^{-5} (E_o/1000)^{1.75} \quad (2.7)$$

where  $E_o$  is measured in electron volts. The number of collisions per unit length is given by

$$\frac{\alpha}{\gamma} \rho \quad (2.8)$$

where  $\rho$  is the density. On the other hand, the electron flux per square meter is given by

$$\frac{I}{e\pi D^2} \frac{D}{v_s} \cong \frac{P}{eDv_s V} \quad (2.9)$$

where  $V$  is voltage.

If we multiply (2.8) by (2.9) and substitute (2.6), we obtain the number of ionizing collisions per unit volume:

$$n = \lambda(z/R) \frac{\rho}{R\gamma} \frac{P}{Dv_s} \quad (2.10)$$

If we define an effective range

$$L_{eff} = \frac{R}{\rho}, \quad (2.11)$$

then (2.10) takes a form similar to (2.3):

$$n = \lambda(z/R) \frac{P}{D\gamma L_{eff} v_s} \quad (2.12)$$

*Rees* [1963] has given atmospheric parameters applicable to the theory. Using (2.2), (2.5), and (2.12) it is possible to construct curves of ionization,  $n$ , versus height as a function of time into afterglow. Results for 1 keV and 5 keV beams are shown in Figures 2.1 and 2.2, respectively. These figures clearly show how increased energy increases the depth of penetration and produces an increasingly pronounced maximum of the electron density with altitude.

If the beam is emitted continuously, a sheet of ionization will be created. On the other hand, if a pulse is emitted, a *picket fence* pattern will be created, each picket corresponding to a pulse. The picket fence pattern is particularly interesting, since

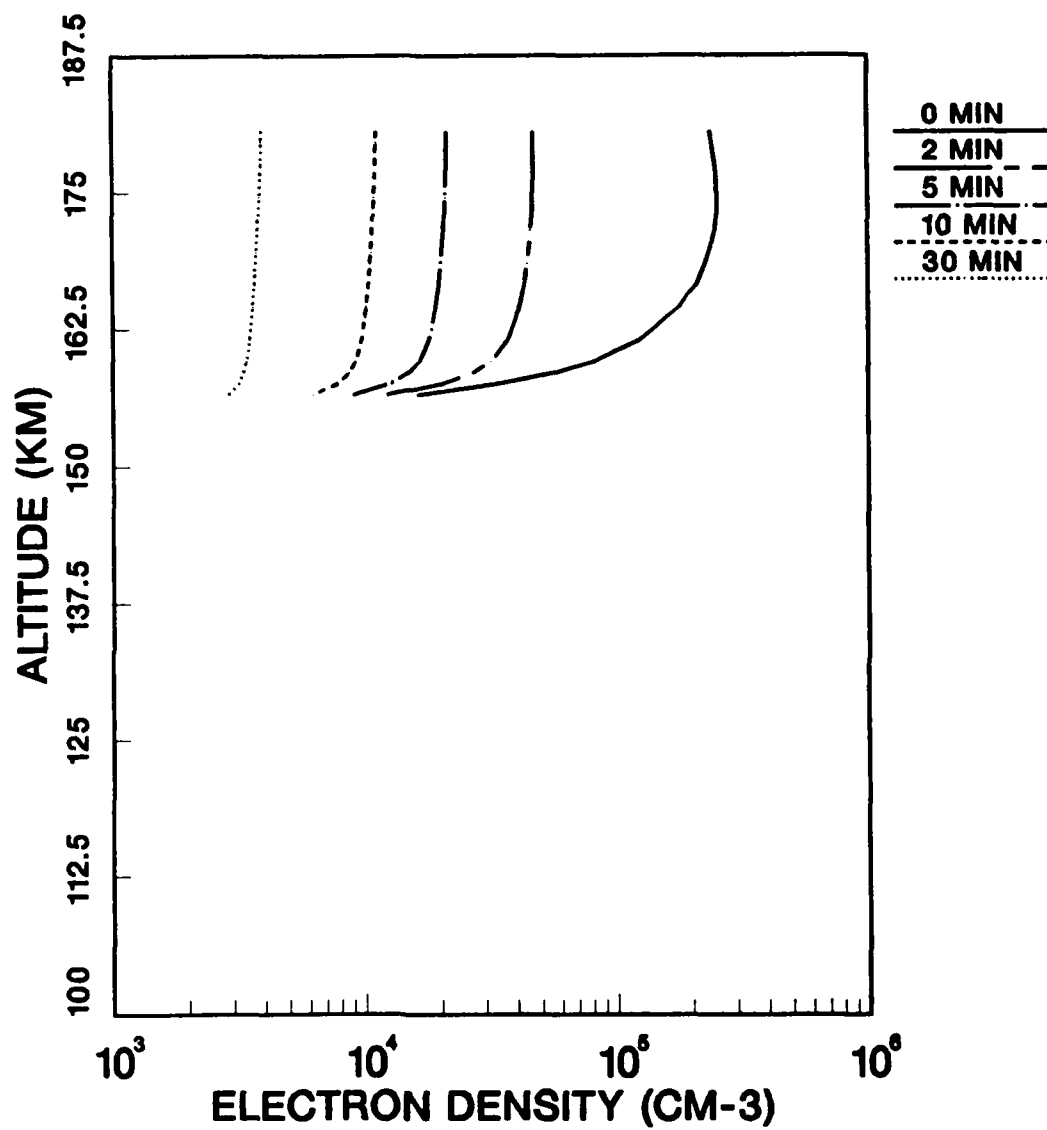


Figure 2.1. Temporal variation of ionization densities produced in a uniform plasma sheet by an 80 mA, 1 keV electron beam from a platform moving at 7 km/sec.

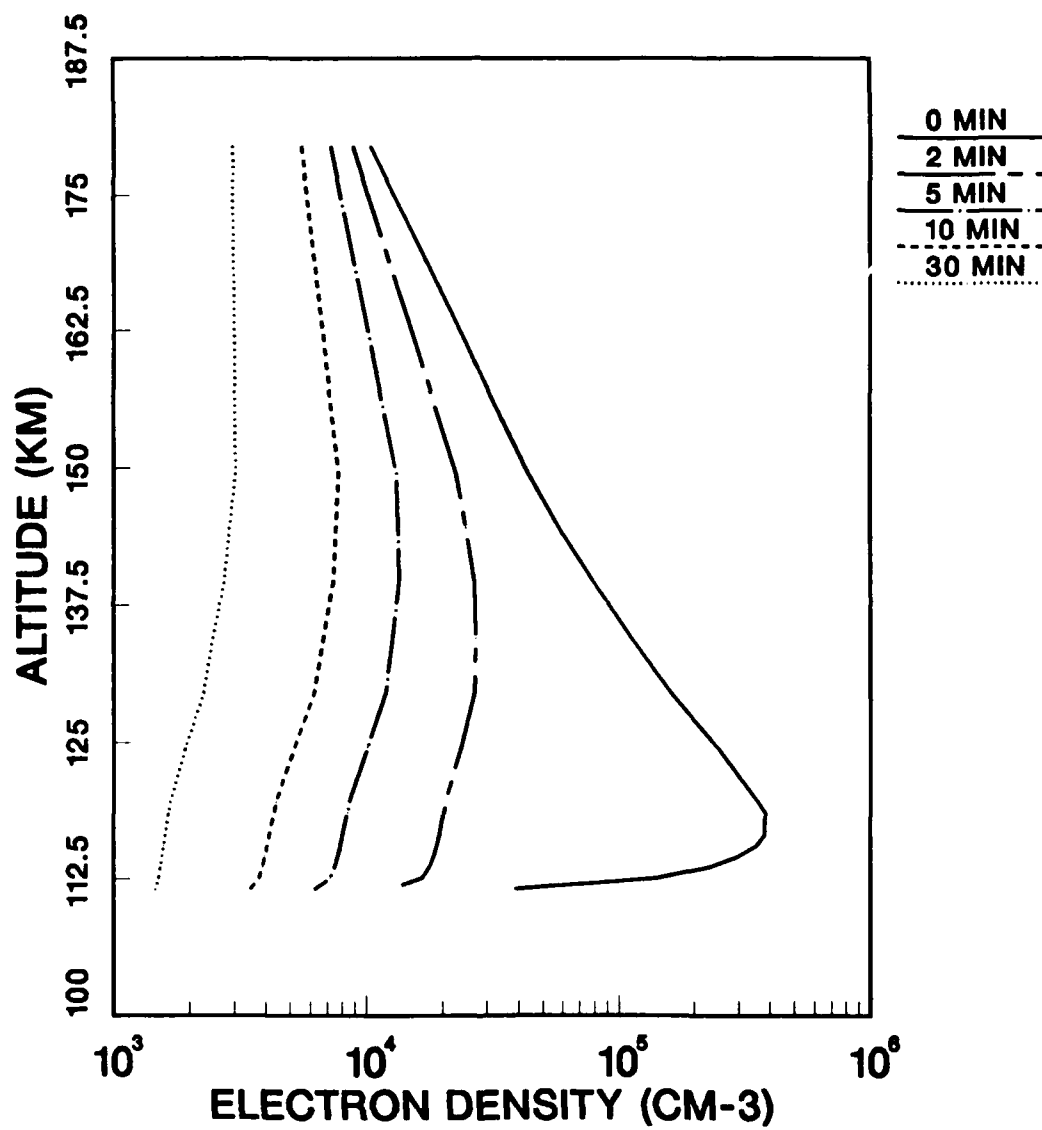


Figure 2.2. Temporal variation of ionization densities produced in a uniform plasma sheet by a 1 A, 5 keV electron beam from a platform moving at 140 m/sec.

it can give rise to Bragg diffraction phenomena due to the periodic structure of the picket fence.

A variety of physical effects should be expected as result of a very localized ionization event. Two examples of this are an outward pressure gradient electrostatic field with corresponding  $\mathbf{E} \times \mathbf{B}$  drifts and the possibility of convective instabilities creating their own spatial structure within the ionization sheet. Also, because of the vertical extent of the ionization sheet, it is possible to provide enhanced coupling between regions with differing ionic properties, such as collision frequency and gyrofrequency.

## 2.2. Electromagnetic Scattering

One of the principal potential applications of ionospheric enhancements is as a scatterer of high frequency electromagnetic waves. This process could therefore be used to remotely probe the affected altitude regimes for scientific purposes, as a reflection site for HF over-the horizon (OTH) ground-based radar, or possibly for communication purposes by scattering signals back to the ground that would otherwise be lost through the ionosphere.

A variety of scattering mechanisms may occur depending on specific electron beam and ionospheric conditions. The simplest is scattering from a single, isolated, nearly cylindrical scattering column resulting from a short pulse of the electron beam. For analysis purposes, this could be thought of as a dielectric medium or it can be treated similarly to the ionization resulting from a meteor trail after it has expanded due to ambipolar diffusion. Scattering from a variety of periodic spatial structures should also be possible. These structures could result naturally from plasma instabilities from the electron beam's propagation through the plasma or from gradients within the resulting ionization enhancement region. Similarly, spatial structures could also be created directly taking advantage of the spacecraft's motion while pulsing the electron gun at the appropriate rate, creating a picket fence sheet structure across the sky. Finally, with sufficient ionization and persistence, completely incoherent scatter effects may be measurable.



### 2.2.1. Column Scattering

In general the strongest signal scattered by a column of plasma occurs for wave vectors which lie in the plane perpendicular to the ionized column (and the coincident magnetic field line) and in which lies also the wave vector of the incident signal.

The measure of the effectiveness of the column as a scatterer is its radar cross-section. This cross-section is determined by solving for the radiation fields which are generated when a plasma column is irradiated by an incident plane wave. This is done by solving simultaneously the plasma equations in conjunction with Maxwell's equations.

An excellent source of material on scattering phenomena is given in the Radar Cross Section Handbook [*Ruck et al.*, 1970]. Under most circumstances the plasma can be described by a dielectric tensor analogously to that for a dielectric medium. When the plasma is subject to a magnetic field, the plasma is represented as an anisotropic dielectric and the tensor becomes very complicated. Formulas for the plasma dielectric tensor may be found in *Ruck et al.* [1970].

*Tang* [1966] has considered the problem of scattering from a plasma column in the absence of magnetic field using an isotropic pressure term. General expressions for the cross-section for both polarizations are given, including the effects of the excitation of longitudinal oscillations. *Gildenburg and Kondrat'ev* [1965] studied the plasma cylinder using the hydromagnetic approximation.

An extensive set of scattering curves for plasma cylinders, which have electron density profiles expressed as polynomials, have been calculated by *Ridder and Peterson* [1962] and *Ridder and Edelberg* [1964]. The Born approximation has been used by *Midzuno* [1961] and *Ruquist* [1964] to calculate the cross section of an electron density distribution, which is arbitrary except for the requirement that the plasma frequency must be much less than the radar frequency.

Axial variations of the permittivity make the variation of the scattered field three dimensional. *Brysk* [1958] has used the Born approximation to compute the scattering for low density meteor trails with axially varying permittivity.

The most interesting and pertinent cases studied are those which include a magnetic field and the corresponding anisotropic plasma dielectric tensor. The homogeneous plasma cylinder in the presence of a uniform axial magnetic field was studied by Wait [1961], Platzman and Ozaki [1960], and Adachi [1962]. Messaien and Vandenplas [1962] found good agreement between theory and experiment for these cases. Wait [1961] also presented solutions for the inhomogeneous plasma case by considering a plasma cylinder consisting of concentric layers with different properties. Messaien and Vandenplas [1966] have studied the existence of a scattered  $E_z$  field which exists even for normal incidence. Dnestrovskiy and Kostomarov [1963] considered a plasma with a diffuse boundary.

Crawford and Harker [1983] considered the nonlinear scattering from such plasma beams. Nonlinear scattering can occur when two separate electromagnetic waves mix in the ionized region, or when a single beam in the ionized region is strong enough to generate harmonics of itself.

When the incident wave has a frequency less than that of the peak plasma frequency (the overdense case), interesting resonance phenomena may arise. These correspond to internal resonances of the plasma column itself. The most well known of these is the dipole resonance, which occurs at  $\omega_p/\sqrt{2}$  [Crawford *et al.*, 1963]. There are, in fact, an infinite series of these resonances, and they are often referred to as the Tonks-Dattner resonances [Parker *et al.*, 1964].

It may be possible to observe these resonances in scattering experiments with artificial auroras, in which case they would appear as greatly enhanced signals at selected frequencies.

Herlofson [1951] studied the problem of plasma column resonance, and described the dipole resonance. Fejer [1964] considered temperature effects, and showed that a series of resonances occurred near  $\omega = \omega_p$ . Parker *et al.* [1964] and Crawford [1963] observed these resonances experimentally and explained them on the basis of plasma pressure theory.

### *2.2.2. Sheet Scattering*

A unique feature of beam particle induced ionization enhancements is the geometry of the ionization region that is created. Because of the relatively narrow diameter of the electron beam and the motion of the spacecraft platform, the resulting ionization enhancement traces out sheets of ionization. The sheet description is particularly appropriate when the extended nature of ionization along the magnetic field is considered. This ionization geometry is in contrast to other ionospheric modification techniques, such as Barium chemical release whose initial localized spherical shape only allows for limited extension along the magnetic field or HF heating, which affects a volume of considerable extent. Naturally occurring ionospheric modification such as sporadic-E or aurora, except for single meteor trail events, typically occur over regions of considerable volume.

Another unique feature of beam particle ionization enhancement is the fact that a picket fence type of structure can be created within the sheet of ionization by pulsing the beam source as the spacecraft moves (see Figure 2.3). This is particularly interesting, since it will give rise to Bragg diffraction phenomena due to the periodic structure of the picket fence that can enhance the scattering process due to coherent addition. The optimal spatial wavelength or diffraction grating spacing will be such that the largest peak to minima ionization is created. This occurs when the beam is operated with a 50% duty cycle and the on time is such that it allows the beam source to move a distance exactly equal to its beam diameter.

Complex viewing geometries are possible depending on the motion of the spacecraft. In particular, we show the geometry associated with a recent rocket experiment, CHARGE-2, flown at White Sands Missile Range. Figure 2.4 shows a computer simulation of the rocket trajectory and portions of the sheet ionization regions created. As can be seen, because of the rocket's trajectory and the given orientation of the earth's magnetic field, the ionization sheet will trace out a complex pattern. Also shown in the figure are ground contours of aspect angle for a specific location along the ionization sheet.

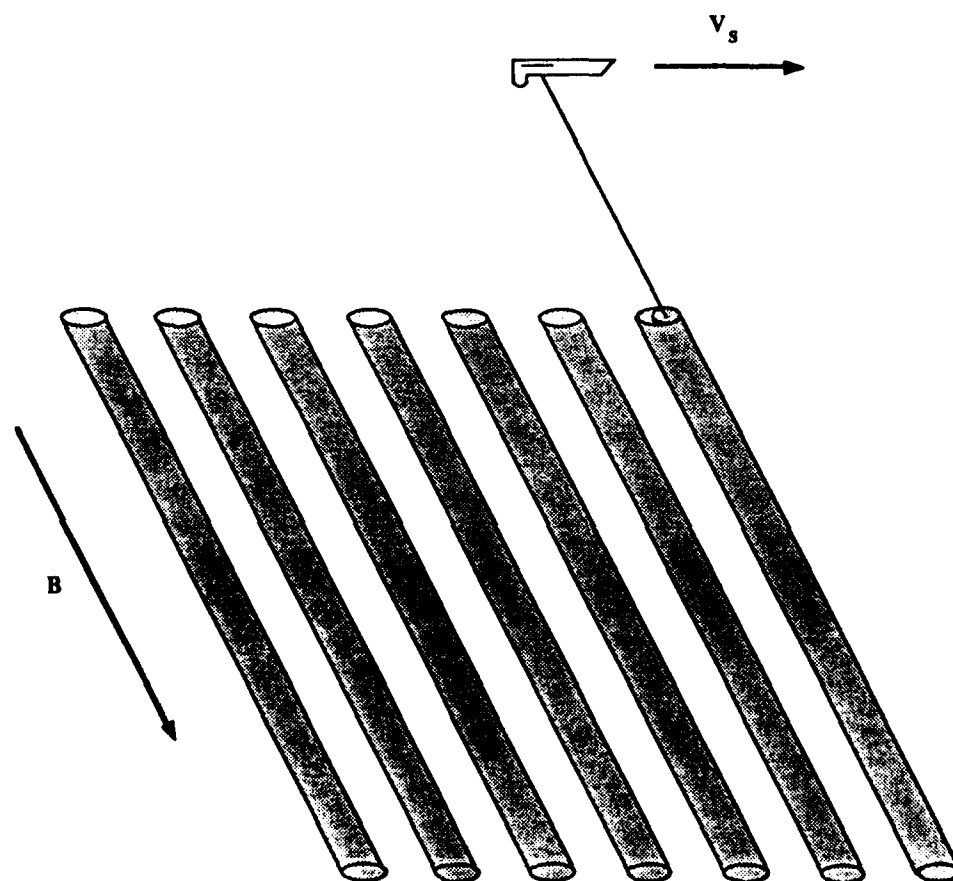


**Figure 2.3.** Schematic diagram showing the creation of a 'picket fence' of comparatively highly ionized columns in the ionosphere by the emission of a periodically pulsed electron beam from a moving source. The electron beam is directed along the earth's magnetic field  $B$  and each column is produced by one of the pulses in the beam.

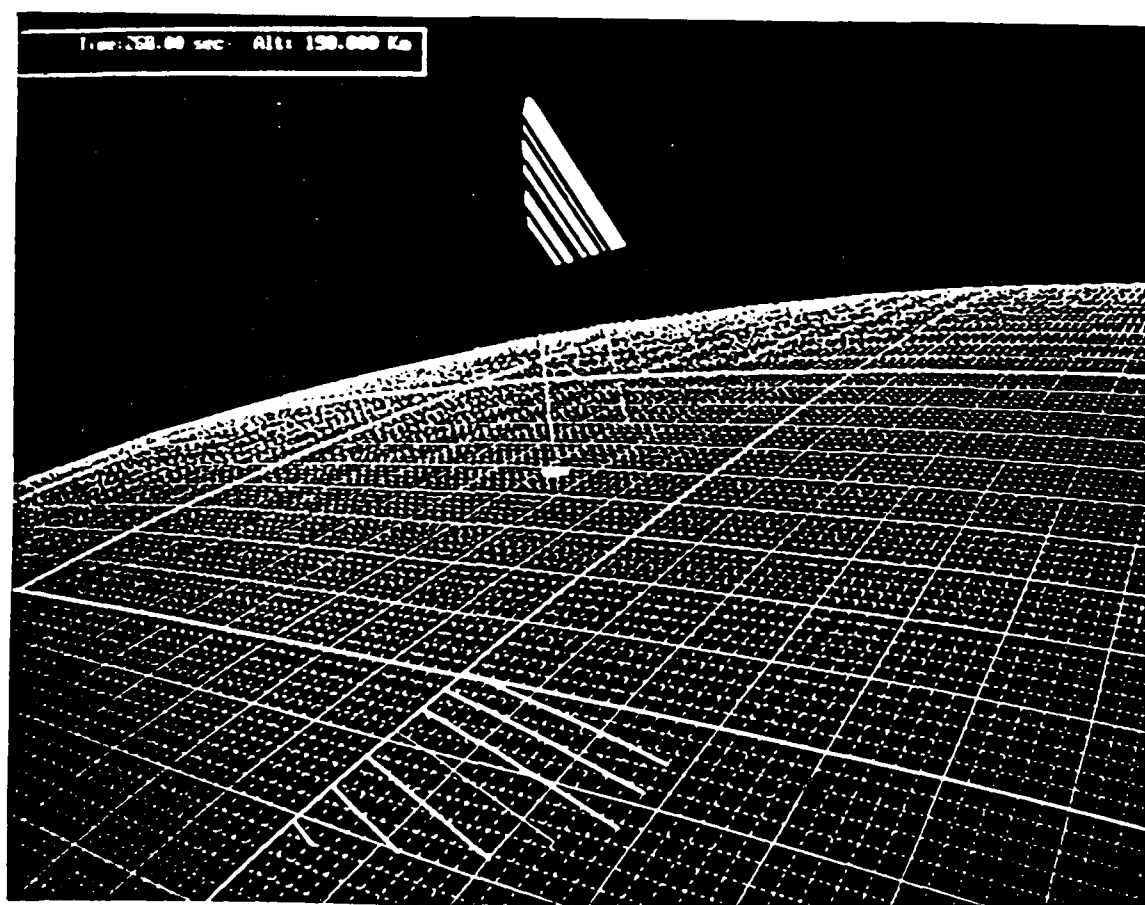


Figure 2.4. Computer simulation of ionospheric modification region for Charge-2 rocket electron beam experiment. Contours in foreground represent aspect angles for a particular location within ionization region assuming line-of-sight propagation.

A variety of radio experiments taking advantage of the unique geometry of the ionization enhancement as well as the periodic striations occurring within the sheet structure should be possible. The spatial wavelengths associated with optimal picket fence structure should be in the HF wavelength regime of 60 to 10 meters, while instability structures may extend to shorter wavelengths in the VHF range. The artificial diffraction screen structure could be used to provide coherent scattering in both the forward and backward directions. This structure should be sensitive to changes along the magnetic field line occurring over dimensions of a Fresnel zone providing a method of observing temporal variations.

### 2.3. Generation of Electromagnetic Waves

Beam injection experiments can tell us a great deal about the space environment, but probably one of the most interesting aspects is the generation of plasma waves by the electron beam in the presence of the background plasma. By monitoring these plasma wave emissions, such as with the PDP on the Shuttle, we can learn much about the interaction processes that take place in the beam-plasma system.

Another important potential use of the electron beam in space is its role as an antenna, i.e., as a generator of electromagnetic waves for communication purposes. The availability of an antenna which uses no wires, but only a modulated beam of electrons in space, offers great potential advantages. Chief among these are long length and thus higher radiation resistance, important for the generation of low frequency waves, and the elimination of metallic ohmic losses.

#### 2.3.1. *Past Work*

A number of systematic investigations have been conducted over recent years into the generation of electromagnetic waves by the passage of a pulsed electron beam through a magnetized plasma. This has been motivated, of course, by numerous experiments and the applications which have been mentioned above. Using a simple model for a pulsed electron beam, it has been possible to obtain a number of important predictions concerning the nature and characteristics of the fields generated.

Basically, there are three main radiation mechanisms that can cause emissions from an electron beam: incoherent spontaneous emission, coherent spontaneous emission, and stimulated emission.

In incoherent spontaneous emission all the electrons radiate independently of one another, giving rise to a radiated power proportional to the number of radiating particles. A number of authors have studied this phenomena in relation to either natural or artificial beams. Their general conclusion has been that incoherent spontaneous emission is not strong enough to give significant radiation from an electron beam of the type currently injected into space from orbiting vehicles.

In coherent spontaneous emission each particle still emits by spontaneous emission, but now the particles are constrained to travel in orbits which force all velocities at each particular position in space to be alike, leading thereby to coherent emission. For a charged particle traversing a magnetoplasma this velocity correlation comes from the fact that all the particles originate from approximately the same region of space and then are constrained to flow along the path of a helix. However, as the beam length increases, these correlations tend to average. If the beam were to remain continuous and become very long, the resulting interference would reduce the coherency to zero. The beam must therefore be broken into segments of the proper length and spacing. This leads to the second criterion for coherent spontaneous emission, namely beam modulation and beam fronts.

In stimulated emission the beam in the presense of the background plasma becomes unstable with respect to wave growth. As opposed to spontaneous emission, emissions are here stimulated by the presense of the wave itself. Since the probability of emission is proportional to the wave strength, the growth rate (in either time or space) is exponential.

Since stimulated emission is not dependent on beam fronts, and hence on modulation, most work on pulsed beams has concentrated on coherent spontaneous emission, since the associated coherency gives rise to the required signal strength, and the pulsed character of the beam satisfies its unique requirement for the presense of fronts.

### 2.3.2. Coherent Spontaneous Emission

#### a. Radiation from beams with a finite pulse train

Harker and Banks [1984a] studied the radiation from a finite pulse train electron beam. The radiation from a single particle traveling through free space permeated by a magnetic field was considered first by these authors. This was later generalized to the multiple pulse case. Finally the complete theoretical treatment to describe the radiation field of a finite pulse train of electrons traveling through a space plasma was presented. In order to simplify the theory, the beam length was assumed to be unbounded, i.e. it was assumed to extend from  $z=-\infty$  to  $\infty$ . Detailed numerical studies were made of the radiation from the lower hybrid to electron cyclotron frequency. Beam voltages considered were 100V, 1 KeV, and 10 KeV, while the beam current and pitch angle were taken as 100 mA and  $30^\circ$ , respectively. The 1 KeV beam voltage was chosen to simulate the FPEG electron gun used in the STS-3 Space Shuttle flight. The theory showed that the power radiated per unit solid angle per pulse typically lies in the vicinity of the free space value of 1mW/sr. There is a great variation with angle and frequency, and for certain angles and frequencies it is not uncommon to find radiated powers per unit solid angle of the order of 1 W/sr. In addition, singularities in the power distribution functions, up to three in number, were observed to occur; it was recommended that the conditions corresponding to these singular points should be studied in experiments, since they have the likeliest probability of detection.

This study showed that the successful use of electron beams as radiators and antennas relies on their use at selected frequencies, observation angles, beam duty cycles, beam modulation frequencies, and pitch angles.

#### b. Radiation from long pulse train beams

Recent experiments have reported the emission of electromagnetic radiation at the modulation frequency of the electron beam when that frequency was in the VLF range. In experiments on STS-3 [Neupert *et al.*, 1982; Banks *et al.*, 1983, 1984; Shawhan *et al.*, 1984] modulation of the beam at 3.1 and 4.8 kHz produced emissions at these frequencies and also at their harmonics up to the maximum observation



frequency of 30 kHz. Pulse trains typically contained 32,768 pulses. Experiments with modulated beams were also carried out on the SEPAC experiment on board Spacelab-1 in November and December 1983 [Obayashi *et al.*, 1982; Taylor and Obayashi, 1984].

Harker and Banks [1985] next extended their theory to cover these latest experiments. First, because of the relatively large number of pulses, they extended their theory to cover infinite pulse trains. Second, because most of the observations have been at frequencies in the range 1-30 kHz, they extended their numerical results to cover the region below the lower hybrid frequency. Third, they made the more realistic assumption that the beam extends only from  $z = 0$  (the gun position) outward, instead of from  $-\infty$  to  $+\infty$ . Finally, they introduced the assumption that the ability of the beam to radiate, for whatever reason, falls off exponentially with distance. The  $e$ -folding distance for this fall-off is a parameter which must be determined from more detailed theories or from experiments. They first derived general results, and then used these to specialize the theory to two cases, the long and short beam, in order to gain as much simplification as possible.

Calculations to determine the radiated power based on the theory were carried out for a range of parameters. One sets of computations was made for a voltage of 1000V, a current of 100 mA and a pitch angle of  $30^\circ$  for comparison with the results of the STS-3 mission with the FPEG. Another set of computations were made for a voltage of 7500V, a current of 1.6A, and a pitch angle of  $45^\circ$ . In all cases results were presented for Cerenkov and normal and anomalous cyclotron radiation.

In their theory for finite pulse train beams, after carrying out the mathematical simplification for the radiated power resulting from contour integrations, they were generally left with two integration variables. When the beam is infinitely long, an additional restraint is imposed in the form of the wave-particle interaction condition, which reduces the number of integration variables to one. This was the case discussed in the finite pulse train paper, where the power distribution function was chosen successively to be a function of the frequency, propagation angle, and ray vector angle.

In the present case, the beam is an unbounded pulse train. This introduces a

new restraint, namely that the frequency is an integral multiple of the modulation frequency, which again reduces the number of integration variables to one. When the beam is long, the wave-particle condition is again imposed, reducing the number of integrations variables to zero, and yielding a single angle for each modulation frequency. This is another way of saying that all of the power has been concentrated into radiation at a single polar angle, i.e. within those angles lying on a thin conical surface. Of course, this angle still varies with the system parameters, such as frequency and pitch angle.

Other authors have also discussed radiation from pulsed electron beams for the special case where the beam is modulated in a spatially sinusoidal manner and is in parallel flow along the magnetic field axis, giving rise thereby to Cerenkov radiation. *Lavergnat and Lehner* [1984] calculated the total power radiated by a beam extending from  $z = 0$  to  $z = vt$ , while *Ohnuki and Adachi* [1984] calculated the far-field in cylindrical coordinates emitted by an infinitely long beam. More recently, *Lavergnat et al.* [1984] have reported results for radiation from a sinusoidally modulated beam ejected at an angle to the magnetic field.

*c. Near fields in the vicinity of pulsed electron beams in space*

One shortcoming of the above work was that it was valid for the far field only. This means that if the beam has a length  $l$ , then the theory is only valid for distances from the beam greater than a factor of three or more times  $l$ . Since most of the measurements on electron beams in space have been taken within 10 m or so of the electron beam generator, it is clear that further work was needed to be done on the near fields generated in the vicinity of pulsed electron beams.

In order to remedy this situation, *Harker and Banks* [1984b, 1986] studied the near fields generated by a pulsed electron beam. Their model, as in our previous studies, assumes that the electrons follow an idealized helical path through the space plasma. The total radiation is obtained, again as above, by adding coherently the radiation from each individual electron in the helix, leading thereby to coherent spontaneous emission. The mathematical technique used consists of taking the Fourier transforms in space and time of Maxwell's equations, including the modulated beam current

terms which act as the driving mechanism for the interaction. The solution is then obtained by taking the inverse transforms to obtain the electric field as a function of the spatial coordinates. An important feature of the theory is the retention of evanescent waves in addition to the propagating waves used in the far field theory. This gives rise to contributions to the field strengths in frequency stop bands of far field theory. Field strengths calculated by the theory were calculated for a representative set of values of ionospheric parameters and electron beam current, voltage, and pitch angle and for a range of modulation frequencies extending from the ion to the electron cyclotron frequency. These predictions were found to be in essential agreement with the most recently available experimental data.

## 2.4. Recommendations for Further Work

### 2.4.1. Theoretical Work

There are four basic theoretical areas associated with electron beam induced ionospheric modification: beam launching and propagation, impact ionization processes, electromagnetic scattering and stimulation, and enhancement decay. All of these, either as part of this or earlier studies, have undergone at least preliminary evaluations. We would make the recommendation that at least two of these areas be pursued further in greater detail.

*Beam Launching and Propagation.* Conditions for proper beam launching and propagation continue to be an area of active theoretical and experimental interest in general. Conditions to achieve the launch of a well defined energy electron beam are not completely known, in particular for high current beam sources. We recommend that these issues be studied and organized in such a way that they could be properly tested on future electron beam experiments.

*Electromagnetic Scattering and Stimulation.* RF scattering and optical stimulation are the two most obvious ways of remotely detecting electron beam induced ionospheric enhancements. Optical observation techniques have been utilized extensively for many years now. This is not the situation for electromagnetic scattering.

There are a variety of possible electromagnetic scattering mechanisms affecting both forward and back scatter. These include Bragg scattering from an artificially generated spatial structure (picket fence), acoustic wave scatter from instabilities generated by gradients within the enhancement regions or by current diffusion parallel to  $B$ , possibly scintillation effects, and finally simple incoherent scatter mechanisms.

We therefore recommend that detailed calculations be made on the possible scattering mechanisms discussed above based on electromagnetic and plasma theory. Existing theory covering plasma columns should be of help in much of this, but the multiple column and resonance enhanced scattering cases will undoubtedly require new theory.

#### *2.4.2. Experimental Work*

An upcoming high power electron beam rocket experiment, called CHARGE-3, to be flown in November 1988 at White Sands Missile Range (WSMR), represents a fortuitous opportunity to investigate ionospheric modification using existing resources. We therefore make the recommendation that a *limited campaign* be undertaken to prepare and conduct remote radar and optical observations as part of the CHARGE-3 mission. The purpose of this effort would specifically be to detect the presence of electron beam generated ionospheric modification and of increasing the knowledge base for beam propagation physics plus the dynamics of the modified region. There are several reasons why we believe this is appropriate to consider at this time:

(1) It would be an efficient use of existing hardware on an existing mission to give information of the important processes associated with electron beam ionospheric modification. By taking advantage of the CHARGE-3 mission to detect the presence of beam generated ionospheric enhancements, we substantially reduce the cost and turn-around time that otherwise would be required for a separate effort. Note that AFGL is already contributing to the funding of CHARGE-3.

(2) CHARGE-3 will have the first low energy electron beam source of significant power (10–15 kW) to be flown on a spacecraft since the electron beam modification concepts first outlined by *Banks and Gilchrist* [1985]. The 10–15 kW power of the

CHARGE-3 gun should allow for peak ionization levels approaching  $10^6 \text{ cm}^{-3}$ , some two orders of magnitude over expected background ionization levels in the nighttime E-region. Earlier attempts, during 1985 (Spacelab-2 and CHARGE-2), used low power ( $\leq 100 \text{ W}$ ) beam sources to attempt detection of ionospheric modification. Neither effort was able to conclusively observe an effect, although it had been calculated that the CHARGE-2 flight, under the proper conditions, had a good probability of success. Unfortunately, the beam source on CHARGE-2 failed to achieve its intended power levels nor was all of the proper ground equipment available for the flight.

(3) Much of the computer programming and logistics planning for CHARGE-2 can be directly utilized in the CHARGE-3 mission, which will help the mission and logistics planning efforts for the latter mission. The computer software now available includes several programs to select both optical and radar ground sites. Having conducted observations as part of CHARGE-2, we are now familiar with the resources available at WSMR and the geography of southwest Texas where ground radar facilities are most likely to be placed.

Finally, (4), the CHARGE-3 mission is still sufficiently in the future that analysis efforts conducted as outlined above for *theoretical work* should be available to contribute to CHARGE-3 remote observations efforts.

## 2.5. Summary

### 2.5.1. Artificial Auroral Ionization

Important ionization enhancement effects in the E and lower F regions, such as the creation of artificial aurora and picket fence type ionization structures, appear possible using low energy electron beams (1–10 keV). These structures are predicted to persist over a period of minutes. The 1 to 10 keV range of beam energy is necessary to produce the principal (peak) ionization enhancement in this altitude regime and offers the advantage of longer persistence when compared to lower altitudes penetrated by higher energy beams because of slower recombination or diffusion rates. The principal area of concern for this energy level of electron beam is in establishing conditions for which the beam will propagate, over extended distances, as a narrow (focused) column

structure.

It should be possible to use the created ionization structures as scatterers of electromagnetic waves. This process could therefore be used to remotely probe these altitude regions for a variety of scientific purposes, as a reflection site for HF over-the-horizon ground based radar, or possibly for communication purposes by scattering back to the ground signals which would otherwise be lost through the ionosphere. It should further be possible to enhance these scattering effects at specific frequencies by resonance scattering phenomena long known in plasma physics.

#### *2.5.2. Generation of Electromagnetic Waves.*

Pulsed electron beams can be used to generate electromagnetic waves by the process of coherent spontaneous emission, among others. We should, therefore, be able to use the electron beam as a non-wire antenna for the generation of electromagnetic waves for communication purposes, for example. The long length of such an antenna can only be rivaled by a device such as the electrodynamic tether. Since the radiation resistance varies as the square of antenna length, and since this type of antenna has no metallic ohmic losses, electron beam antennas should be increasingly useful at lower frequencies.

## 2.6. References

- Adachi, S., Scattering pattern of a plane wave from a magneto-plasma cylinder, *IRE Trans. Antennas Propagation AP-10*, 352, 1962.
- Banks, P. M., and B. E. Gilchrist, Artificial plasma density structures produced by energetic beams from rockets and spacecraft, *Geophys. Res. Lett.*, 12, 125, 1985.
- Banks, P. M., A. C. Fraser-Smith, U. S. Inan, G. Reeves, W. J. Raitt, W. S. Kurth, G. Murphy, R. Anderson and S. D. Shawhan, Observations of VLF emissions from a pulsed electron gun on the Space Shuttle, *EOS*, 65, 1054, 1984.
- Banks, P. M., P. R. Williamson, W. J. Raitt, S. D. Shawhan and G. Murphy, Electron beam experiments aboard the Space Shuttle, *Active Experiments in Space*

Symposium, Alpbach, Austria, May 24-28, 1983.

Brysk, H., Electromagnetic scattering by low density meteor trails, *J. Geophys. Res.*, **63**, 693, 1958.

Crawford, F.W., The mechanism of Tonks-Dattner plasma resonances, *Phys. Letters*, **5**, 244, 1963.

Crawford, F.W., and K.J. Harker, Nonlinear scattering from a plasma column, 1. Theory, *Radio Science*, **18**, 775; Nonlinear scattering from a plasma column, 2. Special Cases, *Radio Science*, **18**, 785, 1983.

Crawford, F.W., G.S. Kino, and A.B. Cannara, Dipole resonances of a plasma in a magnetic field, *J. Appl. Phys.*, **34**, 3168, 1963.

Dnestrovskiy, Yu. N., and D.P. Kostomarov, Diffraction of a plane electromagnetic wave by a circular plasma cylinder, *Radio Eng. Electron. (USSR)* **8**, 359, 1963.

Fejer, J.A., Scattering of electromagnetic waves by a plasma cylinder, *Phys. Fluids*, **7**, 439, 1964.

Gildenburg, V.B., and I.G. Kondrat'ev, Diffraction of electromagnetic waves by a bounded plasma in the presense of spatial dispersion, *Radio Eng. Electron. (USSR)*, **560**, 1965.

Grun, A.E., Energieabsorption im Strahlungsfeld von Elektronenquellen, *Z. Naturforschung*, **129**, 89, 1957.

Harker, K. J., and P. M. Banks, Radiation from pulsed electron beams in space plasmas, *Radio Sci.*, **19**, 454, 1984a.

Harker, K. J., and P. M. Banks, Near fields in the vicinity of pulsed electron beams in space, paper presented at the 21st General Assembly of URSI, Florence, Italy, August 28-September 5, 1984b.

Harker, K. J., and P. M. Banks, Radiation from long pulse train electron beams in space plasmas, *Planet. Space Sci.*, **33**, 953-963, 1985.

Harker, K. J., and P. M. Banks, Near fields in the vicinity of pulsed electron beams in space, *Planet. Space Sci.*, **35**, 11, 1986.

- Herlofson, N., Plasma resonance in ionospheric irregularities, *Arkiv Fysik*, **3**, 247, 1951.
- Lavergnat, J., and T. Lehner, Low frequency radiation characteristics of a modulated electron beam immersed in a magnetized plasma, *IEEE Trans. Antennas Propagat.*, **AP-32**, 177, 1984.
- Lavergnat, J., T. Lehner, and G. Matthieussent, Coherent spontaneous emission from a modulated beam injected in a magnetized plasma, *Phys. Fluids*, **27**, 1632, 1984.
- Messaïen, A.M., and P.E. Vandenplas, Experiment and theory of plasma cylinders in the presense of a magnetic field, *Phys. Letters*, **2**, 192, 1962.
- Messaïen, A.M., and P.E. Vandenplas, High-frequency effect due to the axial drift velocity of a plasma column, *Phys. Rev.*, **149**, 131, 1966.
- Midzuno, Y., Scattering of microwaves from a cylindrical plasma in the Born approximation, *J. Phys. Soc. Japan*, **16**, 971, 1403, 1961.
- Neupert, W. M., *et al.*, Science on the space shuttle, *Nature*, **296**, 193-197, 1982.
- Obayashi, T., N. Kawashima, K. Kuriki, M. Nagatomo, K. Ninomiya, S. Sasaki, A. Ushirokawa, I. Kudo, M. Ejiri, W. T. Roberts, R. Chappell, J. Burch, and P. Banks, Space experiments with particle accelerators (SEPAC), in *Artificial Particle Beams in Space Plasma Studies*, (Edited by B. Grandal), Plenum Press, New York, 1982.
- Ohnuki, S., and S. Adachi, Radiation of electromagnetic waves from an electron beam antenna in an ionosphere, *Radio Science*, **19**, 925, 1984.
- Parker, J.V., J.C. Nickel, and R.W. Gould, Resonance oscillations in a hot nonuniform plasma, *Phys. Fluids*, **7**, 1489, 1964.
- Platzman, P. M., and Ozaki, H. T., Scattering of electromagnetic waves from an infinitely long magnetized cylindrical plasma, *J. Appl. Phys.*, **31**, 1957, 1960.
- Rees, M.H., Auroral Ionization and excitation by incident energetic electrons, *Planet. Space Sci.*, **11**, 1209, 1963.



- Ridder, C.M., and S. Edelberg, Scattering from plasma cylinders with radial variations in electron density, in H. Rotman, K. Moore, and R. Papa (eds.), *Electromagnetic Aspects of Hypersonic Flight*, Spartan Books, Baltimore, MD 286, 1964.
- Ridder, C.M., and L.G. Peterson, Scattering from a homogeneous plasma cylinder of infinite length, MIT Lincoln Laboratory, Report 312G-4, 1962. AD274067
- Ruck, G.T., D.E. Barrick, W.D. Stuart, and C.K. Krichbaum, *Radar Cross Section Handbook*, Vols 1 and 2, Plenum Press, New York, Chapter 10, 1970.
- Ruquist, R.D., A diagnostic theory for cylindrical plasmas based on the Born approximation, Harvard University, AFCRL-65-87, 1964. AD612632
- Shawhan, S.D., G.B. Murphy, P.M. Banks, P.R. Williamson, and W.J. Raitt, Wave emissions from DC and modulated electron beams on STS 3, *Radio Science*, 19, 471, 1984.
- Tang, C.H., Scattering by finite objects in compressible plasma, *Nuovo Cimento*, 46B, 93, 1966.
- Taylor, W. W. L. and T. Obayashi, Wave-particle interactions induced by SEPAC on Spacelab-1. *Proc. 1984 Symposium on The Effects of the Ionosphere on C<sup>3</sup>I Systems*, Alexandria, VA, 1-3 May, 1984.
- Wait, J.R., Some boundary value problems involving plasma media, *J. Res. Natl. Bur. Std.*, 65B, 137 (1961).

### 3. MODERATELY ENERGETIC ELECTRON BEAMS

By this we mean beams of electrons with energies in the range 10–500 keV. The upper limit of this range corresponds roughly to the electron rest mass, so it is a transition value above which relativistic effects are important.

#### 3.1. Previous Space Experiments

Table 1 on page 93 contains a list of the space experiments performed during the past decade (during or after 1975) with artificial electron beams at energies of 10 keV or more. The highest energy reported was 40 keV; we have found no published accounts of any work at higher energies. The successive rows of the table refer to the different experiments, in chronological order. The successive columns contain: (1) the title of the experiment; (2) the date on which it was performed (or dates, if the experiment involved more than one rocket); (3) the range of altitude over which the electron beam was emitted, or the apogee altitude if this range is not given in the published literature; (4) the energy of the electron beam (in some experiments more than one energy was used, or the energy was varied continuously over a certain range); (5) beam current (often the beam was pulsed or otherwise modulated, and the figure quoted is the peak current). This list is not guaranteed complete, but it is certainly representative. Lists of the space electron beam experiments in the years preceding 1975 may be found in two review papers by *Winckler* [1980, 1982].

In all of these experiments the vehicle was a rocket. Though electron beam experiments have also been performed on satellites and on the Space Shuttle, the beam energies have so far always been less than 10 keV.

In none of these experiments was modification of the ionosphere a prime scientific objective, but in some of them it was a means to other ends. Thus, for instance, in the Franco-Soviet 'Araks' experiments [*Cambou*, 1980], the rockets were launched from the Kerguelen Islands in the southern hemisphere, and the ionization produced by the beam in the lower ionosphere at the magnetically conjugate point in the northern hemisphere was the basis for localization of this point by radar [*Pyatsi and*

Zarnitsky, 1980 *Uspensky et al.*, 1980]. Others, such as the Norwegian 'Polar 5' [Grandal, 1982] and 'Electron 2' experiments [Jacobsen *et al.*, 1981], were designed to study ionospheric perturbations produced involuntarily, as results of a beam-plasma discharge (BPD) excited by an electron beam emitted from a rocket. In contrast, the original objectives of the University of Minnesota 'Echo' series of experiments were to use electron beams for investigating beam-plasma interactions and for probing the distant magnetosphere [Winckler, 1980, 1982; Winckler *et al.*, 1984]; for these purposes, the perturbations of the ambient plasma and accompanying perturbations of the electron beam itself were of nuisance value only.

Thus very few of the previous space experiments with electron beams at energies of 10 keV or higher were performed with the deliberate intention of modifying the ionosphere, but nevertheless the data that they have yielded are useful when studying the possibilities for doing so. In this respect, of course, the energy of 10 keV has no special physical significance, and data from experiments at lower energies are helpful as well.

### 3.2. Electron Beam Sources

Winckler [1982] has briefly surveyed progress up to 1980 in the development of electron beam sources for use in space experiments. This effort drew on a knowledge base from the development of powerful electron guns for industrial applications, as in x-ray tubes, or in klystrons and other types of radio-frequency (RF) vacuum tube, or for welding metals under vacuum. In its simplest form, of which the Pierce (1954) design is the post-war prototype, an electron gun comprises a hot cathode that emits electrons, and a set of suitably biased electrodes creating strong electric fields to accelerate, focus, and possibly deflect them. Other electrodes may be used to modulate the beam, and magnetic fields may also be used for focusing and deflection. All the electron guns so far used in space have been of this variety; the highest energy used was about 40 keV, as mentioned earlier. In the laboratory, electron guns have been built for energies up to several MeV; higher energies require induction accelerators

such as betatrons, or RF accelerators such as synchrotrons or linacs. In space, because of the greater difficulty of preventing flash-over, the upper limit of the energy obtainable from straightforward electron guns is probably smaller, but no basis exists for giving a precise figure.

### 3.3. Ionospheric Effects of Electron Beams

#### 3.3.1. Classification

Our mandate is to examine the perspectives for using electron beams to achieve ionospheric modification, which we take in a broad sense to mean effects making appreciable changes in the properties of the ionospheric plasma. Other accompanying effects, such as charging of the vehicle, changes in the properties of the beam, and generation of waves in the plasma, are of interest here only insofar as they relate to this main theme.

For presentation, we may classify the relevant ionospheric effects into those involving direct interaction of the beam with the ambient plasma alone (beam-plasma instability), those involving interaction of the beam with the neutral gas through the intermediary of the plasma (beam-plasma discharge), and those involving direct interaction between the beam and the neutral gas (collisional ionization).

#### 3.3.2. Beam-plasma instability

In theory, a mono-energetic electron beam traveling through a fully ionized thermal plasma becomes unstable as soon as the velocity of the beam exceeds the characteristic thermal velocity of the plasma electrons. The unstable waves are electrostatic in nature, or alternatively, when a magnetic field is present, they may be electromagnetic waves in their quasi-electrostatic limit.

These statements refer to cases where the electron densities of the beam and of the plasma are comparable; in addition, they imply a beam much wider than all of the microscopic plasma scale lengths, and also much wider than the wavelengths of the unstable plasma waves. However, a beam from an electron gun on a spacecraft is

unlikely to satisfy the latter inequality. Generally speaking, narrow beams are more stable than wide ones, because the unstable waves may propagate out of the beam before they have been able to grow very much [*Jones and Kellogg, 1973*].

When an electron gun is operated on a spacecraft, plasma waves may be excited not only by the outgoing electron beam, but also by the return current of thermal electrons from the ambient plasma. Their motion relative to the ions in the plasma can excite both ion acoustic waves and ion cyclotron waves. Under most conditions prevailing in the ionosphere, the ion cyclotron waves are the more unstable, i.e., the threshold current density required to excite them is less than it is for ion acoustic waves [*Kindel and Kennel, 1971*]. In the collisional bottomside ionosphere, electron collisions help to destabilize ion cyclotron waves, contrary to what one might expect [*Satyanarayana et al., 1985*].

Since the beam and the return current are both constrained to follow the magnetic field lines, in most previous experiments they occupied overlapping regions of space, so their respective effects were liable to interact with one another. This difficulty can be overcome in experiments in which two separate payloads are connected together electrically by a 'tether' in the form of a conducting wire coated with an insulating material. Several rocket experiments with tethered sub-payloads have already been performed [*Sasaki et al., 1986a*], and extensive plans have been made for similar experiments on the Space Shuttle [*Banks et al., 1981*].

Besides the experiments in space, many laboratory experiments on beam-plasma instability have been performed. In a very significant recent experiment by *Okuda et al. [1985]*, an electron beam was injected into a magnetized plasma, along the direction of the magnetic field, with a velocity about 10 times the thermal velocity of the plasma electrons. The electron concentration in the beam was about 10% of that in the plasma, and a strong beam-plasma instability developed. The resulting nonlinear electron plasma waves reacted back on the electron population, accelerating appreciable amounts of beam and plasma electrons to velocities well above the initial beam velocity. With increasing distance along the beam, the parallel electron velocity distribution evolved rapidly into a smooth one extending from zero up to 1.5-2 times

the initial beam velocity. Over this entire range it had a negative slope, which meant that the beam had become stable. These phenomena were reproduced subsequently in numerical simulations, which showed that trapping of the electrons by the waves played an important role in the nonlinear development of the beam-plasma instability [Okuda *et al.*, 1987]. One reason why these particular experiments were so successful is that the initial beam velocity was not excessively large compared with the thermal velocity, so the electron distribution function was able to evolve to its final stable form within the dimensions of the apparatus.

Contrariwise, most space experiments have involved initial beam velocities several orders of magnitude greater than thermal velocity, and plasmas much less dense than those commonly used in laboratory experiments. In these circumstances, the beam-plasma instability and its accompanying phenomena evolve over very much greater distances, though their natures are almost certainly the same. In particular, the evolution to a stable velocity distribution, as observed in the laboratory, may help to explain how electron beams are able to travel over long distances in space without losing all their energy to unstable waves and being brought to a halt.

Observations made in the ionospheric plasma near to an artificial electron beam have revealed a wide variety of electrostatic and electromagnetic plasma waves created by beam-plasma instabilities (BPI), extending in frequency from a few kilohertz to well above the local plasma frequency, and including lower-hybrid and whistler-mode waves, electron cyclotron harmonics, and plasma frequency and upper-hybrid emissions. Absorption of these waves can cause appreciable heating of the plasma electrons, up to energies of several electron-volts, and out to distances of more than a hundred metres from the beam [Winckler *et al.*, 1986]; close to the beam, electrons of higher energies are observed, but here, of course, it is difficult to distinguish heated plasma electrons from beam electrons that have been degraded in energy and have diffused outwards from the beam under the influence of the strongly nonlinear plasma waves. This plasma heating is the principal ionospheric modification caused by artificial energetic electron beams at altitudes above about 200 km, where interactions with the neutral atmospheric gas are negligible.

### 3.3.3. Beam-plasma discharge

At lower altitudes, beam-plasma interactions modify the ionosphere to a much greater extent, because the energetic electrons in and around the beam collide with the atoms and molecules of the neutral atmospheric gases, exciting and ionizing them. The resulting increase in the local electron concentration generally intensifies the beam-plasma instabilities that are supplying the energetic electrons, so there is positive feedback from the ionization process to the BPI. If, for a given energy of the beam electrons, the current in the beam is increased progressively, the rate of production of ionization increases faster than the current. Then, when a critical threshold current is attained, the ionization rate jumps discontinuously to a higher level, and so do the electron concentration and the luminous emission from excited neutral atoms. This is the onset of 'beam-plasma discharge' (BPD), a phenomenon that has been studied extensively both in space and in the laboratory. The laboratory experiments have included pre-flight tests of equipment later used in space [Banks *et al.*, 1982; Kawashima, 1983]; these particular experiments were at energies below 10 keV, however. In at least one space experiment, the increase in ionospheric electron concentration due to BPD was sufficient to allow the cloud of dense ionization around the beam to be detected by radar from the ground [Cambou, 1975].

Both the laboratory and the space experiments appear to confirm theoretical predictions that the critical current for the onset of BPD is directly proportional to the  $3/2$  power of the energy of the electrons in the beam, and inversely proportional to the neutral gas pressure [Bernstein *et al.*, 1979; Ingsøy and Friedrich, 1983; Papadopoulos, 1981].

### 3.3.4. Collisional ionization

Even in the absence of BPI or BPD, the energetic electrons in the beam can excite and ionize neutral gas particles by colliding with them. Obviously the most favorable conditions for collisional excitation and ionization exist when the beam descends from space into the atmosphere, encountering neutral gas at ever-increasing densities as its altitude decreases. These conditions were created by the very first

space experiment with a rocket-borne electron gun, in which a 20 keV 0.5 A beam was directed downwards, and produced a streak of artificial auroral light in the altitude range 90–100 km [Hess *et al.*, 1971]. In a later experiment by the same group, a similar beam was directed upwards and the auroral light streak was observed at the magnetically conjugate point [Davis *et al.*, 1980]. A few years later again, in the Araks experiments at a higher magnetic latitude, ionization produced at the conjugate point was observed by radar [Pyatsi and Zarnitsky, 1980]. Rough estimates of the extent of the ionization ‘sheets’ produced during the experiments give  $2^\circ$  of longitude (rocket motion in East-West direction) and  $0.5^\circ$  of latitude (rocket motion in North-South direction).

For the purpose of producing extra ionization in the D region (50–85 km) and E region (85–140 km) of the ionosphere, electron beams in the energy range 10–500 keV are not qualitatively different from beams with lower or higher energies. Indeed there is some quantitative equivalence, because the energy required to produce an electron-ion pair is approximately 35 eV, regardless of the energy of the beam electrons so long as this exceeds 500 eV or so [Banks and Kockarts, 1973]. Hence, at the energies that we are concerned with here, the total rate of production of electron-ion pairs is directly proportional, by a constant factor independent of energy, to the total power of the electron beam.

However, changing the energy of the beam, or its angle with respect to the magnetic field (‘pitch angle’), does change the way in which the rate of production varies with altitude. Electron beams with higher energies or smaller pitch angles penetrate to lower altitudes, and create a greater proportion of their ionization at these altitudes. Graphs of ionization production versus altitude, for downcoming electrons with energies up to 300 keV, have been given by Banks and Kockarts [1973]; at zero pitch angle, the altitude of maximum production varies from 105 km at 10 keV to 70 km at 300 keV.

### 3.4. Possible Future Experiments

Recapitulating, electron beams in the energy range 10–500 keV can modify the



ionosphere by heating the plasma or by producing new ionization. Heating can occur at all altitudes as the result of beam-plasma instability, if the conditions for the latter are met. The production of new ionization, however, requires an adequate neutral gas pressure, which is found only below about 200 km. Around the beam near to its source, both plasma heating and the production of new ionization are favored by the occurrence of beam-plasma discharge, again if the appropriate conditions are met. Under the influence of BPI, with or without BPD, the velocity distribution of the beam evolves towards a stable form. Whether this form is attained or not, the beam electrons can still collide with the neutral particles and produce appreciable amounts of new ionization in the E region, and even down into the D region if their energy is sufficient.

Much space and laboratory experimentation has already been done on these topics, so original experiments on them are hard to suggest. Despite all previous work, however, the ionospheric modifications accompanying BPI and BPD are still imperfectly understood. In space experimentation, at least two factors have contributed to this state of affairs: one is that most experiments have been performed at beam energies above 1 keV, where the spatial scales of such phenomena as the evolution of the beam velocity distribution are so large that they are hard to explore effectively in a single experiment; the other is that the beam current and the return current flowed in the same region of space. It would seem, therefore, that there is still scope for significant experiments at much lower beam energies, from a few eV upwards, using a remote tethered sub-payload to collect the return current; an alternative to the latter would be to eject, into a different region of space, a positive ion beam carrying a current equal and opposite to that of the electron beam.

Electron beams in the energy range 10–500 keV can be used for experiments involving the creation of artificial plasma density structures capable of scattering waves from ground-based radars, as proposed by *Banks and Gilchrist* [1985].

### 3.5. Summary of Proposed Experiments

#### 3.5.1. Investigation of BPI and BPD

Experiments similar to those performed previously in space, but with arrangements made to spatially separate the beam from the return current.

#### 3.5.2. Artificial Plasma Density Structures

Creation as in the proposal by Banks and Gilchrist [1985].

### 3.6. References

- Banks, P.M., and G. Kockarts, *Aeronomy*, Part A, Academic, New York, 1973.
- Banks, P.M., P.R. Williamson, and K.-I. Oyama, Electrical behavior of a Shuttle Electrodynamic Tether System (SETS), *Planet. Space Sci.*, 29, 139-147, 1981.
- Banks, P.M., W.J. Raitt, and W.F. Denig, Studies of beam-plasma interactions in a space simulation chamber using prototype Space-Shuttle instruments, in *Artificial Particle Beams in Space Plasma Studies*, edited by B. Grandal, pp. 393-403, Plenum, New York, 1982.
- Banks, P.M., and B.E. Gilchrist, Artificial plasma density structures produced by energetic electron beams from rockets and spacecraft, *Geophys. Res. Lett.*, 12, 175-178, 1985.
- Bernstein, W., *et al.*, Further laboratory measurements of the beam-plasma discharge, *J. Geophys. Res.*, 84, 7271-7278, 1979.
- Cambou, F., *et al.*, The Zarnitza rocket experiment of electron injection, *Space Research*, 15, 491-500, 1975.
- Cambou, F., *et al.*, General description of the Araks experiments, *Ann. Géophys.*, 36, 271-283, 1980.
- Davis, T.N., *et al.*, Artificial aurora conjugate to a rocket-borne electron accelerator, *J. Geophys. Res.*, 85, 1722-1728, 1980.

- Grandal, B., Highlights of the observations in the Polar 5 electron accelerator rocket experiment, in *Artificial Particle Beams in Space Plasma Studies*, edited by B. Grandal, pp. 159-173, Plenum, New York, 1982.
- Hess, W.N., *et al.*, Artificial aurora experiment: Experiment and principal results, *J. Geophys. Res.*, **76**, 6067-6092, 1971.
- Ingsøy, P., and M. Friedrich, Plasma heating generated by a rocket borne electron accelerator, in *Active Experiments in Space*, edited by W.R. Burke, pp. 129-136, European Space Agency, Noordwijk, Special Publication No. 195, 1983.
- Jacobsen, T.A., *et al.*, Ionospheric electron heating by a rocket borne electron accelerator, *Adv. Space Res.*, **1**(2), 123-127, 1981.
- Jones, J.W., and P.J. Kellogg, Plasma waves artificially induced in the ionosphere, *J. Geophys. Res.*, **78**, 2166-2175, 1973.
- Kawashima, N., Highlights of the electron beam experiments in space in Japan, in *Active Experiments in Space*, edited by W.R. Burke, pp. 141-149, European Space Agency, Paris, Special Publication No. 195, 1983.
- Kindel, J.M., and C.F. Kennel, Topside current instabilities, *J. Geophys. Res.*, **76**, 3055-3078, 1971.
- Okuda, H., *et al.*, Effects of beam plasma instability on current drive via injection of an electron beam into a torus, *Phys. Fluids*, **28**, 3365-3379, 1985.
- Okuda, H., *et al.*, Propagation of a non-relativistic electron beam in a plasma in a magnetic field, *Phys. Fluids*, **30**, 200-208, 1987.
- Papadopoulos, K., Theory of beam plasma discharge, in *Artificial Particle Beams in Space Plasma Studies*, edited by B. Grandal, pp. 505-523, Plenum, New York, 1982.
- Pierce, J.R., *Theory and Design of Electron Beams*, (2nd edn.), Van Nostrand, Princeton, 1954.
- Pyatsi, A.K., and Y.F. Zarnitsky, Electron precipitation in magnetically conjugated

- region in the first Araks experiment from radar data, *Ann. Géophys.*, **36**, 297-302, 1980.
- Sasaki, S., *et al.*, The fourth US-Japan tethered payload experiment — Quick Look Report, Institute of Space and Aeronautical Science, Tokyo, Report No. 323, 1986.
- Satyanarayana, P., *et al.*, Theory of the current-driven ion cyclotron instability in the bottomside ionosphere, *J. Geophys. Res.*, **90**, 12,209-12,218, 1985.
- Uspensky, M.V., *et al.*, "Araks" Doppler radar measurements of the ionospheric effects of artificial electron beam in the North hemisphere, *Ann. Géophys.*, **36**, 303-312, 1980.
- Winckler, J.R., The application of artificial electron beams to magnetospheric research, *Rev. Geophys. Space Phys.*, **18**, 659-682, 1980.
- Winckler, J.R., The use of artificial electron beams as probes of the distant magnetosphere, in *Artificial Particle Beams in Space Plasma Studies* edited by B. Grandal, Plenum, New York, pp. 3-33, 1982.
- Winckler, J.R. *et al.*, Ion resonances and ELF wave production by an electron beam injected into the ionosphere: Echo 6, *J. Geophys. Res.*, **89**, 7565-7571, 1984.
- Winckler, J.R., Y. Abe, and K.N. Erickson, ELF waves and ion resonances produced by an electron beam emitting rocket in the ionosphere, in *Ion Acceleration in the Magnetosphere and Ionosphere*, edited by T. Chang, pp. 191-200, American Geophysical Union, Washington, Geophysical Monograph No. 38, 1986.

## 4. RELATIVISTIC ELECTRON BEAMS

### 4.1. Introduction

Previous experiments with electron beams in space have been limited by practical considerations to relatively low particle energies: To the best of our knowledge the maximum electron energy yet used in a conventional space experiment is of the order of 40 keV. The motivation for the present study has come from a realization that linac electron accelerators have reached a state of technology permitting relatively small units to be mounted in payloads suitable for research rockets and/or the Space Shuttle. Thus, it is now worth considering the full range of consequences of using such a beam for a variety of purposes, including the creating of plasma density irregularities in the lower ionosphere and the probing of electrodynamic regions of the middle atmosphere.

In the following sections we describe the possible consequences of operating a moderately powerful ( $\sim 5$  MW), relativistic ( $\sim 5$  MeV) electron accelerator from a satellite or rocket platform. In such an experiment, a beam of relativistic electrons fired downwards from space will create, by means of electron impact ionization, an ionized column whose length and cross sectional area will be set by electron energy loss and scattering. As discussed later, owing to the relatively small cross section for electron interaction with matter at relativistic energies, a single pulse from such a beam will penetrate to the lower mesosphere and upper stratosphere, creating a dense column of free electrons and positive ions. At high altitudes this structure remains relatively static, decaying only slowly under the influence of recombination. At low altitudes, however, the electrons are rapidly lost via attachment reactions with  $O_2$  to form  $O_2^-$ . While the column is composed largely of free electrons, it can scatter electromagnetic radiation and, surprisingly, may even initiate an intense upward traveling electrical discharge similar to lightning.

Before passing to the calculations of beam interactions, however, it is informative to compare the ionizing effects of electrons and photons. Generally speaking, electrons in the energy range 1 to 5 MeV have appreciably smaller interaction cross sections with matter than easily obtainable EUV photons or X-rays. Even hard X-rays, for which

there are as yet no convenient space payload sources, only penetrate to the altitude range of 50 to 60 km. Thus, if there is a need to produce appreciable ionization as deep as the upper stratosphere, relativistic electrons are the logical choice.

Another factor relates to the net energy flux carried by electron beams. Unlike high energy photon sources, which have a generally broad beam divergence and accompanying  $r^{-2}$  energy diminuation with distance from the source, electron beams are constrained to remain geometrically confined, varying in intensity only in response to changes in the strength of the magnetic field and transverse spreading associated with scattering by atmospheric particles. Thus, it can be expected that a relativistic electron beam, if injected at a small pitch angle with respect to the magnetic field, will remain confined until it has lost a substantial fraction of its initial kinetic energy. Furthermore, a surprisingly large fraction ( $\sim 20\%$ ) of the initial beam energy will be expended in producing atmospheric ionization along the path of the beam.

In the following sections we describe the physical processes which accompany the firing of a pulsed relativistic electron beam downwards along a magnetic field line into the middle atmosphere. Consideration is given to the resulting altitude profile of ionization, the conversion of the initial atmospheric positive ions and free electrons into an end product state of positive ions, electrons, and negative ions, and the possibility that the resulting beam column of ionization may lead to a high voltage breakdown condition mimicking, to some extent, natural lightning.

## 4.2. Ionization Column Dynamics

### 4.2.1. Ionization Production Rates

Consider a relativistic electron beam of current  $I$  composed of monoenergetic electrons of velocity  $v$  fired parallel to the local magnetic field. We assume that the beam emerges from an aperture of area  $A_s$  and expands slowly with distance along the magnetic field such that the area of the beam is  $A_r$  at a distance  $r$  from the source. The beam current is assumed to be pulsed at the source with an on period of  $t$  seconds each pulsing cycle. As the beam travels downwards along the magnetic field, ionization is produced through electron impact.

Following the treatment of *Evans* [1955], the number of ionization pairs per unit path length in air at STP produced for each incident electron is approximated by the ionization formula

$$\frac{dN}{ds} \cong \frac{45 \text{ ion pairs}}{\beta^2 \text{ air - cm}} \quad (4.1)$$

where  $s$  is measured along the local magnetic field and  $\beta = V/c$  is the ratio of particle velocity to the speed of light,  $c$ . Equations of greater detail also exist and are extensively discussed in Appendix A.

As the electron beam moves downwards into the atmosphere, each electron of the beam will gradually lose kinetic energy as a consequence of inelastic collisions with the atmospheric gases. This effect is shown in Figure 4.1, and is based on Appendix A equations. The figure gives the average energy per particle of the incident beam as a function of altitude. For altitudes down to about 70 km there is little energy loss. Below this point, however, the exponentially increasing density of the atmosphere, coupled with the rise of energy loss rate with decreasing electron energy, dictates a progressively greater decrease in beam particle energy. By the time that the beam has reached 40 km, virtually all of the original beam energy has been deposited in the atmosphere.

Using the results of Appendix A, it is possible to compute the local rate of energy loss per unit distance of beam travel as a function of altitude. The typical profile of energy deposition is shown here as Figure 4.2. The interesting result is that the rate of energy deposition is generally proportional to the neutral gas concentration and that a large amount of energy is deposited in the atmosphere at the end of the beam penetration. This arises because of the large increase in beam energy loss rate at low electron energies. The consequence is that there can be a substantial increase in local electron density in the terminus zone of beam penetration. This general effect is discussed in more detail following a discussion of the effects of beam scattering.

For a beam of current,  $I$ , and projected area,  $A_s$ , normal to the magnetic field, the local rate of production of electrons and ions per  $\text{cm}^3$  per second,  $p$ , is given by

the expression

$$p = \frac{45}{\beta^2} \left( \frac{I}{eA_s} \right) \left( \frac{n}{n_0} \right) \text{ cm}^{-3} \text{ sec}^{-1} \quad (4.2)$$

where  $n$  is the neutral gas concentration at the observation point and  $n_0$  is the concentration of the atmosphere at STP ( $n_0 = 2.67 \times 10^{19} \text{ molecules cm}^{-3}$ ).

Knowledge of the area,  $A_s$ , of the beam at any point in the trajectory is an important part of calculating the local ionization production rate. As individual electrons pass through matter, minute deflections occur as a consequence of Coulomb interactions with atmospheric atoms and molecules. These angular deflections are equivalent to the introduction of perpendicular (to the local magnetic field) velocity to the beam electrons so that after many kilometers of travel there can be appreciable spread of the beam in pitch angle. This effect spreads the total ionization production over a significant area, lowering the local enhancement of the electron and ion density.

There is extensive knowledge of electron scattering in various materials, including air; e.g., *ICRU# 35* [1984]. Using standard approaches, it is even possible to compute the angular scatter effects of low density materials where perpendicular transit is an important part of the final beam area distribution. However, up to the present time we have been unable to discover any method which adequately takes into account the confining effect of a magnetic field on a strongly peaked (energy and angle) electron beam. Figure 4.3 illustrates this situation by following the trajectory of a single electron. As it leaves the source the electron initially travels directly down the magnetic field. At some point, however, it suffers a scattering collision which changes its pitch angle. Such scattering interactions continue with increasing frequency until the electron has lost all of its initial energy. As a consequence of the accumulated angular scattering, the electron may be substantially deflected in a lateral direction with respect to the original magnetic field line trajectory. This behavior is indicated in Figure 4.3 by showing hypothetical scattering collisions and the envelope of an electron's helical motion.

In this situation, we find that the traditional calculations of electron beam spreading are incorrect since they ignore the confining effects of the geomagnetic field. *Walt*



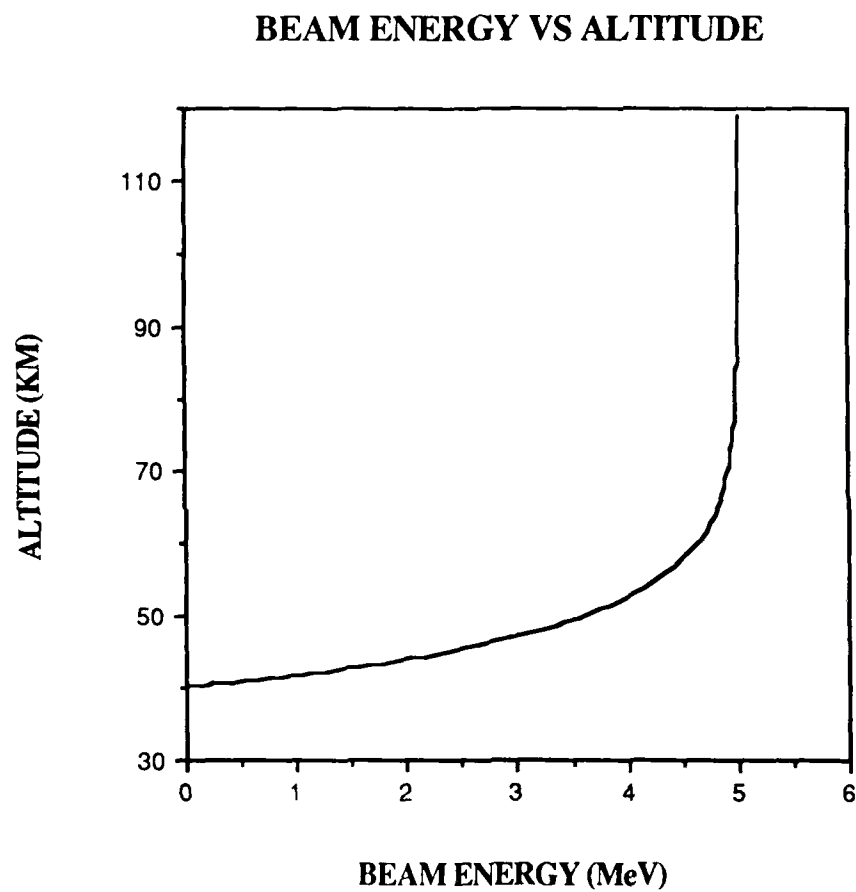


**Figure 4.1.** Average energy per particle of a 5 MeV electron beam penetrating vertically into the middle atmosphere. Details of the calculation are given in Appendix A.

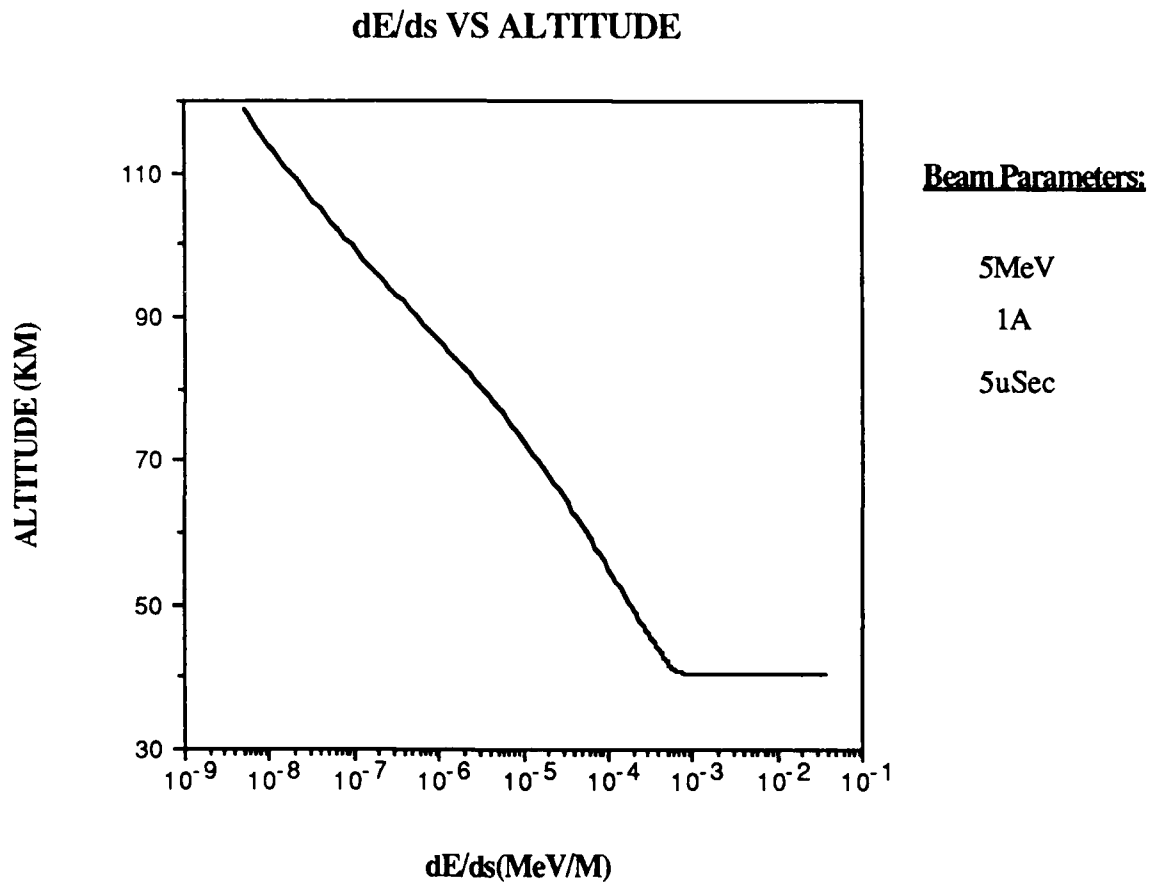


**Figure 4.2.** Relativistic electron beam energy loss rate shown as a function of altitude in the middle atmosphere. The peak deposition at the end of the path is due to the rapid rise in energy loss which occurs at low electron energies. Details of the calculation are given in Appendix A.

*et al.* [1967] have attacked this problem for the case of a non-peaked relativistic electron beam, and they derived analytic expressions for the ionization rate as a function of altitude, but the results may not be accurate for the case at hand.

Calculations for the highly peaked distributions considered here could be made in a guiding center formalism which would take into account the gradual outward diffusion of electrons resulting from scattering. However, this new work has not been practical within the limits of the present study. Instead, we use three approximations to the electron beam area: An area which corresponds to no scattering by the atmosphere ( $A_s = \pi/4 \text{ m}^2$ ), an area which corresponds to the gyroradius of the relativistic electrons at the energy of the source ( $A_s = 600^2 \pi \text{ m}^2$ ), and the full scattering predicted from non-magnetic, conventional scattering equations ( $A_s = 10^8 \text{ m}^2$  at 50 km altitude). In addition, we simply assume that at the very end of the beam penetration there is a substantial spatial blooming of the beam as scattering assumes great importance in the last few kilometers of beam travel.

The result of these assumptions is to give the model of the region of electron beam ionization enhancement shown in Figure 4.4. The overall shape of the ionization region produced by the beam can be compared with that of a mushroom anchor: A long, increasingly thick column of ionization eventually meets a thick, radially broad cap, a consequence of electron scattering.

We now return to quantitative calculations. Using the energy loss rate, altitude profiles of the plasma produced by single pulses from an electron source can be made taking into account the full range of energy degradation process. Since charged particle recombination operates on time scales of many milliseconds, a beam pulsed with relatively short, microsecond bursts will give a net production of new ionization equal to the product of the local production rate and the beam on time. The newly introduced charged particles then decay according to recombination and other ionic and electronic reactions with the gases of the middle atmosphere.

Figure 4.5 shows ionization production rate as a function of altitude calculated for a 1 A, 5 MeV electron beam pulsed on for 5  $\mu$ seconds with different assumptions about the beam area. The production is proportional to the neutral gas number

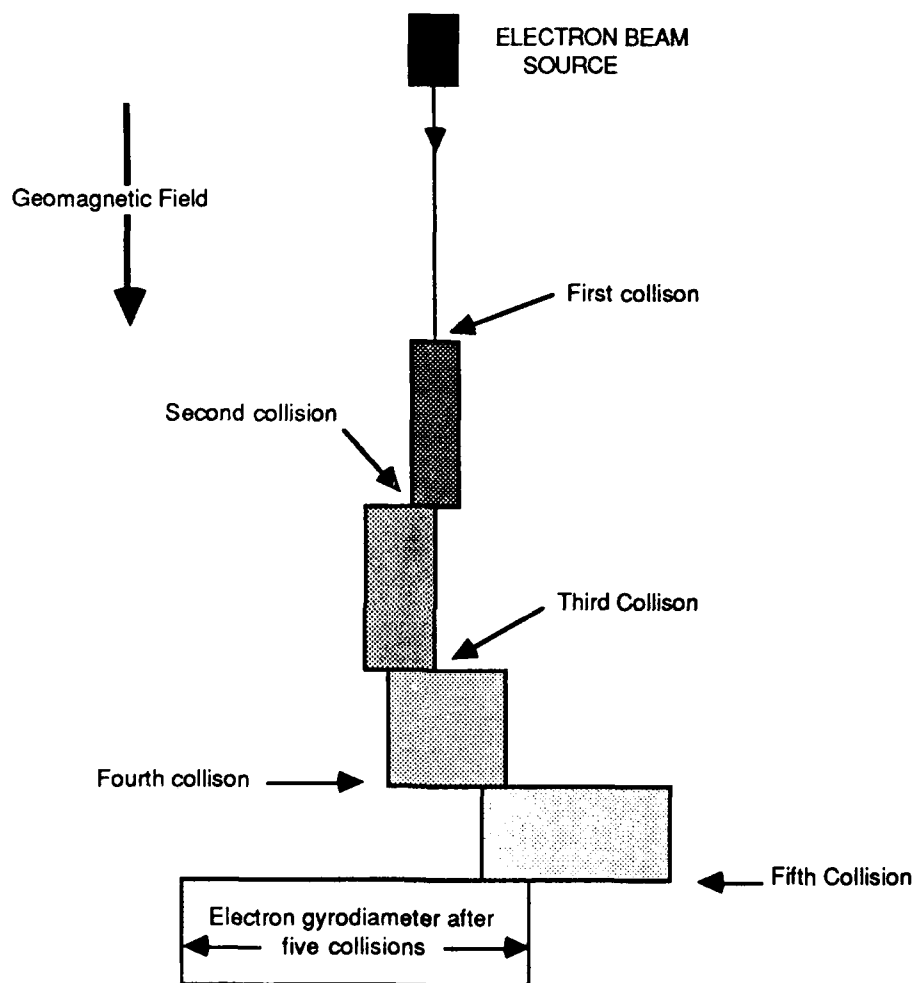


**Figure 4.3.** Schematic view of the effects of small angle scattering on the pitch angle and lateral deflection of an energetic electron initially moving parallel to the local magnetic field. Each collision enlarges the gyroradius of the electron motion. Since each collision occurs at a random point within the gyrating trajectory, such collisions can give a lateral deflection of the particle which is limited by the intrinsic scale size of the full gyroradius of the electron.

density for most of the path, but large ionization rates obtained near the end of the beam show where scattering is important with consequent large lateral dispersions.

The initial burst of new ionization from a relativistic electron beam can have a high "contrast" with respect to the pre-existing, background plasma. Figure 4.6 shows typical day and night electron densities for the middle atmospheric regions. Also included is the new density calculated above for a single 5  $\mu$ second burst. It can be seen that the beam-associated ionization can be much larger than the ambient ionization for altitudes depending on the particular beam cross sectional area.

More complete analyses of electron beam penetration must take into account beam divergence arising from the finite range of pitch angles at the beam source, the confining feature of the magnetic field, and the important effects of electron scattering which accompany traversal through the atmosphere. A description of these is given in Appendix A, which provides the basis for the ionization production rate discussion of this section.

#### 4.2.2. Plasma Chemistry

The initial ionization created by the pulsed electron beam consists of positive atmospheric ions ( $O_2^+$ ,  $N_2^+$ ) and free secondary electrons. Once created, the positive ions will undergo reactions with the ambient gases of the atmosphere, resulting in a variety of final positive ion products which can be computed using atmosphere chemistry codes. Typically, large cluster positive ions will begin to form in competition with dissociative recombination, a process which is rapid at the high plasma densities of the narrower models of the ionization column.

The secondary electrons, in contrast, undergo two more stages of activity. First, those having significant energies will have subsequent additional energy losses, including optical excitation and impact ionization of atmospheric gases. Electrons of lower energy will cool to atmospheric temperature by means of various inelastic collisions with atmospheric gases and, thereby, become part of the background D-region and upper stratospheric plasma.

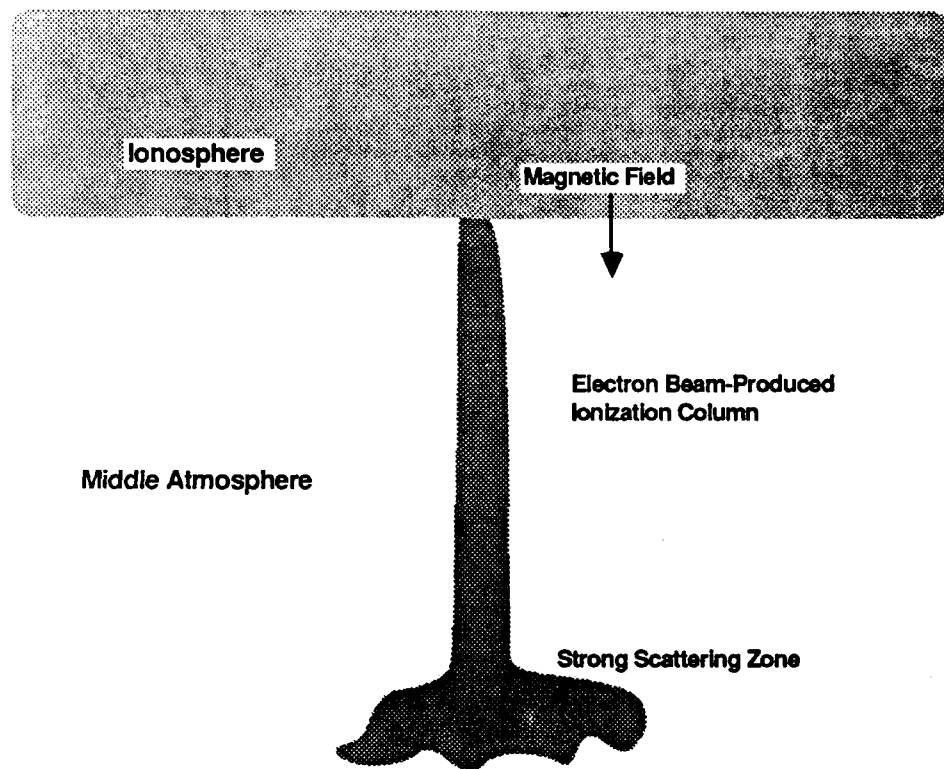


**Figure 4.4.** Illustrating the penetration of the electron beam into the middle atmosphere. The plasma density of the beam-produced ionization column will be much greater than the ambient ionospheric density. In addition, owing to strong scattering at the end of the trajectory, we expect a substantial "blooming" of the ionization structure. It is assumed that the beam is launched parallel to the local magnetic field.

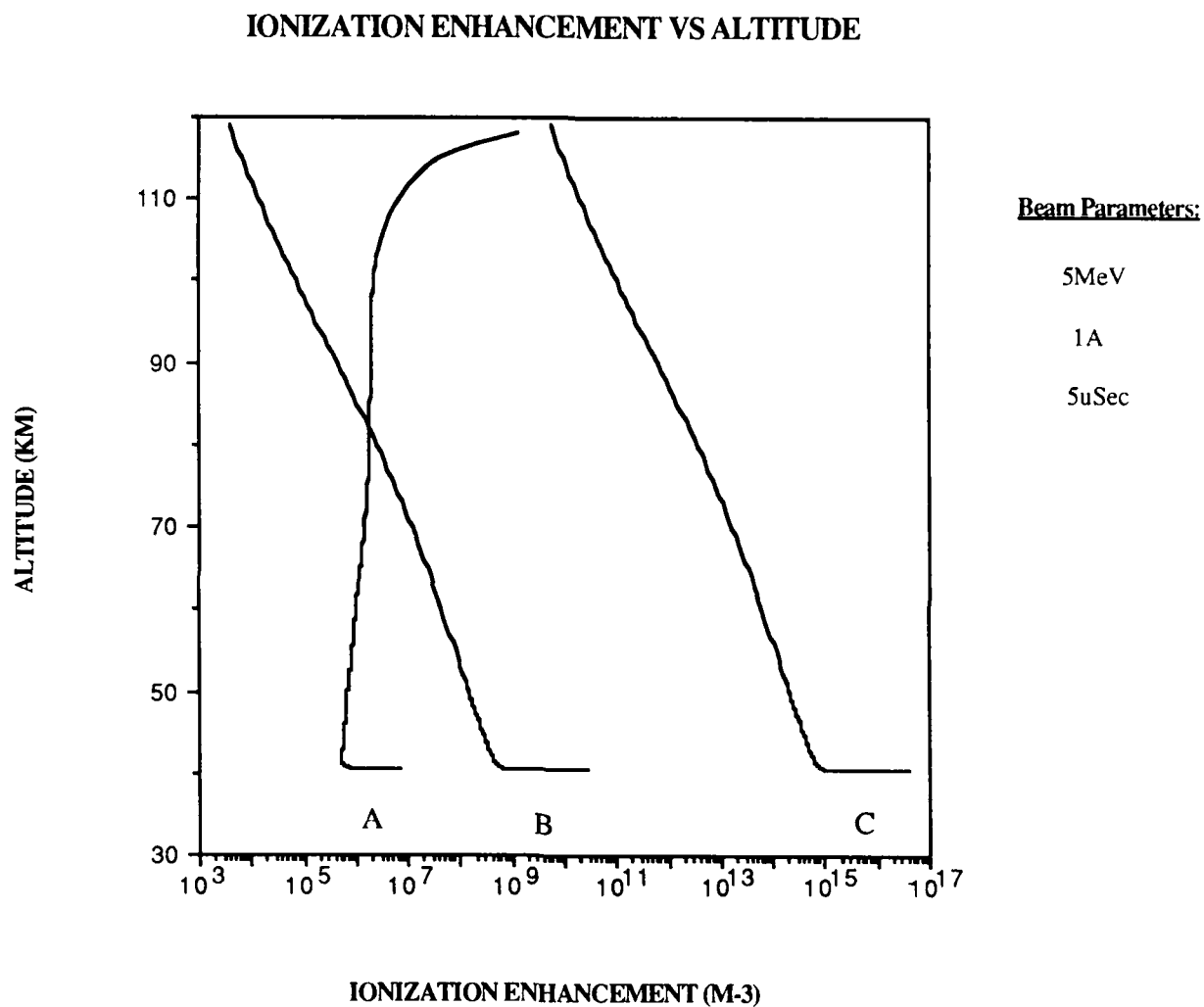


**Figure 4.5.** Ionization production as a function of altitude for 5  $\mu$ second, 5 MeV, 1 A, electron beam for three different beam cross sections. Contour A is for a variable beam cross section due to atmospheric scattering without a magnetic field. Curve B and C assumes constant cross section radii of 602 and 0.5 meters, respectively. The 602 radius represents the relativistic gyroradius of a 5 MeV beam.

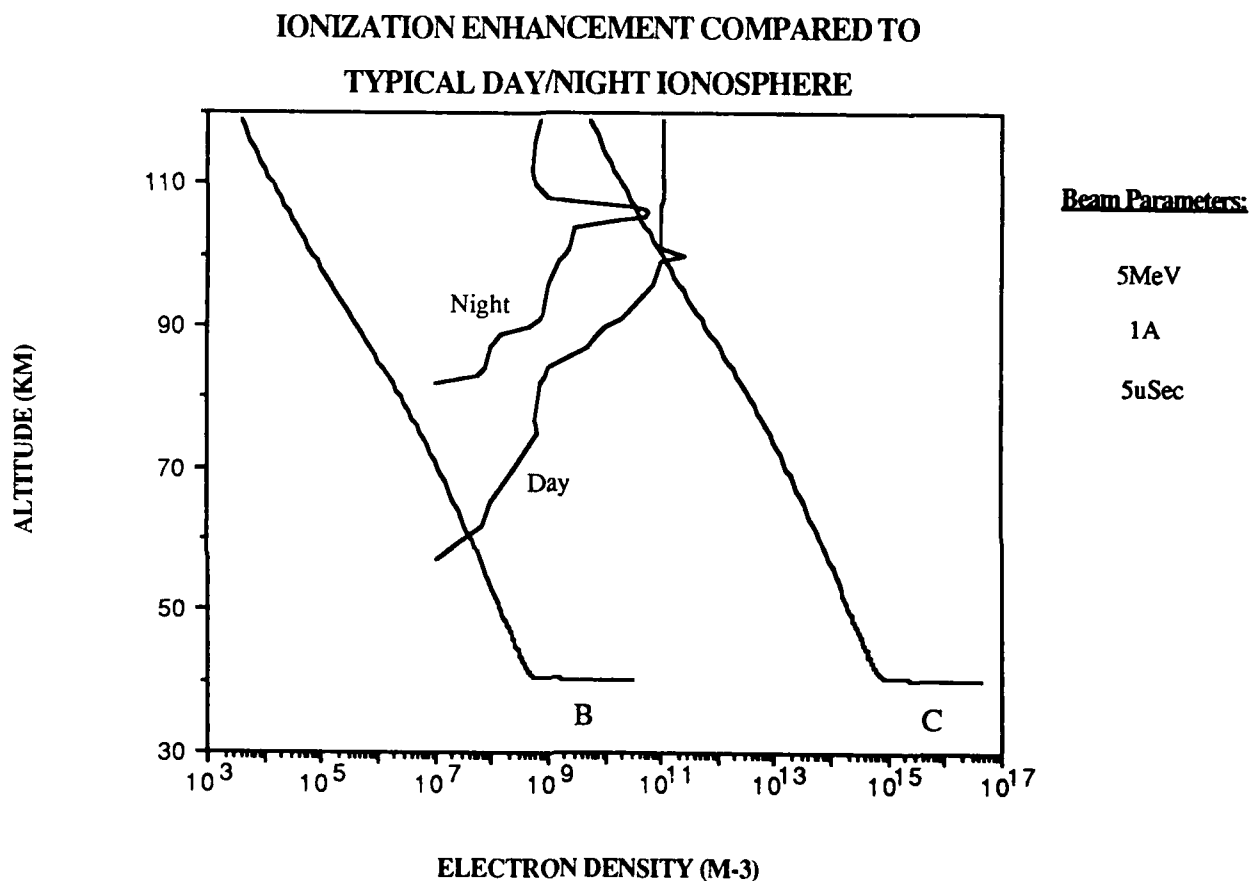


**Figure 4.6.** Comparison of initial ionization enhancement produced per unit value with the average ambient density of the E- and D-regions for day and night conditions. Curves B and C are defined in Figure 4.5.



Since it is the electrons which interact most strongly with electromagnetic radiation, it is important to understand the various processes which affect their density decay. On the one hand, recombination with ions occurs at a certain rate in proportion to the ion concentration. The time constant for this is set by the dissociative recombination coefficient,  $\alpha$ , and the density of ambient ions. A useful expression for the time constant for dissociative recombination is given by

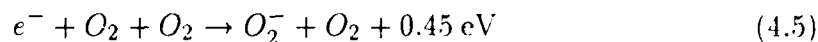
$$\tau_D = \frac{1}{\alpha_D n_e} \quad (4.3)$$

where

$$\alpha_D = 3 \times 10^{-7} \left( \frac{300}{T} \right)^{\frac{1}{3}} \text{cm}^3 \text{sec}^{-1} \quad (4.4)$$

and,  $T$ , is the electron temperature. Typical plasma densities of  $10^4$  to  $10^6 \text{ cm}^{-3}$  within the beam-produced ionization column give recombination decay times of seconds or more.

A more important loss process for cold electrons is attachment to neutral  $O_2$  to form  $O_2^-$  ions. This three-body reaction progresses according to the reaction



which has a rate coefficient [Banks *et al.*, 1973] given by

$$k = 1.5 \times 10^{-29} \left( \frac{300}{T} \right) e^{-600/T} n^2(O_2) \text{ sec}^{-1} \quad (4.6)$$

where  $T$  is the temperature of the background neutral atmosphere and  $n(O_2)$  is the molecular oxygen density. Calculations show that such attachment of free electrons becomes a very important process below about 70 km altitude in the mesosphere. As shown below, it is the primary limitation on the lifetime of free electron densities arising from the relativistic electron beam experiment.

To understand this effect, we must consider the overall balance between electrons and  $O_2^-$  ions. While electron attachment removes the free electrons, there are several

reactions serving to liberate them, including photodetachment (in sunlight) and reactions of  $O_2^-$  with  $O_3$  and  $O$ . For the present models, it seems reasonable to ignore these last two reactions: The  $O$  and  $O_3$  densities are sufficiently low in the regions between 40 km and 70 km for their detachment reactions with  $O_2^-$  to be ignored. Thus, to model the time-dependent electron density in the beam column, we can approximate the real situation by considering only electron attachment to  $O_2$  and photodetachment in sunlight.

The photodetachment of electrons from  $O_2^-$  is expressed as:



where  $J = 0.3 \text{ sec}^{-1}$  at zero optical depth [Banks *et al.*, 1973].

Competition between electron attachment and photodetachment can be studied by a simple time dependent model of ionization loss which ignores recombination. If there is an initial electron density,  $N_0$ , at time  $t = 0$ , the electron density at a later time is given by the expression

$$\frac{n_e}{N_0} = [1 - \tau k(1 - e^{-t/\tau})] \quad (4.8)$$

where  $\tau$  is a time constant for reaching equilibrium conditions given by the expression

$$\tau = \frac{1}{(J + k)} \quad (4.9)$$

where  $k$  is the attachment rate for equation (5) and  $J$  is the zero optical depth photodetachment rate for  $O_2^-$ . Values of this time constant as a function of altitude are given in Table 1.

Figure 4.7 shows the time history of the equilibrium ratio of electron density to initial ion density,  $\gamma$ , at several altitudes. It is clear that at low altitudes even in daylight, electrons will quickly be transformed to negative ions.

From the foregoing we can conclude that an appreciable concentration of free electrons can be created by an initial pulse of relativistic electrons. However, these

**Table 1**  
**Electron-Negative Ion Equilibrium Time Constant**

| Height (km) | Time Constant (sec)  |
|-------------|----------------------|
| 30          | $1.2 \times 10^{-4}$ |
| 40          | $1.9 \times 10^{-3}$ |
| 50          | $2.3 \times 10^{-2}$ |
| 60          | $2.5 \times 10^{-1}$ |
| 70          | $1.9 \times 10^0$    |
| 80          | $3.3 \times 10^0$    |

will disappear by two major processes: Attachment with  $O_2$  and, at a slower pace, by recombination with positive ions. At altitudes above 70 km the lifetime of the electrons is long, measured in terms of seconds. Below 70 km, attachment becomes increasingly important, such that at altitudes of 50 km free electron lifetimes are measured in terms of milliseconds, even in daytime.

#### 4.3. Electrodynamics of an Ionization Column in the Middle Atmosphere

It is well known that the middle atmosphere plays an active part in global electrodynamics, serving as a conducting medium for the spatially dispersed currents arising from thunderstorm activity throughout the world. Although the largest values for the atmospheric electric fields are found within the troposphere near the earth's surface, *in situ* observations indicate that substantial potential drops are still possible in the upper stratosphere and mesosphere. Using several different measuring methods, *Maynard* and *Hale* and their co-workers have found, on occasion, electric fields on the order of volts per meter in the D-region, implying that there may be total potential drops on the order of 10's of kilovolts over distances of 10's of kilometers [*Maynard et al.*, 1981; *Hale et al.*, 1981].

Within the context of the present study it is appropriate to investigate the interactions might occur between a transient, highly conducting ionization column and ambient electric fields of the middle atmosphere. This is done in the following way.

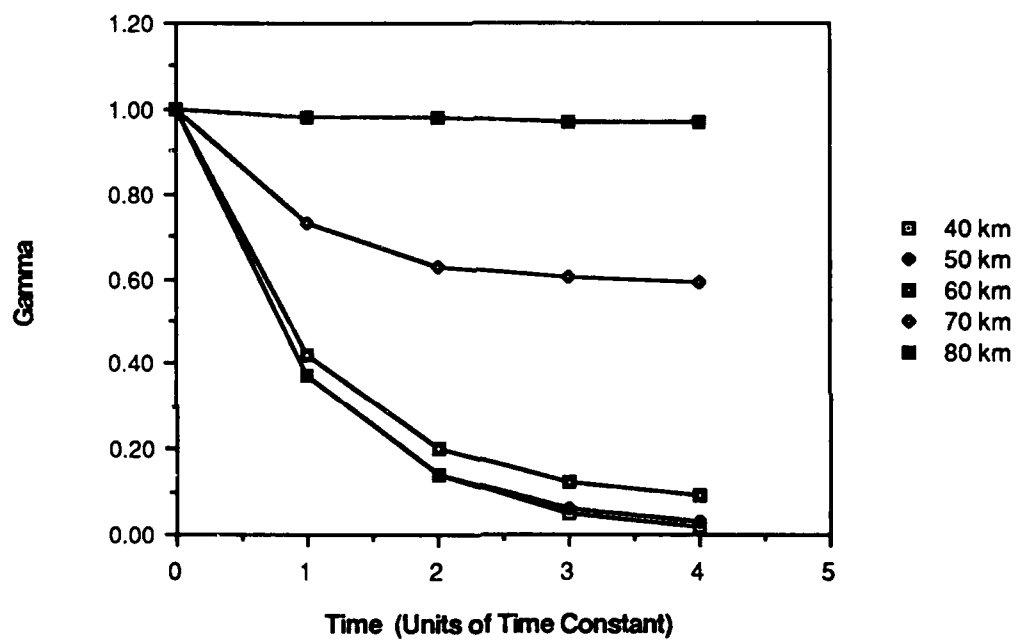


Figure 4.7. Showing the ratio of equilibrium electron to initial ion density,  $\gamma$ , as a function of altitude. These results demonstrate the idea that free electrons are rapidly converted to negative ions at low altitudes.

First, we assume that the ionization column is produced instantaneously with a certain altitude profile of electron density and beam area. Next, under the action of the existing atmospheric electric fields, currents will be established in the column, leading it to charge at a certain rate to the potential of the highly conducting ionosphere lying above. At each point along the column the potential difference between the column and the surrounding atmosphere will also rise. At some point it may be the case that the associated electric fields are sufficiently large to accelerate ambient and ionization column electrons to sufficiently large energies to cause additional ionization; i.e., breakdown will occur. In this situation, a discharge would be initiated with the possibility of subsequent large currents occurring in the ambient medium and the conducting ionization column. Such a discharge, the equivalent of lightning, would continue until the ionization column-associated electric field is reduced below the breakdown level of the atmosphere.

To proceed, we first compute the resistivity and charging time of the beam-produced ionization column. This time is shown, for typical parameters, to be somewhat less than the time for loss of the electrons due to attachment. Next, a computation is made of the breakdown electric field for conditions within the middle atmosphere. Using a model for the distribution of electric potential along the ionization column and typical values of middle atmosphere electric fields, it is shown that it is likely that some portion of the ionization column will establish electric fields which exceed the threshold for breakdown. This then leads to a discussion of subsequent effects which are important to the magnitude and duration of the discharge current.

#### *4.3.1. Resistance and Charging of the Ionization Column.*

We consider a simple model where the ambient electric field,  $E$ , is parallel to the vertical ionization column.

When the ionization column is created, current will pass along it at a magnitude set by the resistivity of the column and the magnitude of the external electric field. Owing to its high conductivity, however, the interior electric field will quickly

change, introducing a net potential difference between the column and the exterior atmosphere. If the column were perfectly conducting, it would achieve the same, uniform potential as the ionosphere. Figure 4.8 illustrates this situation in terms of equipotential contours in the vicinity of the column. Owing to the high electrical conductivity of the column, the local contours of electrostatic potential are altered, producing large potential gradients in the vicinity of the column.

To begin the computation of the resistivity of the ionization column, the relationship between the local current density,  $j$ , and the local electric field,  $E$ , is given by

$$j = \sigma E \quad (4.10)$$

where  $\sigma$  is the ordinary Pedersen conductivity of the ionospheric medium. If we then assume that a current  $I$  passes through an area  $A$  of the column, we have

$$I = (\sigma A)E \quad (4.11)$$

Next, we adopt the standard expression for the conductivity:

$$\sigma = \frac{n_e e^2}{m_e \nu_{en}} \quad (4.12)$$

where  $n_e$  is the ambient electron density,  $\nu_{en}$  is the electron-neutral collision frequency,  $m_e$  is the electron mass, and  $e$  is the magnitude of the electron charge.

Further progress can be made by noting that the electron-neutral collision frequency and the initial electron density are both proportional to the neutral gas density. Thus, if we normalize our results to the values of initial electron density and collision frequency at some reference altitude, we can write the relation between column current and electric field as

$$I = \left[ \frac{n_e^0 e^2 A}{m_e \nu_{en}^0} \right] E \quad (4.13)$$

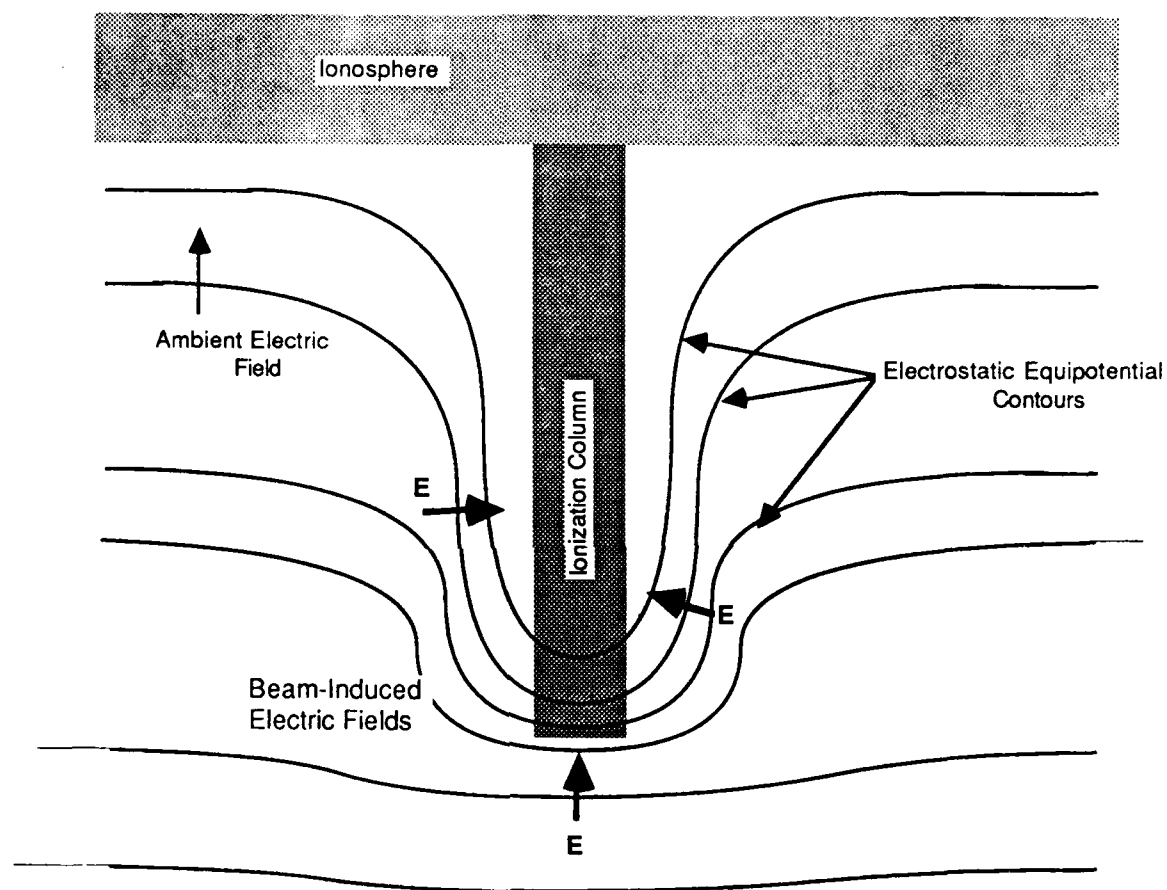


**Figure 4.8.** Electrostatic effect of introducing a conducting plasma column into the ambient middle atmosphere. It is assumed here that the ambient electric field is uniform and vertical. Note the large electric fields which surround the region near the surface of the ionization column.

To obtain the resistivity of a column of length  $L$ , we note that if there is a voltage  $V$  present over a distance  $L$ , Eqn. (4.13) becomes

$$V = \left[ \frac{m_e \nu_{en}^0 L}{n_e^0 e^2 A} \right] I \quad (4.14)$$

so that the column resistance per unit length,  $r$ , can be written as

$$r = \frac{m_e \nu_{en}^0 L}{n_e^0 e^2 A} \quad (4.15)$$

Values for the collision frequency can be obtained from the CIRA reference atmosphere. Normalizing to 50 km altitude, using these values and the electron density from Figure 4.5 gives a resistance per unit length of

$$r = 35 \, \Omega \text{m}^{-1}. \quad (4.16)$$

or, for a total length of, say, 40 km, a total column resistance of 1.4 M $\Omega$ .

From this, we find that the resistance of the ionization column is substantial and that a potential drop of about 20 kV will result in a current of tens of milliamperes. In this situation, the time constant for charging of the column does not follow from the usual transmission line equations of electrical charging: They apply only to cases where the resistance per unit length is a small part of the line impedance provided by the capacitance and inductance per unit length. In this instance another approach is needed, and this is discussed in Appendix B in terms of a diffusion-controlled electric field. The result applicable to the present circumstances is that the time constant,  $\tau_c$ , for the beam column charging can be approximated by the expression

$$\tau_c \simeq \frac{\nu_{en}}{\omega_p^2} \quad (4.17)$$

where  $\nu_{en}$  is the electron-neutral collision frequency and  $\omega_p$  is the plasma frequency. For the situation outlined here, the time constant for charging of the column is on the order of 10's of  $\mu$ seconds. Thus, as seen from an attachment time scale of 10's



of milliseconds, the ionization column rises to the ionospheric potential very quickly, leading to the electrical model shown in Figure 4.8.

As a consequence of these calculations, we see that not only does the electron beam pulse create a channel of highly conductive plasma, albeit for a relatively short time of 10's of milliseconds at low altitudes, but also that the ambient electric fields of the middle atmosphere will drive current within this structure, bringing it quickly (on time scales of 10's of  $\mu$ seconds) to the potential of the overlying ionosphere.

#### 4.3.2. *Electric Discharge of the Beam Column*

As the potential of the beam column rises with respect to the background, an electric field is generated within the surrounding medium. This situation was illustrated in Figure 4.8, where we showed the equipotential contours of the middle atmosphere as they have responded to the increasing potential of the beam-induced plasma column. The concentration of potential contours near the lower tip of the column indicates the increasing electric field there, and opens the question of the possibility of creating the conditions necessary for an electrical discharge.

To resolve this possibility, two separate issues must be investigated: (1) The magnitude of the breakdown electric field in the middle atmosphere, and (2) the magnitude of the electric field in the vicinity of the beam structure. Each of these is presented in the following sections.

*a. The Breakdown Electric Field.* Electrical breakdown occurs in a partially ionized gas when the local electric field is sufficiently large to accelerate ambient electrons to ionizing energies, typically of the order of 15 eV. The tendency of electric field accelerated electrons to rise in energy towards breakdown energies is opposed by electron collisions with the ambient neutral gas: In each energetic electron-neutral collision the energy imparted to the electron by the electric field is largely lost. The problem in its simplest form, then, is to compute the energy of an individual electron under combined effects of the accelerating electric field and the momentum lost in electron-neutral collisions. In fact, more accurate theories of breakdown would include the distribution of velocities of the electrons, and the fact that it is the high

energy portions of the electron velocity distribution function that lead to the initial avalanche ionizations that result in electrical breakdown. However, for this discussion, the simple model of breakdown is probably sufficiently accurate to indicate the magnitudes of fields needed.

We wish to compute the energy acquired by an electron between collisions with neutral gas particles. If there is an ambient electric field of magnitude  $E$ , the velocity,  $v$ , after a time,  $t$ , has elapsed since the last collision is

$$v = \left( \frac{eEt}{m_e} \right) \quad (4.18)$$

where  $e$  is the magnitude of electron charge and  $m_e$  is the electron mass. The electron energy,  $\epsilon$ , then follows as

$$\epsilon = \frac{1}{2} m_e \left( \frac{eE}{m_e} \right)^2 t^2 \quad (4.19)$$

If  $\nu_{en}$  is the collision frequency for electron-neutral gas collisions, the time,  $T$ , between collisions is  $T = 1/\nu_{en}$  and the relation between electron energy and collision frequency becomes

$$\epsilon = \frac{e^2 E^2}{2m_e \nu_{en}^2} \quad (4.20)$$

If we adopt a value of 10 eV as the mean energy of the electron gas to acquire between collisions to initiate the ionizations necessary for breakdown, we arrive at the desired relation between breakdown electric field,  $E_b$ , and the collision frequency between electrons and neutrals:

$$E_b \cong \frac{1.1 \times 10^{-5}}{\nu_{en}} \quad (\text{volt m}^{-1}) \quad (4.21)$$

Figure 4.9 plots values of  $E_b$  as a function of altitude in the middle atmosphere. The results indicate that relatively small fields of 100 to 1000 V/m will initiate electrical discharge in the regions between 50 km and 70 km altitude, the zone of principal interest in this study.

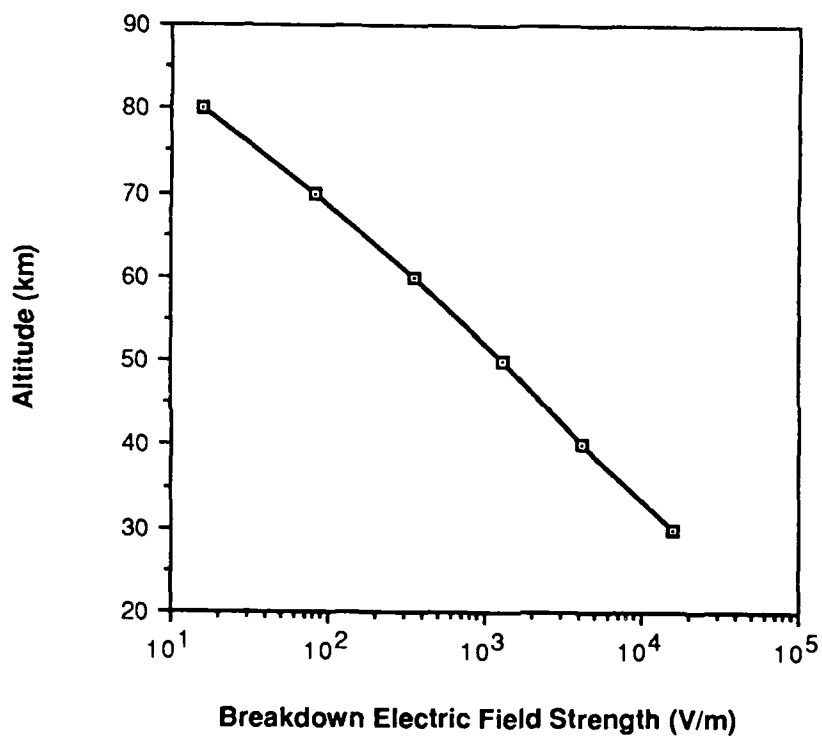


**Figure 4.9.** Showing the d.c. breakdown electric field strength as a function of altitude in the middle atmosphere.

*b. Electric Fields Near the Plasma Column.* Figure 4.8 shows the general situation of electric equipotential contours near the beam column. Up to this point we have assumed that the beam has a geometry set by the initial pulse of high energy electrons: i.e., that a long, thin structure is created with the diameter set by atmospheric scattering. Furthermore, we have been able to show that this plasma structure will rapidly charge itself towards the potential of the overlying ionosphere, yielding progressively larger radial potential differences between the plasma column and the ambient ionosphere as one progresses downwards. Now, however, a difficult problem arises; namely, how to estimate the local electric field. If the potential changes rapidly with distance, then a large electric field will be present and the conditions required for electrical breakdown may be present. If, on the other hand, the potential is distributed over a large radial distance, only weak fields will occur and no cataclysmic effects can be expected.

The core structure of the ionization column is determined by atmospheric scattering. In the absence of accurate numerical results in the literature, we have estimated that the beam will achieve a diameter which is much larger than the source area,  $A_s$ , but substantially less than one gyrodiameter (600 meters for a 3.5 MeV electron). In fact, the column will not be uniform in radial dimension. Consequently, the potential of the core of the beam will be higher than even the outside edges, indicating that the correct calculation for the distribution of electric potential must include not only the time-dependent effects, but also the dimensionality of the electron distribution in the radial direction. This difficult task lies beyond the scope of the present report. Instead, we can indicate the possible values based on typical potentials and characteristic radii of the ionization column.

For example, if the core of the column has a diameter of 20 m, and if there is a 20 kV potential drop, then it might be possible to have a radial electric field of 1 kV/m within this extended zone. According to Figure 4.9, this would be sufficient to create breakdown above 50 km. On the other hand, if the diameter is 200 meters and the potential drop only 10 kV, then the radial electric field will be on the order of 50 V/m, which is probably too low to meet the requirements for breakdown except

above 74 km altitude.

At this time, with our lack of knowledge about the actual distribution of electric fields in the middle atmosphere and the redistribution of fields which will accompany the establishment of a conducting column of ionization in the same region, we can't state categorically that electrical discharge is an inevitable consequence of the relativistic electron beam experiment. Part of this uncertainty can be removed by more thorough calculations of the electrodynamics of the column. But, in the face of poor information about the spatial and temporal variability of middle atmosphere electric fields, it will probably not be possible to have full confidence in the breakdown hypothesis: A suitable *in situ* experiment will be needed to test all of the complex factors.

#### 4.3.3. *Consequences of a Discharge.*

It is interesting to speculate what might happen if, indeed, it is possible to initiate an electrical breakdown at some point in the column. In this situation, we first expect that additional electrons will be liberated to carry current. This might occur through the formation of filaments or leaders which would extend away from the column into the surrounding gases. The subsequent rush of free electrons would produce an electromagnetic pulse whose principal frequencies would be determined by both the duration of the breakdown and any characteristic oscillations that might accompany the formation and decay of leaders in the gas.

The general effect of the discharge would be to transport electric charge along the column. With sufficient fields, such a discharge could conceivably extend the full length of the beam. Heating of the atmosphere would be a slight consequence, and optical emissions would provide a way of seeing the development of the discharge process.

The decay of the discharge would be determined by the change in local potential and electric fields. As the region of enhanced density grows in size, the potential drop will become spread out, lowering the electric field strength until it falls below that required for breakdown. However, since this threshold depends on altitude, a

complicated pattern of discharge might result, with prolonged discharge occurring at higher altitudes along the beam column. Countering this would be the diminuation of the local fields with altitude as one approaches the conducting regions of the D-layer.

#### 4.4. A Proposed Experiment

As stated at the begining of this section, current technology is available for a rocket-borne relativistic electron beam experiment. The goal of such an experiment should be to assess a variety of phenomena associated with firing a high energy beam into the atmosphere. These include: (1) The formation of a highly ionized column of ionization extending downwards to the upper stratosphere, (2) The formation of a large lateral cap of ionization at the end of the beam travel, as implied by Figure 4.4, (3) The time dependent decay of the free electrons in the column, (4) The possibility of creating a large scale electrical discharge in the middle atmosphere, and (5) Understanding the physics of the interaction of the energetic particles with the atmosphere, as seen in the geometry of the beam and the character of energetic particles reflected back into space.

The most suitable experiments would be done with the nighttime launch of a recoverable rocket payload at White Sands Missile Range. The rocket trajectory could be chosen to minimize the cross-magnetic field velocity, permitting the accelerator to fire many pulses into the same general region of the atmosphere. The payload would consist of the accelerator and various on-board detectors, including those related to measuring the performance of the pulsed beam, the electrical charging of the rocket, and high energy particle detectors capable of measuring the fast backscatter of electrons from the atmosphere. Other remote diagnostic devices could also be flown on the rocket to permit characterization of the ionization column, as seen from immediately above. These could be optical and UV detectors capable of seeing by-product radiation arising from beam interactions with the atmosphere and broadband radio receivers.

Coordinated ground observations would also be essential. Optical imagers would provide information about the geometry of the beam, while radars of various fre-

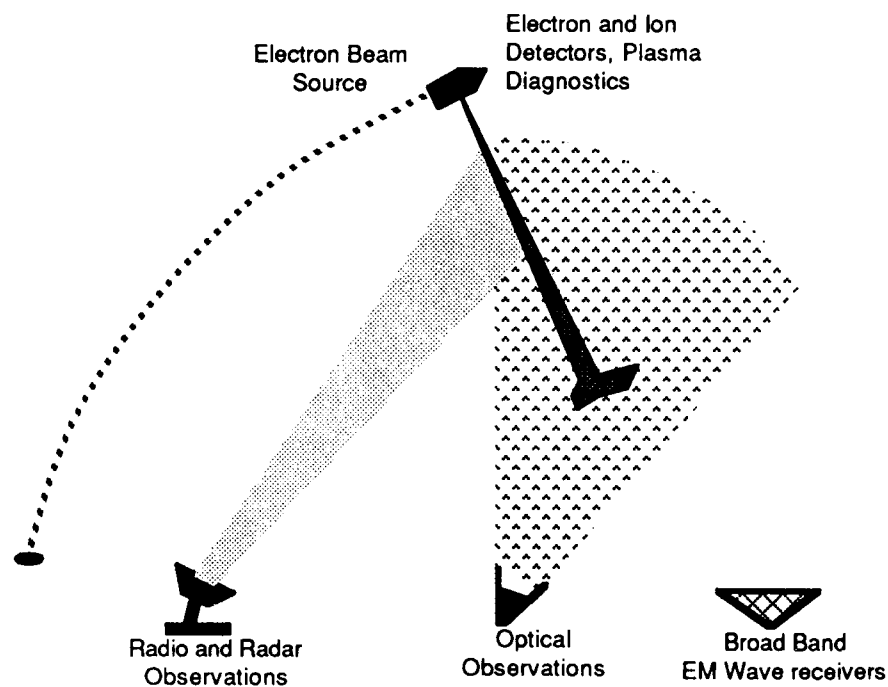


**Figure 4.10.** Illustrating the geometry of a relativistic electron beam rocket experiment. Ground sites provide optical, radar, and radio measurements of the beam characteristics, while diagnostics of the rocket measure vehicle charging, backscattered electron and ion fluxes, and image photon emission from the underlying ionization structure.

quencies could probe the extent to which the column ionization interacts with the incident radiation. Broad-band radio receivers would also help to assess the emission of any initial electromagnetic radiation (expected to be weak) and the possible stronger emissions following from an electrical discharge.

A schematic view of the experimental situation is given in Figure 4.10.

#### 4.5. Closing Remarks

There are many interesting features of relativistic electron beam experiments in space. Here, we have focused on problems relating to the interaction of the beam with the atmosphere to produce ionization enhancements. It is seen that the high energy of the beam electrons means that interaction with the middle atmosphere is possible, and that there are a number of subsidiary phenomena which may come into play. In the face of substantial theoretical uncertainties, firm understanding of the physical consequences will require an experimental program involving, at the least, several rocket flights with supporting ground and space observations. This should be done in connection with an extensive theoretical analysis of the important features of beam production, scattering, and electrodynamic consequences.

#### 4.6 References

- Banks, P. M., and G. Kocharts, *Aeronomy, Vol. A and B*, Academic Press, New York, 1973.
- Cospar International Reference Atmosphere (CIRA) - 1965, North-Holland Publishing, Amsterdam, 1965.
- Evans, Robley D., *The Atomic Nucleus*, McGraw-Hill, New York, 1955.
- Gilchrist, B. E., and L. G. Smith, Rocket Radio Measurement of Electron Density in the Nighttime Ionosphere, University of Illinois-Urbana, Aeronomy Report No. 85, 1979.
- Hale, L. C., C. L. Croskey, J. D. Mitchell. Measurements of middle-atmosphere electric fields and associated electrical conductivities, *Geophy. Res. Lett.*, 8(8), 927, August 1981.



- ICRU# 35, Radiation dosimetry: Electron beams with energies between 1 and 50 MeV, International Commission on Radiation Units and Measurement, Bethesda, MD, 15 September 1984.
- Maeda, K., Diffusion of auroral electrons in the atmosphere, NASA TN D-2612, 1965.
- Mahlum, B. N., Particle precipitation: Scattering and absorption, in *Cosmical Geophysics*, (Ed. A. Egeland, O. Holter, and A. Omholt), Universitetsforlaget, Oslo, Norway, p. 211, 1970.
- Maynard, N. C., C. L. Croskey, J. D. Mitchell, L. C. Hale, Measurement of volt/meter vertical electrical fields in the middle atmosphere, *Geophys. Res. Lett.*, 8(8), 923, August 1981.
- Rees, M. H., Auroral ionization and excitation by incident energetic electrons, *Planet. Space Sci.*, 11, 1209, 1963.
- Rossi, B., *High-Energy Particles*, Prentice-Hall, Englewood Cliff, NJ, 1952.
- Walt, Martin, W. M. MacDonald, and W. E. Franci, Penetration of auroral electrons into the atmosphere, in *Physics of the Magnetosphere*, (Ed. R. L. Carovillano, J. F. McClay, and R. R. Radoski), Reidel, Dordrecht, p. 534, 1967.
- Wedde, T., Internal Report E-162, Norwegian Defense Research Establishment, 1970.

#### 4.7. Appendix A

Calculations of predicted ionization for relativistic electron beams in the atmosphere can be divided into two specific areas. First, is the energy loss of the electron beam per unit length ( $dE/ds$ ) as it penetrates through the atmosphere. It is assumed that most of this beam energy loss is consumed in the process of impact ionization with the neutral background of the plasma. An immediate result of this calculation should be the penetration depth of the beam and also the ionization per unit length as a function of distance. The second area is the estimation of the lateral extent (perpendicular to B) of the primary beam resulting in an incident primary electron flux,  $\Phi(s)$ . Both sets of calculations are necessary to estimate the ionization densities that are to result for the relativistic electron beam.

Given the above, it is straightforward to estimate the ionization rate,  $q$ , at any given altitude as

$$q = \frac{dE}{ds} \frac{\Phi(s)}{\Delta\epsilon} \quad (A.1)$$

where  $\Delta\epsilon$  is the required average ionization energy with a value of 35eV used here [Banks *et al.*, 1973]. Assuming a short duration pulse, the value in Eq. A.1 can be multiplied by the on-time of the beam pulse to estimate the additional ionization or ionization enhancement that is created by the relativistic electron beam.

In the following, the two calculations will be discussed separately keeping in mind that both are necessary to provide the final predictions of electron densities as a function of penetration. The results presented are intended for use with relativistic beam energy levels up to approximately 5 MeV, although it may be satisfactory for some applications to extend up to the 10 MeV level.

##### 1. ENERGY LOSS AND IONIZATION RATE PER UNIT LENGTH, $dE/ds$

Atmospheric ionization and penetration of energetic electron beams in the non-relativistic range greater than 1 KeV can be straightforwardly calculated based on a variety of methods. For example, *Rees* [1963] used experimentally verified energy

distribution functions to calculate the penetration and ionization deposition versus altitude. These results are useful for first order calculations in the lower energy ranges (1-300 keV). For beam energies above about 0.5 MeV, where the electron kinetic energy is approximately equal to the electron rest mass, it is necessary to include relativistic effects in these calculations.

Both ionization and penetration calculations start by estimating the electron beam energy loss per unit path length and assuming that all of the energy loss goes into ionization at that altitude. A form of the Bethe equation that accounts for relativistic effects therefore can be used [Evans, 1955]

$$\frac{dE}{ds} = 4\pi r_o^2 \frac{m_o c^2}{\beta^2} N Z \left\{ \ln \left[ \beta \frac{E + m_o c^2}{I} \sqrt{\frac{E}{m_o c^2}} \right] - \frac{1}{2} \beta^2 \right\} \frac{\text{MeV}}{m} \quad (\text{A.2})$$

where

$E$  = incident electron beam kinetic energy (MeV)

$r_o$  = classical electron radius

$NZ$  = electrons/m<sup>3</sup>

$\beta^2 = \left(\frac{V}{c}\right)^2 = 1 - \left[\frac{E}{m_o c^2} + 1\right]^{-2}$

$m_o c^2 = 0.511 \text{ MeV}$

The original Bethe equation is basically a summary of detailed quantum mechanical calculations of soft collision energy loss between an energetic particle and bound electrons (by soft or conversely hard, we are referring to whether the struck electrons are initially considered bound or free). This was later extended to include relativistic effects. Although the Bethe equation is calculated assuming soft collisions only, it has been found to be an adequate first order estimate of total energy loss from both hard and soft collisions when it is extended to consider up to the maximum possible energy loss per collision of  $E/2$ . This has been done in Eq. A.2.

The use of Eq. A.2 to estimate  $dE/ds$  ignores contributions to energy loss from Bremsstrahlung radiation and straggling effects. However, for electron beam energies up through 10 MeV, radiative losses remain at least an order of magnitude lower [Evans]. Also ignored in Eq. A.2, is the effect of electron back-scattering, which

would decrease the incident flux at any given altitude but which would represent an additional ionizing electron flux contribution in the reverse direction. The effect from back-scattering is not expected to be significant except near the end of the electron beam path. Figure 4.2 shows the variation of  $dE/ds$  as a function of altitude for a 5 MeV beam, while Figure 4.1 shows the actual energy of the 5 MeV as it penetrates the atmosphere.

## 2. PRIMARY BEAM ELECTRON FLUX, $\phi(s)$

While the loss of electron beam energy, as the beam penetrates the atmosphere, plays the principal role in determining penetration depth and ionization per unit length, it is the radial expansion of the primary beam that sets the enhancement densities that are ultimately achieved within the ionization column. Factors that can play a role in determining radial expansion include initial beam source divergence, confining magnetic field forces, and electron scattering from interactions with the neutral atmosphere. How these effects interact becomes a very significant physical and computational problem, especially for the case of a narrow energetic beam source. *Walt et al.* [1967] used a formulation of the Fokker-Planck diffusion equation to, in part, predict radial expansion of auroral flux. Their method was not considered to be easily applied to distributions that were strongly peaked in either energy or angle; precisely the situation under consideration here. Another complimentary approach integrates the diffusion equations using Monte Carlo techniques, as in *Wedde* [1970] and *Maeda* [1965]. It is implicitly assumed that the primary beam and secondary flux electrons all behave independently, following single particle motions, and interact only with neutral atmosphere particles and the earth's magnetic field.

Results from *Walt et al.* [1967], indicated that typical perpendicular-to-B diffusion of an auroral (non-relativistic) flux with broad energy and angular spread was on the order of an electron gyroradius; indicative of the confining effect of the magnetic field. That the magnetic field should still be necessary to confine the radial expansion of a narrow relativistic monoenergetic electron beam launched nearly parallel to B in a tenuous atmosphere is not necessarily obvious. After all, as beam energy increases the scattering cross-sections decrease [*Machlum*, 1970] and highly focused relativis-

tic beam generators are available. As will be shown, even in tenuous atmospheric conditions present for upper stratospheric and higher altitudes (neutral atmosphere molecular densities levels are at least three to seven orders lower than STP density levels), the relativistic electron-neutral elastic scattering collisions still can cause substantial radial beam diffusion without the presence of the earth's magnetic field.

To demonstrate this fact, standard equations collected and published by the International Commission on Radiation Units and Measurements (ICRU) can be utilized to predict radial beam expansion [ICRU Report 35] in a reference atmosphere [CIRA, 1965] due to small angle scattering. Small angle scattering assumes that any large angle scattering events are relatively infrequent and can therefore be ignored. Fundamental to small angle scattering calculations is the fact that the mean square angular scatter for each electron-neutral collision is statistically independent and therefore additive [Rossi, 1952]. This fact can be used to estimate the mean square radius of a narrow Gaussian electron beam as a function of penetration depth,  $s$ , given by

$$\overline{r^2}(s) = \overline{r_i^2} + 2\overline{r\theta_i}s + \overline{\theta_i^2}s^2 + \int_0^s (s-u)^2 T(u) du \quad (A.3)$$

where the terms are defined as follows:

$\overline{r_i^2}$  = initial mean square radial spread of the beam

$\overline{r\theta_i}$  = initial covariance of the simultaneous radial and angular distribution

$\overline{\theta_i^2}$  = initial mean square angular spread of the beam

$T(u)$  = change in mean square angle of scattering per unit length, where

$$T(u) = \sum_i d \frac{\overline{\theta_i^2}}{du} = \sum_i 4\pi r_o^2 N_i \left( \frac{Z_i}{(\tau+1)\beta^2} \right)^2 \left\{ \ln[1 + (\theta_{mi}/\theta_{ui})^2] + 1 + [1 + (\theta_{mi}/\theta_{ui})^2]^{-1} \right\} \quad (A.4)$$

where

$$\theta_{mi} = \frac{2A_i^{-\frac{1}{3}}}{\alpha\beta(\tau+1)} \text{ or } 1, \text{ whichever is smaller} \quad (A.5)$$

$$\theta_{ui} = 1.130 \frac{\alpha Z_i^{-\frac{1}{3}}}{\beta(\tau + 1)} \quad (A.6)$$

$A_i$  = nucleon number

$$\alpha = (\text{the fine structure constant}) = 1/137$$

$\theta_{mi}$  is the cut-off angle due to the finite size of the nucleus given by the ratio of the reduced de Broglie wavelength of the electron to the nuclear radius.  $\theta_{ui}$  is the screening angle due to the screening of the nucleus by the orbital electrons and is given by the ratio of the reduced de Broglie wavelength to the atomic radius.

As indicated in Eq. A.4,  $T(u)$  is the sum of the mean square angle scattering contributions from each neutral atmospheric constituent. Mean square angle scattering for each constituent is proportional to its respective density and the square of the nucleus charge number. For a narrow, well focused beam, the integral in Eq. A.3 completely dominates radial expansion and need be the only term considered. The integral weights scattering that occurs early, along the path of the beam, more heavily than scattering occurring near the end of the integration path.

Figure A.1 shows the predicted rms beam radius, assuming an initially narrow (1 cm radius) 5 MeV beam focused at infinity with no magnetic field, as it traverses vertically down from an altitude of 119 km. As seen, the beam spread due to elastic scattering would be substantial; well beyond the gyroradius for a 5 MeV electron (602 m). The somewhat surprising result here is that significant beam spread is predicted to occur even due to the scattering levels present in the highest altitude portion of the beam path where collisions are the most infrequent. For example, in transiting from 119 to 118 km,  $T(u)$  has the average value

$$T(u) = T_o = 1.26 \times 10^{-9} \text{ rad}^2/\text{m} \quad (A.7)$$

In transiting one kilometer the rms angular spread of an initially columnar beam would thus increase to approximately 1 milliradian. Without any additional scattering

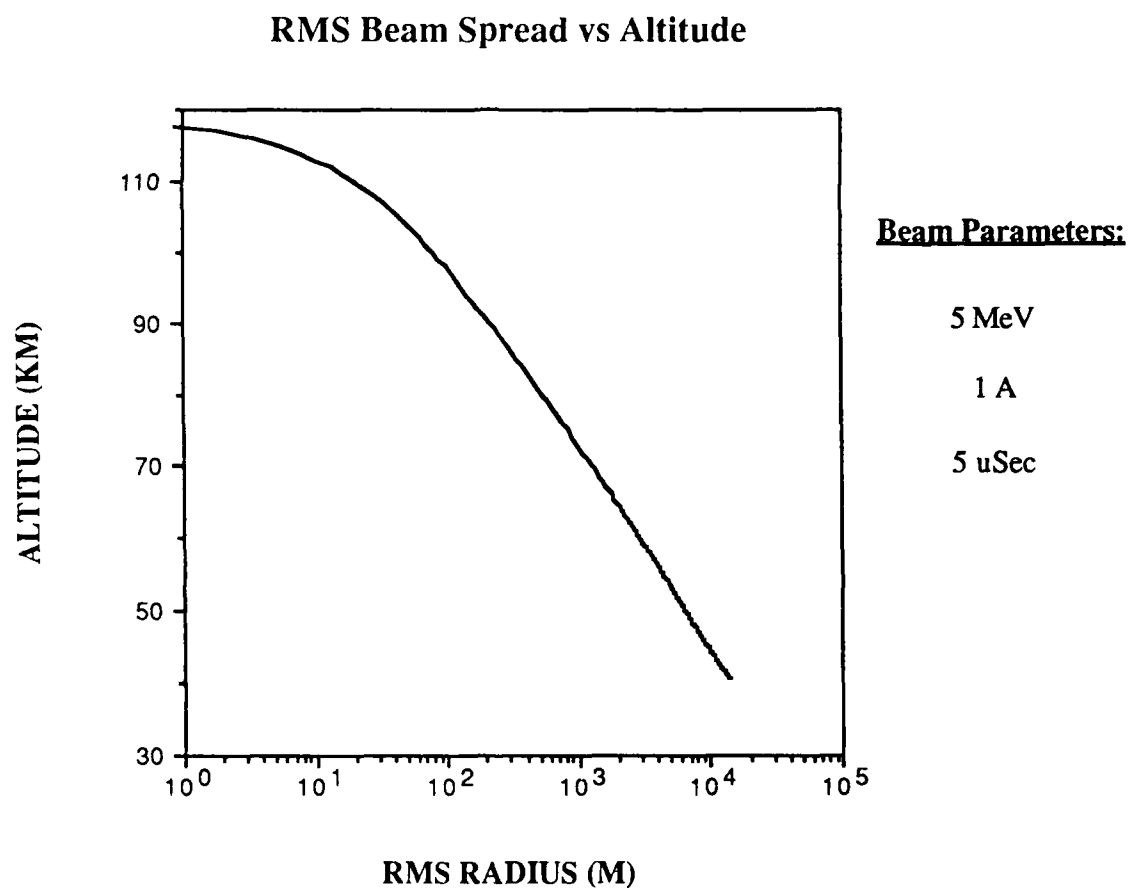


**Figure A.1.** Predicted rms beam radius versus altitude for 5 MeV beam that starts with a 1 cm radius. No magnetic field assumed.

collisions, this angular spread would cause the average beam radius to increase to approximately 80 m after penetrating down to a depth near 40 km; substantially less than a gyroradius. If instead,  $T(u)$  was maintained at the value in Eq. A.7, the integral in Eq. A.3 could be straightforwardly solved resulting in an approximate mean square radius of

$$\overline{r^2}(s) = \frac{1}{3}s^3T_o \quad (A.8)$$

which when evaluated at maximum range gives an rms radius of 460 m. However, since the beam must penetrate at least ten scale heights down to 40 km (for a 5 MeV beam),  $T(u)$  will increase correspondingly and so would the rms radius as shown in Figure A.1, without the presence of the magnetic field. Placement of the beam source at higher or lower altitudes would modify the integrated mean square scattering and therefore the resulting radial spread shown in Figure A.1.

Even with the reduced scattering cross-section of a relativistic electron beam, each primary electron experiences many elastic small angle scattering events as it penetrates through the atmosphere [Maehlum, 1970]. This will cause substantial spread in the angular distribution function describing the primary beam flux, even for the case of a focused narrow beam, directed down the magnetic field. Therefore, without the presence of the magnetic field, it would not be possible to keep a narrow, focused relativistic electron beam from having significant radial diffusion as it penetrated the atmosphere.

The problem of specifically including the confining effect of the magnetic field's Lorentz force with the statistical behavior of the electrons, due to elastic and inelastic collisions, is much more complicated, most likely requiring the methods of *Walt et al.* [1967], *Wedde* [1970], or *Maeda* [1965]. However, it is probably safe to assume that the electron beam will not spread to much beyond a gyroradius, following the results of *Walt et al.* [1967], at least until the beam penetrates sufficiently deep into the atmosphere where large angle scattering collisions become significant.

There are several assumptions that have been made in generating the above. For example, straggling and reflection effects have not been included (Although most re-



flections tend to come from deep along the electron path [*Maehlum*, 1970 and *Walt*, 1967]). In the above analysis it has been implicitly assumed that the primary electrons, having identical initial conditions, all penetrate to the same final altitude. In actuality, different primary electrons in the beam will penetrate to different altitudes and possibly be reflected based on their unique collision history. This would have the effect of spreading out the very pronounced peaks that occur at the end of the beam penetration in Figure 4.5 over several kilometers or to reduce the incident flux somewhat.

We have also assumed that all secondary electrons produced, which on the average have sufficient energy to produce approximately two additional ion-electron pairs, will stay within the same location where it was initially generated. However, it can easily move along the magnetic field lines within a mean free path before generating additional ionization. This will also have the tendency to reduce and broaden the pronounced peak observed at beam termination in Figure 4.5.

Finally, under certain conditions it is predicted that the mean square scattering angle will reach an equilibrium value, so that much beyond 0.3 to 0.5 of the mass weighted range the electrons will reach a state of full diffusion and a rms value of approximately  $45^\circ$  [ICRU #35]. The explanation for this is that electrons scattered over larger angles are rapidly lost from the beam so that the largest depths are only reached by electrons with nearly straight paths. However, for the case under consideration here, the stated mass weighted range is only reached at approximately the last atmospheric scale height. Further, the effect of a confining magnetic field was apparently not considered, which should prevent large-angle scattered electrons from moving more than a gyroradius away and leaving the beam.

To summarize, the neutral atmospheric densities in the mesospheric and stratospheric altitudes under consideration here are sufficient to cause enough angular spread, on an initially narrow electron beam, such that without the presence of the magnetic field there would be substantial radial diffusion of the beam flux. The elastic collisional effect can be thought of as random walk of the primary electron guiding center. Therefore, for a first order estimate of the column ionization density, we

would propose to use the initial beam energy gyroradius to set the primary electron flux and further assume that the flux is uniformly distributed within this gyroradius. This is the gyroradius curve (curve B) of Figure 4.5 where a much narrower column radius (0.5 m) is also included (curve C). In practice we would expect to see the actual ionization enhancement start with values near the 0.5m curve and then move towards the gyroradius curve as the beam penetrated into the atmosphere. At the end of beam penetration, it may also be that the primary electron beam will diffuse slightly beyond a gyroradius, causing the resulting ionization density to dip below the gyroradius curve. Finally, we would expect that a variety of effects, such as electron straggling, will tend to broaden and reduce the peak levels of ionization predicted at the end of beam penetration in Figure 4.5.

#### 4.8. Appendix B: Relocation of Ionized Column to Uniform Potential

Consider the ionized column in Figure B.1 and the initial ambient potential profile in Figure B.2.

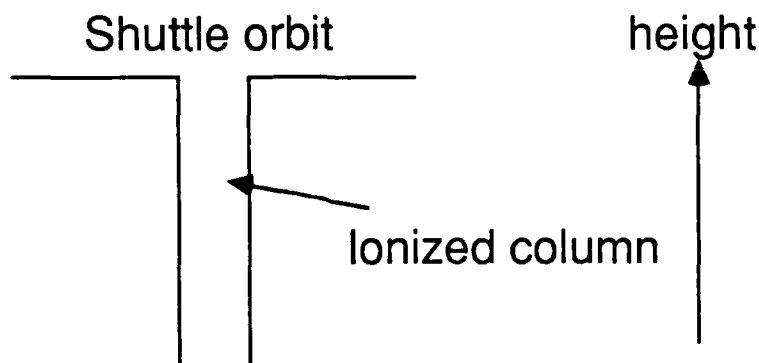


Figure B.1. Ionized column in the ionosphere.

The governing equations in the column are

$$\nabla \cdot E = -ne/\epsilon_0 \quad (B.1)$$

$$\frac{\partial n}{\partial t} = -\nabla \cdot nv \quad (B.2)$$

where  $n$  and  $v$  are the electron density and velocity, respectively, and

$$\frac{\partial v}{\partial t} = -\eta E - \frac{\kappa T \nabla n}{mn} - \nu v = 0 \quad (B.3)$$

##### A. Solution for $\nu \gg$ plasma frequency

In this case we can ignore the term on the left hand side of Eq. (B.3). Rearranging (B.3) then gives

$$nv = -\frac{n\eta E}{\nu} - \frac{kT\nabla n}{\nu m} \quad (B.4)$$

Substituting this in (B.2) gives

$$\frac{\partial n}{\partial t} = \nabla \cdot \frac{n\eta E}{\nu} + \frac{kT}{\nu m} \nabla^2 n \quad (B.5)$$

Now we substitute (1) to get

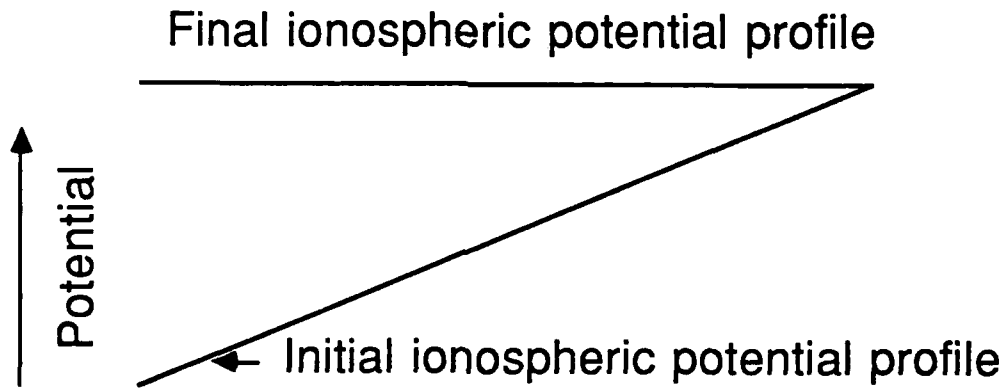


Figure B.2. Initial and final ionospheric potential particles.

$$-\frac{\partial}{\partial t} \frac{\epsilon_o}{e} \nabla \cdot E = \nabla \cdot \frac{n\eta E}{\nu} - \frac{kT}{\nu m} \nabla^2 \frac{\epsilon_o}{e} \nabla \cdot E \quad (B.6)$$

Rearranging gives

$$\frac{\partial}{\partial t} \nabla \cdot E = -\nabla \cdot \frac{\omega_p^2}{\nu} E + \frac{v_e^2}{\nu} \nabla^2 \nabla \cdot E = 0 \quad (B.7)$$

or

$$\nabla \cdot \left\{ \frac{\partial E}{\partial t} + \frac{\omega_p^2}{\nu} E - \frac{v_e^2}{\nu} \nabla^2 E \right\} = 0 \quad (B.8)$$

One possible solution is

$$\frac{\partial E}{\partial t} = -\frac{\omega_p^2}{\nu} E + \frac{v_e^2}{\nu} \nabla^2 E \quad (B.9)$$

Let us assume a one-dimensional solution in the z-direction so that

$$\frac{\partial E_z}{\partial t} = -\frac{\omega_p^2}{\nu} E_z + \frac{v_e^2}{\nu} \frac{\partial^2 E_z}{\partial z^2} \quad (B.10)$$

If we also assume an initial beam profile

$$V = -Az + B \quad \text{and} \quad E_z = A \quad (B.11)$$

then the solution to (B.10) is

$$E_z = Ae^{-\frac{t}{\nu/\omega_p^2}} \quad (B.12)$$

i.e., the  $E_z$  field relaxes to zero in a characteristic time,  $t_o$ , equal to  $\nu/\omega_p^2$ .

If  $\nu$  is  $10^6 \text{ sec}^{-1}$  and  $\omega_p$  is  $10^6 \text{ sec}^{-1}$ , then

$$t_o = \frac{\nu}{\omega_p^2} = 10^{-6} \text{ sec}$$

### B. Solution for general case

In the general case the governing equations are

$$\nabla \cdot E = -ne/\epsilon_o \quad (B.13)$$

$$\frac{\partial n}{\partial t} = -n_o \nabla \cdot v \quad (B.14)$$

$$n_o \frac{\partial v}{\partial t} = -\eta n_o E - \frac{\kappa T}{m} \nabla n - n_o \nu v \quad (B.15)$$

Taking the divergence of (B.15) gives

$$n_o \frac{\partial}{\partial t} \nabla \cdot v = -\eta n_o \nabla \cdot E - \frac{\kappa T}{m} \nabla^2 n - n_o \nu \nabla \cdot v \quad (B.16)$$

If we rewrite (B.13) as

$$n = -\frac{\epsilon_o}{e} \nabla \cdot E, \quad (B.17)$$

and substitute it into (B.14), we obtain

$$\nabla \cdot v = -\frac{1}{n_o} \frac{\partial n}{\partial t} = -\frac{1}{n_o} \frac{\partial}{\partial t} \left( -\frac{\epsilon_o}{e} \right) \nabla \cdot E = \frac{\epsilon_o}{en_o} \frac{\partial}{\partial t} \nabla \cdot E \quad (B.18)$$

Substituting (B.17) and (B.18) into (B.16) yields the equation

$$n_o \frac{\partial}{\partial t} \frac{\epsilon_o}{en_o} \frac{\partial}{\partial t} \nabla \cdot E = -\eta n_o \nabla \cdot E + \frac{\kappa T}{m} \nabla^2 \frac{\epsilon_o}{e} \nabla \cdot E - n_o \nu \frac{\epsilon_o}{en_o} \frac{\partial}{\partial t} \nabla \cdot E \quad (B.19)$$

or, in simpler form,

$$\frac{\partial^2 E}{\partial t^2} = -\omega_p^2 E + v_e^2 \nabla^2 E - \nu \frac{\partial E}{\partial t} \quad (B.20)$$

or

$$\frac{\partial^2 E}{\partial t^2} + \nu \frac{\partial E}{\partial t} = -\omega_p^2 E + v_e^2 \nabla^2 E \quad (B.21)$$

Let  $E = A\tilde{E}(t)$

Then

$$\frac{\partial^2 \tilde{E}}{\partial t^2} + \nu \frac{\partial \tilde{E}}{\partial t} + \omega_p^2 \tilde{E} = 0 \quad (B.22)$$

If  $\nu > 2\omega_p$ , then

$$E = Ae^{[-\frac{\nu + \sqrt{\nu^2 - 4\omega_p^2}}{2}]t} \quad (B.23)$$

If  $\nu < 2\omega_p$ , then

$$E = Ae^{-\nu t/2} \sin \sqrt{\frac{4\omega_p^2 - \nu^2}{2}} t \quad (B.24)$$

If  $\nu \gg 2\omega_p$ , then

$$E = Ae^{-\omega_p^2 t/\nu} \quad (B.25)$$

This corresponds to Eqn. (B.12).

## 5. ION AND PLASMA BEAMS

### 5.1. Previous Space Experiments

Our literature search has not turned up any published accounts of space experiments involving non-neutral beams of ions, positive or negative (however, see p. 133); here 'non-neutral beams' means beams in which the electric space charge of the positive or negative ions is not neutralized by the emission of equal numbers of oppositely charged particles from the sources of the beams. Probably the main reason for the lack of interest in such experiments is that no scientific objectives have been proposed for them that could not be attained more readily using either electron beams, as described above, or plasma beams, as will be described below. Other reasons are technological: ion beams are relatively difficult to produce and to use. Electrons can be extracted simply from a heated cathode, which need be no more than a simple filament of a refractory metal such as tungsten. Positive ions, however, are generally produced by extraction from gas discharges. It is possible to extract ions from heated solid cathodes, but these have to have relatively complicated structures if they are to avoid being eroded in the process. Negative ions, which are less stable than positive ions, are even more difficult to produce in quantity.

Moreover, the use of intense non-neutral positive ion beams in space experiments would create a severe problem of spacecraft neutralization. For a given beam current, passive neutralization (i.e., neutralization by charge deposition from the ambient plasma onto any conducting outer surfaces of the spacecraft body) is more difficult to achieve when the beam is of positive ions, because the body is then required to collect ionospheric positive ions instead of the much more mobile ionospheric electrons. It is true that the same problem would not arise with negative ion beams, but their advantage in this respect would be outweighed by the greater difficulty of producing them.

Seemingly, therefore, space experimentation with intense non-neutral positive ion beams would entail the use of active methods for spacecraft neutralization. One such method might be to embark a separate electron beam source, and to arrange for it



to emit an electron current equal in magnitude to the positive ion current. However, quite apart from the technological inconvenience of having two separate and different sources of particle beams on the same spacecraft, this arrangement would be open to the scientific objection that the effects caused by the two beams might be difficult to distinguish from each other.

A much simpler active method for neutralization of a spacecraft carrying a source of energetic positive ions is to arrange for an equal number of electrons to be emitted from the same source. In other words, the source emits a plasma beam instead of an ion beam. When the ion and electron sources are separate, space charge limits the currents — and hence the particle fluxes — of both species. But when the two sources are combined, the space charges due to the two particle species neutralize one another, with the result that very much greater fluxes can be emitted. Thus, for instance, in Table 1 the largest current reported for an electron beam is 0.8 A, whereas in Table 2 the corresponding figure for a plasma beam is 1.6 kA.

Of course, the beam emitted from a plasma source, besides having no net space charge, also carries no net current; the beam is said to be current-neutral as well as charge-neutral. This is true, at least, so long as no other device, such as an electron beam source or a tethered sub-payload, is bringing current to the spacecraft. Thus the source emits equal and opposite ion and electron currents, and the figures quoted in the last column of Table 2 are their absolute values.

Whether it be for these or for other reasons, all the space experiments performed up to now with energetic ions have used plasma beams rather than non-neutral ion beams. A list of those performed since the beginning of 1975 is given in Table 2. The format is similar to that of Table 1, except that the nature of the positive ion is specified in an additional column; usually the ions were either of alkali metals such as caesium, or of inert gases such as argon.

Although in most of these experiments the vehicles were rockets, there were some exceptions. The Soviet 'Meteor' experiment was performed from a satellite [Grebner *et al.*, 1981], while the Japanese SEPAC experiment was part of the Spacelab-1 payload on the NASA Space Shuttle [Obayashi *et al.*, 1985]. Plasma sources were also

Table 1. Space experiments with electron beams of energies of 10 keV or more, since 1-1-75

| TITLE      | DATE                       | ALTITUDE                 | ENERGY           | CURRENT       |
|------------|----------------------------|--------------------------|------------------|---------------|
| ARAKS      | (1) 1-26-75<br>(2) 2-15-75 | (1) 190 km<br>(2) 185 km | 15 and<br>27 Kev | 0.5 A         |
| ECHO 4     | 1/31/76                    | 215 km                   | 40 keV           | 0.1 A         |
| POLAR 5    | 2/1/76                     | 110-220 km               | 10 keV           | 0.13 mA       |
| ELECTRON 2 | 11/27/78                   | 120-192 km               | 10keV            | 0.01 - 0.1 mA |
| ECHO 5     | 11/13/79                   | 100-120 km               | 40 keV           | 0.8 A         |
| ECHO 6     | 3/30/83                    | 200 km                   | 10-36 keV        | 0.23 A        |

Table 2. Space experiments with positive ion (plasma) beams, since 1-1-75

| TITLE     | DATE   | ALTITUDE                             | ION                             | ENERGY                 | CURRENT   |
|-----------|--|--------------------------------------|---------------------------------|------------------------|-----------|
| ARAKS     | (1) 1-26-75<br>(2) 2-15-75                                   | (1) 190 km<br>(2) 185 km             | Caesium                         | 50 eV                  | 10 A      |
| ARIEL     | (1) 10-29-77<br>(2) 10-30-77<br>(3) 11-30-78<br>(4) 11-18-79 | (1,2) 115-160 km<br>(3,4) 110-145 km | (1,4) Barium<br>(2,3) Uncertain | Uncertain              | Uncertain |
| METEOR    | 1977-79  | 850-900 km                           | Xenon                           | 130 eV                 | Uncertain |
| AELITA    | (1) 10-06-78<br>(2) 10-25-79                                 | 100-145 km                           | Lithium                         | 4-10 eV                | 300 A     |
| PORCUPINE | (1) 3-19-79<br>(2) 3-31-79                                   | (1) 196-464 km<br>(2) 191-451 km     | Xenon                           | 200 eV                 | 4 A       |
| ARCS      | (1) 1-27-80<br>(2) 11-14-82                                  | (1) 120 - 220 km<br>(2) 120 - 451 km | Argon                           | (1) 25 eV<br>(2) 33 eV | 0.1 A     |
| SEPAC     | 11-28-83   | 240 km                               | Argon                           | 110 eV                 | 1.6 kA    |
| ARCS 3    | 2-10-85  | 129-406 km                           | Argon                           | 200 eV                 | 0.2 A     |

embarked on the geosynchronous satellites ATS-5, ATS-6, and SCATHA, but these experiments have not been listed in the table because the sources concerned were too small to be useful for ionospheric modification.

The figures quoted for the energies are those of the positive ions. The corresponding velocities are, of course, very much less (by the square root of the mass ratio) than those of electrons with the same energy. In the SEPAC experiment, for instance, the velocity of the 110 eV argon ions in the plasma beam was about 23 km/s [*Sasaki et al.*, 1986b]. Since the beam is electrically neutral, the bulk velocity of the electrons in it is the same as the velocity of the ions, which is much less than the electron thermal velocity. Thus the neutralizing electrons are thermal, in the sense that their energies are essentially those of their random thermal motions: usually these amount just to a few eV, which is nevertheless an order of magnitude greater than the thermal energies of the ambient ionospheric electrons.

In some space experiments, a plasma source was put on board the spacecraft primarily as a source of neutralizing electrons rather than of energetic ions. This was the case, for instance, in Araks, the first of the experiments listed in Table 2. Each of the Araks payloads had an electron gun as the main active experimental device (see Table 1), while the purpose of the plasma source was to promote neutralization during the electron beam emissions [*Morozov et al.*, 1978; *Cambou*, 1980]. The source was operated continuously, and the plasma was ejected more or less perpendicularly to the local magnetic field, so that it tended to remain near the payload. Thus the payload should have been surrounded by a dense cloud of hot plasma, from which it could collect neutralizing electrons more readily than from the ambient ionosphere. Whether the plasma source actually succeeded in restraining the excursions of payload potential is not clear from the Araks data [*Fiala*, 1981]. On the other hand, the plasma sources on the ATS-6 and SCATHA satellites were quite successful in this respect [*Purvis and Bartlett*, 1980; *Gussenhoven and Mullen*, 1983]. Plasma sources used primarily as means for stabilizing spacecraft potential are sometimes referred to as 'plasma contactors' or 'plasma bridges'.

In all the remaining experiments listed in Table 2, the plasma source itself was

the main active experimental device. In most cases it operated in pulses rather than continuously, so that comparison could be made between the effects observed with the source in action and with it switched off. The very large ion current used in the SEPAC experiment was emitted in 1 ms pulses, separated by relatively long intervals; the value quoted for the current has been estimated from the published figure of  $10^{19}$  for the total number of electron-ion pairs emitted in a pulse [Sasaki *et al.*, 1986]. The power was supplied from a capacitor bank, which accumulated electrical energy relatively slowly and then discharged it impulsively into the source; the discharge energy was 2 kJ [Ijichi *et al.*, 1981]. However, some of the other experiments used pulses lasting 1 s or more, approximating continuous operation. In the Soviet 'Aelita' experiments, for instance, the 300 A lithium plasma beam was emitted in pulses 2 s long with 1 s between them; the resulting plasma clouds, launched into the ionosphere in the 90-150 km altitude range, were sufficiently large and sufficiently dense to be observable by radar from the ground [Sagdeev *et al.*, 1981].

The scientific objectives of most of these experiments were to study the propagation of plasma beams through the ionospheric plasma in the presence of the Earth's magnetic field. The theoretically anticipated behavior depends very much on the direction of propagation of the beam relative to the field: it is very different for the perpendicular and parallel directions. In some of the experiments the beam was directed more or less perpendicular to the field, and in others more or less parallel, depending on the objectives. The theory of plasma beam propagation and the effects that have been observed experimentally are discussed in §5.3.

## 5.2. Ion and Plasma Beam Sources

### 5.2.1. Introduction

Sources of ion beams and of plasma beams are far more diverse than sources of electron beams are. A comprehensive review of research and development work on ion and plasma beam sources up to the beginning of 1973 has been published by Green [1974]; his discussion of basic principles and extensive bibliography are especially valuable. The review concentrates on the production of beams by gaseous discharges,

which is the classical method, and it covers the three main aspects of the subject: these are, firstly, the actual discharge in which ions of the species needed can be produced at controlled rates, preferably with spatial and temporal uniformity; secondly, the extraction of the beam from the discharge, preferably with only a small spread in velocity; and thirdly, the transport of the beam away from the source, in the possible presence of strong space-charge forces. We now discuss briefly these three aspects of the classical discharge source, then describe some alternative plasma sources, many of which were developed originally for the electric propulsion of spacecraft [Jahn, 1968]. Finally we outline the progress that has been accomplished in developing plasma sources over the past decade.

### 5.2.2. *Gas Discharge*

In a discharge, neutral gas is ionized and turned into plasma by bombardment with energetic electrons. These may be emitted from a cathode, which generally is heated to promote emission. Alternatively, once the discharge has started, they may be electrons liberated by the ionization of the gas. In either case, they are given energy by acceleration in electric fields, which may be uni-directional or oscillatory. Rapidly oscillating radio-frequency (RF) fields offer the advantage of not driving the electrons systematically towards and into the anode, as is liable to happen with uni-directional fields: thus the electrons remain in contact longer with the neutral gas, and have a better chance of making ionizing collisions.

To this same end, in sources energized by uni-directional electric fields, magnetic fields are often used to confine the electrons and thus stop them from moving promptly to the anode. One family of sources of this kind is based on the principle of the Penning Ionization Gauge (PIG), otherwise known as the reflex discharge source. In its simplest form, the PIG has axial symmetry, and a uniform magnetic field is applied parallel to its axis. This field prevents the electrons from escaping radially, while they are prevented from escaping axially by means of two negatively biased circular disks, one at each end of the discharge, which face one another and form the cathodes. The anode is a cylinder, which often forms the outer wall of the device. The 'pigatron'

and 'duopigatron' are examples of sources that use this principle; other varieties, such as the 'duoplasmatron', also use confining magnetic fields but in different ways.

### 5.2.3. Beam Extraction

At the instant when it is formed in a gas discharge, a positive ion has just the random thermal velocity of its neutral parent particle, and for some purposes this velocity would be quite sufficient. If, for instance, the source is to be used as a plasma contactor, then there is no need for the plasma to emerge as a directed beam, so long as the emitted ion and electron currents exceed the value required for spacecraft neutralization. Indeed, it is better that the plasma should emerge slowly and diffusely, so as to form a dense cloud around the spacecraft. Hence a plasma contactor may consist simply of a gas discharge tube, for example of the hollow cathode type, with a hole at one end to let the plasma out. If the discharge is produced by means of an RF field, the ions will emerge at their thermal velocities corresponding to the temperature of the gas in the source: a particularly efficient type of RF plasma source has been developed recently by *Boswell* [1984].

However, if a static electric field is used to produce the discharge, then the average velocity of the emergent ions, and the spread in their velocities around the average, are generally much greater than the ion thermal velocity at the temperature of the gas in the source. The reason for this is the existence, within the discharge, of variations of electric potential from point to point. Besides its thermal kinetic energy, an ion acquires additional kinetic energy equal to the difference between the potential of the point in the discharge where it was formed, and the potential of the ambient plasma. Thus, for instance, the ion gun used in the ARCS 1 and 2 experiments consisted of a hollow-cathode discharge, in which electrons from a filament were accelerated towards a cylindrical anode on the axis, while being confined by a coaxial magnetic field. The ions, which had radii of gyration greater than the dimensions of the source, were not confined. The ion beam had a  $60^\circ$  cone angle, and a distribution in energy with a full width at half maximum of approximately 25% centered on an energy of 25–30 eV, when 60 V were applied to the anode [*Moore et al.*, 1982, 1983; *Kaufmann et al.*, 1985]; a similar type of source, but producing a 200 eV ion beam, was used in ARCS

3 [Erlandson *et al.*, 1987]. Nevertheless, even though these energies are one or two orders of magnitude greater than the ion thermal energy, it is still the ion thermal velocity that governs the flux, or current, of the emergent ions, as we shall see in a moment.

A source operated as described above produces a broad beam of ions, but for many purposes, such as spacecraft propulsion, a directed beam is required. This means that additional velocity in one direction must be imparted to the ions as they emerge from the source, and the simplest way to do so is with an electric field. Ions can be extracted from the plasma and accelerated by applying a negative potential to an external electrode.

Needless to say, care must be taken to ensure that the extracted ions are not all collected by this electrode. The usual precaution is to employ an electrode with one or more holes in it, through which the ions pass. In the limit, the electrode can be a thin mesh grid, the holes in which have a much greater total area than the wires of the grid, in which case only a small fraction of the extracted ions ends up on the wires.

There is, however, a limit to the density of the current that can be drawn from the plasma in this way. On account of the shielding action of the electrons, an electric field applied to the surface of a plasma does not normally penetrate deeply; its influence is limited to a thin layer at the surface of the plasma, just a few Debye lengths thick, which is called the 'ion sheath' because it contains more ions than electrons. In the bulk plasma the ion and electron concentrations are equal, and the highly mobile electrons normally keep the electric field small. The consequence is that while the potential applied to the extraction electrode governs the energy of the ion beam, it has very little effect on the beam current density. Once the ions have entered the plasma sheath, they are accelerated by the externally applied field, but they come to the sheath from the bulk plasma only with their thermal velocities. Thus the surface density  $J_i$  of the ion current entering the sheath from the bulk plasma is approximately

$$J_i \approx en_i v_i \quad (5.1)$$



where  $e$  is the elementary charge,  $n_i$  is the ion concentration in the plasma, and  $v_i$  is the ion thermal velocity:

$$v_i = \left( \frac{kT_i}{M_i} \right)^{\frac{1}{2}} \quad (5.2)$$

Here  $k$  is Boltzmann's constant,  $T_i$  is the ion temperature, and  $M_i$  the mass of an ion.  $J_i$  is the maximum beam current density that can be extracted, unless some method can be found for accelerating the ions within the plasma itself. Some sources that employ such methods will be described in §5.2.5. First, however, we discuss the transport of an ion beam extracted from a gas discharge by means of an electric field.

#### 5.2.4. Beam Transport

We now consider how the quality of the beam can be preserved as it is transported away from the source. At the outlet from the discharge, the negatively biased electrode that attracts the ions also repels the electrons, so initially the beam consists entirely of ions. Since these repel one another electrostatically, the emerging ion beam would expand rapidly as it receded from the source, if no steps were taken to prevent this from happening. Close to the source, the beam can be focused by electric or magnetic fields, but once it has left their influence, the only effective way of preventing it from expanding is to neutralize its space charge. When the source is being operated in the ionosphere, neutralization can occur naturally, by influx of ionospheric electrons. This process cannot be relied on, however, unless the ion concentration in the beam is of the order of or less than the electron concentration in the ambient plasma. Moreover, even when natural beam neutralization is feasible, reliance upon it would still leave the problem of how to neutralize the spacecraft carrying the source.

For these reasons, some of which we already noted in §5.1, arrangements are often made to neutralize the ion beam artificially as it emerges from the source, thus transforming it into a plasma beam. The simplest arrangement is to place an electrically heated and negatively biased filament in the path of the beam, beyond the extraction electrode; this hot cathode emits thermal electrons, which neutralize the beam. If the beam is intense, however, bombardment by the ions may overheat

and destroy the cathode. Hence it is often better to place the cathode off to one side, or to use a cathode in the form of a ring surrounding the beam.

Magnetic fields exacerbate the problem of beam neutralization. When the source is of the type that employs a magnetic field to confine the electrons in the discharge, care must be taken to keep this field away from the neutralizer, so that the thermally emitted electrons are not confined as well. Moreover, even when the beam has escaped from its source entirely, the Earth's magnetic field is still to be reckoned with, since it hinders the neutralizing electrons in their attempt to follow the ions. The influence of the Earth's field on plasma beam propagation will be mentioned again in §5.3.

#### 5.2.5. *Alternative Sources*

We now describe briefly various alternative types of plasma source, all of which produce a directed plasma beam without using an extraction electrode, and are capable of yielding ion current densities higher than that given by equation (5.1).

In the type of source known as an electrothermal accelerator, or arcjet, these results are achieved by means of an intensely hot electric discharge, sustained at sufficiently high pressure for the gas to be thoroughly collisional [Tuczek, 1967]. An arcjet is basically a rocket motor in which the propellant is heated electrically instead of being burned. Usually the propellant is an inert gas, which is both heated and ionized by an electric arc. Since the gas is collisional, it accelerates to supersonic speeds, much greater than the ion thermal speed, as it emerges through the nozzle of the source. Such devices form quite efficient thrusters, but are not very efficient as plasma sources because the propellant gas is only slightly ionized. Their efficiency as plasma sources can be much improved by using, instead of an inert gas, the vapor of some alkali metal such as caesium, which has a very low ionization potential (3.9 eV); the plasma contactor used in the Araks rocket experiments was of this variety [Morozov *et al.* 1978].

In most of the other types of source that we shall now discuss, the plasma is accelerated and formed into a beam by electromagnetic fields acting within the discharge itself. Many different types of source have been built using this general principle.

One way of classifying them is according to whether they use static or time-varying fields; the latter may be pulsed or oscillatory. We shall consider these various types in turn.

In electromagnetic plasma beam sources using static electric and magnetic fields, these fields fill the whole volume of the discharge, and the plasma is expelled by the  $\mathbf{j} \times \mathbf{B}$  motive force. The electric field  $\mathbf{E}$  is more or less perpendicular to the magnetic field  $\mathbf{B}$  at all points; the parallel component of  $\mathbf{E}$  is relatively small because the plasma conducts so well in this direction. The design of such a source depends on the gas pressure at which it is intended to operate, since this variable governs the electron-neutral collision frequency, and hence the ratio of the transverse direct (or Pedersen) conductivity to the Hall conductivity.

In sources operating at the highest pressures, the Pedersen conductivity dominates, so the current  $\mathbf{j}$  is more or less parallel to the electric field  $\mathbf{E}$ . The simplest design has the gas flowing in a conduit with a rectangular cross-section. Two opposite walls of the conduit are electrodes, between which an electric field is applied, creating a discharge and ionizing the gas. The other pair of walls are the poles of an electromagnet, or permanent magnet, which create a static magnetic field perpendicular to the electric field. The  $\mathbf{j} \times \mathbf{B}$  force drives the plasma along the conduit and out of the end into space. This design of source, sometimes called a 'Faraday-type crossed-field accelerator', may be regarded as a classical magnetohydrodynamic (MHD) electric power generator run in reverse, i.e., it is being supplied with power and used as a motor.

A disadvantage of the simple crossed-field accelerator is its lack of axial symmetry, and this is overcome in a more elaborate design known as the 'magnetoplasma dynamic arcjet'. Essentially an MPD arcjet is a hollow-cathode discharge source, in which an arc is struck between a cylindrical rod anode on the axis, and a hollow cylindrical cathode forming the outer wall of the device. Its distinctive feature is that the current flowing axially along the anode is large enough to create a strong azimuthal magnetic field in the discharge space between the anode and the cathode. This azimuthal field, crossed with the radial discharge current, yields the propulsive force along the axis.

Since this force is proportional to the square of the current, an MPD arcjet works best at high currents. The plasma source used in the Japanese SEPAC experiment on Spacelab-1 was of this kind [Obayashi *et al.*, 1985]; pulsed power supply provided the very high current required, in pulses 1 ms long. The even more powerful quasi-continuous source used in the Soviet Aelita rocket experiments was also an MPD arcjet, with the particularity that the lithium vapor for the plasma was evaporated, by the heat of the arc, from a button of lithium metal attached to the end of the anode rod [Dorodnov, 1978; Sagdeev *et al.*, 1981]. Like the straightforward arcjets mentioned above, MPD arcjets expel much neutral gas along with the jet of plasma.

For producing a plasma jet with relatively few neutrals, the so-called 'Hall-effect accelerator' is superior. Its principle, indeed, assumes a discharge plasma in which collisions between charged and neutral particles are rare. Once again, static electric and magnetic fields are applied to the plasma in directions perpendicular to one another. The electric field  $\mathbf{E}$ , which is created by an extraction electrode, is more or less parallel to the axis of the device. The strength of the magnetic field  $\mathbf{B}$  is such that the particle gyro-radii, in comparison with the dimensions of the device, are small for the electrons but large for the ions. Hence the electrons are tied to the field lines, and drift in the direction of  $\mathbf{E} \times \mathbf{B}$ , carrying the Hall current. They cannot move in the direction of  $\mathbf{E}$  to neutralize this field, as they would if  $\mathbf{B}$  were not there, so  $\mathbf{E}$  permeates the plasma instead of being localized in a sheath at its surface. The ions, which are almost unaffected by  $\mathbf{B}$ , are accelerated by  $\mathbf{E}$  and extracted from the plasma. The ions formed at different points acquire different kinetic energies from the electric field, so they emerge from the plasma widely spread in energy. Since the plasma electrons cannot follow them, other electrons have to be fed into the emergent ion beam from a neutralizer, as was described in §5.2.4.

We shall deal only very briefly with plasma sources in which pulsed or oscillatory electromagnetic fields are used to accelerate the plasma. Most of them rely on the fact that a time-varying magnetic field cannot readily penetrate into a highly ionized plasma that contains no magnetic field initially. It is kept out by electric currents induced on the surface of the plasma, and their interaction with the field creates a

$\mathbf{j} \times \mathbf{B}$  force (the 'magnetic pressure') pushing the plasma away from the region of space occupied by the field. 'Plasma rail-guns' and 'conical theta-pinches' are examples of pulsed sources based on this principle [Tuczek, 1967]. In a similar way, 'traveling-wave accelerators' use RF fields to expel a stream of plasma blobs [Heflinger *et al.*, 1965; Jahn, 1968]. For more complete information about these types of source, the reader should consult the publications cited.

The pulses or blobs of plasma that these sources emit are often referred to as 'plasmoids'. If their electric conductivity were perfect, then the magnetic fields that propel them would not penetrate into them at all. In practice, the plasma has some resistivity, with the result that partial penetration occurs and the emergent plasma blobs have some magnetic field embedded in them. With certain types of pulsed source, such as the coaxial plasma gun or 'Marshall gun' [Marshall, 1960], the operating conditions can be chosen so that the embedded field is quite large. The blob then has the form of a torus, with the magnetic field lines winding helically around the minor axis. The interest of this kind of plasmoid is that it holds itself together much longer than a blob with no embedded field does; fusion plasma physicists call it a 'spheromak' [Okabayashi *et al.*, 1981; Hammer, 1984]. Such plasma entities were first produced by Bostick [1956, 1957], who gave the name 'plasmoids' to them, but later the meaning of this term was extended to cover any type of plasma blob, with or without an embedded magnetic field [Lockner *et al.*, 1985].

#### 5.2.6. Recent Developments

During the past decade, the design of classical gas-discharge plasma sources has evolved and their performance has improved considerably. Progress up to about the end of 1979 in the development of sources for electric propulsion has been presented by Finke [1981]. A modern ion thruster, suitable for quasi-continuous operation on the Space Shuttle, can produce a 10 A beam of 1 keV argon ions for a total power expenditure of 12 kW [Byers, 1986].

A new incentive to develop very powerful (multi-megawatt) ion beam sources has been provided by their application to heating magnetically confined fusion plasmas,

a proceeding that calls for quasi-continuous beams of light ions such as protons or deuterons. These are converted, by charge exchange, into beams of neutral atoms, which are able to traverse the confining magnetic field into the heart of the plasma. There they become ionized again, are trapped by the field, and give up their energy to the plasma. As an example, a quasi-steady-state (30 s pulse) source of the duopigatron type, developed for fusion applications, can produce a 45 A beam of protons or a 33 A beam of deuterons, both at 80 keV [Menon *et al.*, 1985]. Other, quite different types of ion beam source, producing very intense but very short pulses, have been developed as alternatives to lasers for the purposes of inertial confinement fusion, namely compressing and heating the target pellets [Dolan, 1982; Miller, 1982].

More useful for space applications is a type of Hall-effect accelerator that is capable of producing large quasi-continuous currents at relatively low energies. In this device, which has axial symmetry, the discharge takes place in the space between two insulating coaxial cylinders. An electric field, applied parallel to the axis, extracts the ions from the discharge; an external cathode supplies neutralizing electrons. The reason why the device is very efficient as a plasma source is that, within the discharge, the  $\mathbf{E} \times \mathbf{B}$  drift motion of the electrons is in the azimuthal direction, so it does not carry them to the walls. Some authors use the acronym ACED, for 'Accelerator with Closed Electron Drift', to denote this type of source.

The development of the ACED was initiated in the USA [Lary *et al.*, 1962; Seikel and Reshotko, 1962; Cann and Marlotte, 1964; Pinsley *et al.*, 1964; Brown and Pinsley, 1965; Grossman *et al.*, 1965; Janes and Lowder, 1966], but appears to have been abandoned here in the mid-1960's. and subsequently it was taken up again in the USSR [Morozov *et al.*, 1972; Bishaev and Kim, 1978; Dorodnov, 1978; Askhabov *et al.*, 1981]. An ACED thruster was used to adjust the near-synchronous orbit of one of the 'Meteor' satellites [Artsimovich *et al.*, 1974]; thrusters of the same or of a similar design were used on two later members of the Meteor series [Grebnev *et al.*, 1981]. ACED plasma beam sources delivering 4 A of xenon ions at 200 eV were supplied by the Soviet participants in the West-German 'Porcupine' program of rocket experiments in the auroral ionosphere [Haerendel and Sagdeev, 1981].

To conclude this review, we should mention several means that exist for creating a plasma beam in space without using an electric discharge. The simplest means is to release, in sunlight, a vapor cloud of a readily photoionized metal such as barium; usually this is done by igniting a canister of thermite, or detonating a bomb, containing some of the metal in question. A directed beam may be obtained by employing a shaped explosive charge; for instance, a magnetic-field-aligned barium ion cloud released from a rocket-borne shaped charge in the auroral ionosphere has been used to measure parallel electric fields at altitudes of several thousand kilometers [Haerendel *et al.*, 1976]. Another way to produce a beam is to release a cloud of barium vapor from a rapidly-moving vehicle such as a satellite; the newly born ions then possess the orbital velocity of the vehicle [Heppner *et al.*, 1981]. A related method is to release a cloud of a neutral gas such as argon, and to ionize it with an electron or ion beam from a source on the vehicle; a charged particle beam has to be used because photoionization by sunlight is too slow. Finally, if an ionizable cloud is released in interplanetary space, as in the AMPTE ('Active Magnetospheric Particle Tracer Explorers') artificial comet experiments [Valenzuela *et al.*, 1986], it constitutes a beam because the ambient solar-wind plasma is flowing outwards from the Sun at speeds of several hundred kilometres per second.

The suggestion has been made that ion beams are created inadvertently by all satellites in low Earth orbits, as the result of partial specular reflection of ionospheric ions at their forward surfaces, i.e., the parts of their surfaces facing into the direction of the orbital motion. Relative to the ambient plasma, the reflected ions would have twice the orbital velocity of the satellite, and their motion through the plasma might give rise to instabilities. It has been suggested that these processes are responsible for the luminous emission known as 'Shuttle glow', which has been observed close to the forward surfaces of the Space Shuttle [Papadopoulos, 1984].

Be that as it may, a related suggestion has been made by Stenzel [1985] for a way in which similar beams could be created deliberately, for experimental purposes, on the future NASA Space Station. His proposal is to erect, outside the Station, a plane multi-grid electrostatic probe in the form of a flat panel several metres across. This

panel would consist of a frame supporting a set of several fine metal grids, one behind the other. It would be facing more or less into the direction of orbital motion of the Station, and appropriate potentials would be applied to the grids so as to reflect some of the oncoming flux of ionospheric ions, together with an equal flux of neutralizing electrons; the reflection process would be specular, and the reflection coefficient could be adjusted by varying the applied potentials. The large space directly in front of the panel would then be filled with an ion beam having well known and precisely controllable characteristics, counterstreaming through the oncoming ionospheric plasma. The resulting two-stream instabilities would be accessible to experimental study in quite exceptional conditions of plasma cleanliness and uniformity.

### 5.3. Ionospheric Effects of Ion and Plasma Beams

Among the various factors that govern the behavior of a plasma beam traveling through the ionosphere in the presence of the Earth's magnetic field, two of the most important are, firstly, the angle between the beam and the magnetic field, and secondly, the beta factor for the beam. For simplicity, most space experiments with plasma beams have been designed to inject the beam either perpendicular or parallel to the field, so we shall discuss the observed effects under these two headings. The beta factor, or  $\beta$ , is the ratio of the kinetic pressure of the plasma in the beam to the magnetic pressure of the Earth's field; it decreases steadily as the beam expands away from the source.

#### 5.3.1. Beams Injected Perpendicular to the Field

The propagation of a beam of plasma perpendicular to a magnetic field has been a subject of interest for many years, both on theoretical and on practical grounds.

It is of theoretical interest because it is a classical example of how the particles in a plasma can behave collectively in ways very different from their individual behavior. An individual charged particle launched in a direction perpendicular to the field moves in a circle, right-handedly around the field for an electron and left-handedly for a positive ion, with the radius appropriate to its charge, mass, and velocity. In



contrast, a plasma beam is able to travel some distance across the magnetic field in a straight line, for reasons that will be discussed shortly.

Theoretical study of the interaction between a plasma beam and a perpendicular magnetic field was first undertaken by *Chapman and Ferraro*, in connection with their classical theory of geomagnetic storms: see *Ferraro* [1952], and the references given there to earlier papers, beginning in 1931. These authors considered what would happen if a beam of plasma emitted from the Sun encountered the Earth's magnetic field. At the time when they wrote, it was not known that the Sun emits plasma continuously in the form of the solar wind, and they conceived of these plasma emissions as isolated events, rather than as the intensifications of a continuous emission that we now understand them to be. *Chapman and Ferraro* discovered much of the basic physics, and initiated the theoretical research on plasma flow around the magnetosphere that continues to this day, but the relevance of their work to the propagation of artificial plasma beams in the ionosphere is restricted by the fact the solar wind plasma beam is much wider than the spatial scale of the Earth's magnetic field. In these circumstances, the oncoming beam compresses the field on the sunward side of the Earth, just so long as its momentum flux, or 'ram pressure',

$$P_{ram} = NMV^2, \quad (5.3)$$

exceeds the magnetic pressure

$$P_{mag} = \frac{B_0^2}{2\mu_0}. \quad (5.4)$$

Here  $N$  is the ion concentration in the solar wind and  $M$  the mass of a solar-wind ion, so  $NM$  is the mass density of the plasma, while  $NMV$  is its momentum density, with  $V$  the flow velocity.  $B_0$  is the strength of the Earth's magnetic field, and  $\mu_0$  is the permeability of free space. When the field is compressed,  $B_0$  rises until finally the magnetic pressure becomes sufficient to halt the motion towards the Earth, obliging the beam to diverge so as to flow around this obstacle. Thus the balance of  $P_{ram}$  and  $P_{mag}$  governs the geocentric distance of the magnetopause at the stagnation point of the flow, close to the sub-solar point.

Much of the foregoing analysis applies to a plasma beam injected into the ionosphere perpendicularly to the Earth's magnetic field, even though this is the opposite situation where the width of the beam is much less than the spatial scale of the field. For the moment, we are picturing a cylindrical beam of fully ionized plasma moving in a direction parallel to its axis. The beam will propagate only if its ram pressure exceeds the magnetic pressure, in which case, however, the magnetic field lines are pushed aside by the head of the beam as it advances through them.

Initially, the beam excludes the magnetic field: it is a 'diamagnetic cavity'. Within the beam, the plasma exerts its gas kinetic pressure, whereas outside the beam there is just the pressure of the magnetic field, neglecting the kinetic pressure of the ionospheric plasma which is relatively small. Thus the edge or boundary of the beam, which is sharp, is a kind of magnetopause. According to whether the plasma pressure is greater or less than the magnetic pressure, the boundary will expand or contract to establish equilibrium [*Haerendel and Sagdeev*, 1981]; most of the plasma sources used in space experiments have  $\beta \gg 1$  at their outlets, so initial expansion is the rule.

This state of affairs is short-lived, however, because the magnetic field diffuses into the plasma. If the diffusion occurred in a purely classical fashion, through collisional dissipation of the currents flowing in the boundary, then it would take a time of the order of

$$\tau = \mu_0 D^2 / \eta , \quad (5.5)$$

where  $D$  is the diameter of the beam and  $\eta$  is the classical resistivity of a fully ionized plasma; to find the expression for  $\eta$  and the derivation of (5.5), see pp. 179-181 and 205-207 respectively of *Chen* [1984]. Experimentally, however, the magnetic field penetrates into the beam much more rapidly than (5.5) suggests. Evidence to this effect, from the Porcupine rocket experiments, has been presented by *Häusler et al.* [1986a]. For the 4 A xenon plasma beam used in these experiments, the theoretical diffusion time according to (5.5) was about 2.5 ms, whereas the experimental value was about 0.2 ms; the latter was estimated from the observed diamagnetic field perturbation, which disappeared within less than 5 m from the source. This anomalously rapid

diffusion is believed to be caused by instability of the currents in the boundary layer, the unstable waves being electrostatic in nature, with frequencies of the order of the lower hybrid frequency [*Mishin et al.*, 1986a,b]. As the field penetrates into the beam, the beam expands outwards into the field so as to preserve pressure balance. The end result of their interdiffusion is a low-beta plasma beam permeated by the magnetic field.

Independent evidence of anomalously rapid magnetic field diffusion was found in the AMPTE artificial comet experiment, which, for reasons explained at the end of §5.2.6, can also be regarded as a beam injection. In this experiment, a diamagnetic cavity about 100 km in diameter was created by releasing a cloud of barium vapor into the solar wind. The initial motion of the cloud was very curious indeed: during the first 4.5 m after its formation, it moved perpendicularly to the direction of the solar wind through a distance of about 500 km before being accelerated downwind. As soon as the cloud was formed, the interplanetary magnetic field began to diffuse back inwards, and its return was observed by a magnetometer on the vehicle from which the cloud had been released. Surprisingly, no very strong electrostatic wave activity was observed at the boundary between the field and the cloud, and for the moment the mechanism of their rapid interdiffusion remains obscure [*Gurnett et al.*, 1985; *Hatrendel et al.*, 1986; *Valenzuela et al.*, 1986]. Similar results had been obtained previously during the AMPTE solar wind lithium cloud releases [*Häusler et al.*, 1986b].

Even when the magnetic field has permeated it completely, the beam or cloud can continue to travel perpendicularly across the magnetic field, thanks to the collective action of the plasma particles. Interacting individually with the field, electrons would be deflected sideways in one sense and ions in the other, but as soon as these processes start to occur in a beam, free polarization charges appear on the sides of it. These create an electric polarization field within the beam, enabling the plasma particles of both species to continue their forward motion undeflected, as an  $\mathbf{E} \times \mathbf{B}$  drift. The kinetic theory of this form of collective behavior was begun by *Schmidt* [1960], who argued that the condition on which it can happen is that the transverse dielectric

constant of the magnetoplasma,

$$\epsilon = \frac{NM}{\epsilon_0 B^2}, \quad (5.6)$$

should be much greater than unity; otherwise, the particles execute their individual motions in the magnetic field. Subsequently *Peter and Rostoker* [1982] showed that the stronger condition

$$\epsilon \gg (M/m)^{\frac{1}{2}} \quad (5.7)$$

was necessary, where  $M$  and  $m$  are the ion and electron masses. Other recent contributors to the theory of the propagation of low-beta plasma beams across magnetic fields are *Treumann et al.* [1983], *Katz* [1984], *Treumann and Häusler* [1985], and *Cheng* [1987].

Laboratory experiments demonstrating the propagation of low-beta plasma beams or plasmoids across magnetic fields have been performed by *Eubank and Wilkerson* [1961], *Baker and Hammel* [1965], *Lindberg* [1978], *Wessel and Robertson* [1981], and *Robertson et al.* [1981], among others. The work described in the two most recent of these papers demonstrated the relevance of the condition (5.7). It was motivated by eventual practical applications to magnetic confinement fusion, namely the possibilities for using charge-neutral ion beams to heat or drive currents in a fusion reactor, instead of having first to convert them into beams of neutral atoms [*Ott and Mannheimer*, 1977]. Even more recently, a series of experiments covering a range of beta from 0.01 to 100 has been performed by *Li et al.* [1986].

When a low-beta plasma beam or plasmoid propagates across a magnetic field, the plasma on its flanks is eroded. The reason is that, while the plasma at the center of the beam is acted upon by the full polarization field and moves at the velocity  $\mathbf{E} \times \mathbf{B}/B^2$ , the plasma in the boundary layer experiences a lesser field so it lags behind [*Crow et al.*, 1978; *Curtis and Grebowsky*, 1980]. Experimentally, the erosion of a plasmoid traveling across a magnetic field was first observed in the laboratory by *Bostick* [1956]; in space, it was observed dramatically in the AMPTE artificial comet

experiment [Valenzuela *et al.*, 1986]. As a result, the beam or plasmoid is dispersed and ultimately slowed to a halt.

The dispersion and slowing are enhanced if plasma is already present in the magnetic field through which the beam or plasmoid is moving, because currents flowing in this background plasma partially neutralize the space charges on the flanks, reduce the polarization field, and dissipate the kinetic energy of motion [Haerendel and Sagdeev, 1981; Treumann *et al.*, 1983]. In addition, the intense velocity shear in the boundary layer may excite a collisionless form of the Kelvin-Helmholtz instability, enhancing the erosion; at Stanford University a Ph.D. student, D. Cai, is now investigating this possibility theoretically, and a 3-D particle simulation of this and related phenomena is the subject of a pending research proposal by Buneman *et al.* [1986]. The larger the ratio of background plasma density to beam plasma density, the more important these effects are likely to be, and in fact they are conspicuous in beam injection experiments in the ionosphere. In the Porcupine experiments, for instance, beyond 15 m from the source, electric field measurements inside the xenon plasma beam revealed a transverse polarization field of only about 10% of the value corresponding to the initial beam velocity. At these distances, most of the particles were executing their individual motions in the Earth's field. The beam electrons, having gyro-radii of about 10 cm, were virtually 'frozen' to the magnetic field lines, while the ions, with gyro-radii of about 500 m, continued onwards to twice this distance before turning around. This ion beam, though largely charge-neutralized by electrons from the background plasma, carried a net electric current of about 90% of the initial 4 A ion current [Häusler *et al.*, 1986; Sagdeev *et al.*, 1986].

The separation of the beam electrons from the ions had a number of side-effects, the first of which was the creation of a system of intense field-aligned currents of suprathermal electrons. Once the beam electrons had become frozen to the field lines, the only directions in which they could escape from the vicinity of the source were up and down these lines. Häusler *et al.* [1986] have estimated the current density as 140 mA/m<sup>2</sup> in each of the two directions, which is much greater than ever occurs naturally. Moreover, the number density of these electrons on the beam axis, at 4 m

from the source, must have been about  $10^8 \text{ cm}^{-3}$ , which was two to three orders of magnitude larger than the ambient plasma density [Häusler *et al.*, 1986]. Thus, when they emerged from the beam, their space charge could not have been neutralized by ions from the ambient plasma, so their mutual electrostatic repulsion would then have accelerated them along the field lines to suprathermal energies. Since the total energy (in eV) gained by an electron was just the potential difference between the source and the ambient plasma, the source had to acquire a negative potential in order for such acceleration to occur. By this means, the energy given to the electrons was taken from the ions in the beam. Provided that this was the only way in which the ions lost energy, the gain in energy by the electrons could be determined by measuring the mean energy of the ions and comparing it with its nominal value. In this respect, the data from Porcupine were inconclusive, but data from the very similar ARCS 3 experiment (see Table 2) showed clearly that the sub-payload carrying the source became charged to a negative potential exceeding half the initial beam energy [Erlandson *et al.*, 1987]. A quantitative theory of the charging process has yet to be developed.

Independent data supporting this scenario were obtained in the Soviet Aclita rocket experiments (see Table 2), which involved much more intense plasma beams injected more or less perpendicularly to the field [Sagdeev *et al.*, 1981]. On the evidence, the diamagnetic cavity extended 1-10 m from the source, then the beam became electrically polarized and remained so for another 10-20 m, and finally the ions continued alone out to a total distance of about 100 m. The beam was so dense that it could be observed by radar from the ground, and the radar data showed that the cross-field velocity of the ions did not exceed 200-300 m/s, compared with 10 km/s at the source, which may be regarded in retrospect as evidence of strong negative charging of the source. Further relevant data were obtained in the Ariel rocket experiments, where pulsed plasma sources were used [Alexandrov *et al.*, 1981a,b].

The experimental evidence that the electrons in the plasma beam become attached to the field lines, soon after leaving the source, raises the question of how the ion beam is neutralized thereafter. The fact that it is indeed quasi-neutral is confirmed by the absence of the strong electric fields that a non neutral ion beam would

create. Obviously the answer must be that it is neutralized by electrons from the ambient plasma, but this cannot be a simple process. Under the almost collisionless conditions of the Porcupine experiment, for instance, ambient electrons attracted by the positive space charge in the ion beam would be accelerated along the field lines towards the core of the beam, but on reaching it they would have high velocities, relative to their thermal velocities, so their momentum would carry them on through the core and out the other side. Their concentration within the core would actually be less than in the unperturbed plasma far from the beam. In reality, however, some process equivalent to collisions, such as a two-stream instability excited by the counterstreaming of the electrons attracted into the beam from the plasma above and below it, must be acting so as to allow these electrons to become electrostatically trapped inside the beam, and thus to neutralize it.

If the distribution of the beam ions in space were constant in time, the neutralization of the beam would be a transient process, completed very soon after the source of the beam was switched on. But if the source is modulated, or if the vehicle carrying it is spinning or is moving through the plasma, which is usually the case, then neutralization is a dynamic, never-ending process. Continually, electrons from the ambient plasma must flow up and down the field lines, towards points where the beam ion concentration is increasing and away from points where it is decreasing. Thus modulation or motion of the beam gives rise to a complicated pattern of field-aligned currents of thermal electrons, in the region of space formed by the projection of the ion beam up and down the magnetic field lines.

Since the electrons in the beam are diverted into field-aligned currents within a few metres of the source, whereas the ions continue out to distances of the order of their gyro-radius, the currents that these two particle species carry are effectively dumped into the ionosphere at different points. Thus a perpendicularly injected plasma beam acts as a current dipole, and if the beam is modulated it should excite waves. At the lowest frequencies, these would be Alfvén waves. Alexandrov *et al.* have suggested that such waves, interacting with and scattering radiation-belt electrons at energies greater than 40 keV, were responsible for increases observed in the flux of

such electrons precipitating into the ionosphere, coincident with pulsed plasma beam injections, in the Ariel 1 and Ariel 2 experiments. Even larger increases in these fluxes, apparently stimulated by the plasma beam, were observed in the Aelita experiments and reported by Sagdeev *et al.*, who, however, preferred the view that they were due to ionospheric electrons accelerated by some unspecified collective process accompanying beam injection.

As the beam ions travel through the background plasma, they excite a variety of electrostatic plasma waves propagating more or less perpendicularly to the magnetic field. In the Porcupine experiments, ion cyclotron harmonic waves excited by the xenon ion beam were observed at frequencies up to about 16 kHz [Jones, 1981; Kintner and Kelley, 1981]; they occurred at harmonics of the local proton gyrofrequency, and were particularly intense around the local lower hybrid frequency. Kintner *et al.* [1986] have compared the plasma waves observed, under similar conditions, in the Porcupine and ARCS series of rocket experiments. In the Meteor satellite experiments, a xenon plasma beam was injected into the ionosphere in the direction of orbital motion, and excited intense waves in the 5-20 kHz band [Grebnev *et al.*, 1981]. Ionospheric  $O^+$  ions, after having passed through the turbulent plasma beam, arrived at the satellite with their energy spectrum broadened; this effect became more and more pronounced as the beam velocity vector approached the plane perpendicular to the magnetic field. The mechanisms by which these low-frequency waves are generated are fairly well understood, qualitatively at least [Kintner and Kelley, 1983; Roth *et al.*, 1983; Hudson and Roth, 1984; Malingre and Pottelette, 1985]; weaker waves accompanying plasma beam injections have also been observed at higher frequencies, in the whistler-mode frequency band between the lower hybrid frequency and the electron gyrofrequency [Thiel *et al.*, 1984], and also around the plasma and upper hybrid frequencies [Pottelette *et al.*, 1984], but their generation mechanisms are still uncertain.

Related data from the SEPAC experiment on Spacelab-1 have been presented by Sasaki *et al.* [1986]. Whenever the MPD arcjet injected a plasmoid into the ionosphere, there was a burst of waves with its spectral peak near the lower hybrid



frequency. Additionally, when the plasmoid was injected in the direction of orbital motion, and the component of the orbital velocity perpendicular to the magnetic field exceeded about 6 km/s, there was an enhancement of local plasma density lasting several tens of milliseconds. The SEPAC experimenters believe that this was produced by Alfvén's critical velocity ionization process: the nonlinear waves are assumed to heat some of the electrons present, which then ionize some of the neutral gas [Alfvén, 1954]. The duration of the plasma density enhancement indicates that, before the neutral gas in question became ionized, it must have been moving with the Shuttle, so it must have been either atmospheric gas escaping from the payload bay, or neutral argon emitted by the MPD arcjet. Even after it became ionized, it would have continued to move with the Shuttle through polarization of the plasma cloud, and some independent evidence for the existence of the electric polarization field was found.

Summarizing, the injection of a plasma beam perpendicularly to the Earth's magnetic field modifies the ionosphere by introducing new plasma, by setting up a system of intense field-aligned currents of suprathermal electrons, and by creating plasma turbulence, primarily at low frequencies; in some special situations, the turbulence can lead to electron heating and hence to ionization of the neutral gas.

### 5.3.2. Beams Injected Parallel to the Field

With the exceptions of Araks and Porcupine, all the space experiments listed in Table 2 involved plasma beams injected parallel as well as perpendicular to the Earth's magnetic field. The most recent series of rocket experiments, ARCS 1-3, was planned so as to provide good data for comparing the effects of parallel and perpendicular injections under otherwise similar circumstances [Kintner *et al.*, 1986].

With parallel injection, the initial behavior of the beam just after it has emerged from the source is much the same as it is with perpendicular injection: at first the beam expands freely, pushing the magnetic field before it, but then the field diffuses back into the beam faster than classical processes would allow. The subsequent evolution of the magnetized beam is simpler, however, because with parallel injection

there is no conflict between the individual and collective behavior of the plasma particles. Both the ions and the electrons can move freely along the field lines, so their joint parallel motion does not lead to any charge separation. If collisions with neutral particles and ionospheric ions are negligible, the plasma cloud expands freely in the direction parallel to the field, as into a vacuum, but if collisions are appreciable they slow down the expansion, rendering it diffusive.

Because the expansion can proceed more freely in the parallel direction than perpendicularly, and because most of the plasma sources used in space experiments produce rather broad beams (cone angle 30–60°), it can happen that even in an experiment with nominally perpendicular injection, the resulting plasma cloud extends further along the field than across it. In the Aclita experiments, for instance, the cloud was about 1 km long compared with 70–100 m in the perpendicular direction; the ion concentration within it was about  $10^6 \text{ cm}^{-3}$ , substantially greater than in the ambient E region.

The fact that the electrons and ions in the beam can travel together along the field, with nothing but collisions to stop them, means that a parallel beam injection does not create the system of intense field-aligned currents that a perpendicular injection does. Correspondingly, the strong negative charging of the source that the ARCS 3 experimenters observed with perpendicular injection (see §5.3.1) was not observed with parallel injection [Erlandson *et al.*, 1987].

Plasma beam injections parallel to the field excite low-frequency plasma waves, but generally these are weaker than those accompanying perpendicular injections [Grebner *et al.*, 1981; Erlandson *et al.*, 1986]. A curious effect apparently related to wave excitation was observed in the ARCS 1 rocket experiment and was reported by Moore *et al.* [1982]: this experiment was performed in the auroral zone, and operation of the plasma gun within an auroral arc produced striking enhancements in the natural fluxes of precipitating electrons at energies below 1 keV. These data can be explained by assuming that all downcoming energetic electrons had been accelerated by a parallel electric field in the plasma above the rocket, and the most plausible means for creating such a field appears to be anomalous plasma resistivity

due to small-scale turbulence. The anomalously enhanced resistivity would offer an obstacle to the local auroral current, the major part of which is assumed to be directed upwards in the conventional sense, and carried by downcoming thermal electrons which, unlike the more energetic ones, are strongly scattered by the turbulent waves. Because the enhancements of the energetic electron fluxes were equally strong for parallel and for perpendicular beam injection, *Kaufmann et al.* [1985] have argued that the instabilities leading to plasma turbulence were created not by the ion beam, but by the associated system of field-aligned electron currents; this must be regarded as uncertain, however, since the later results from the ARCS 3 experiment suggest that these field-aligned currents also are weaker for parallel injection, as already mentioned [*Erlandson et al.*, 1987].

Many laboratory experiments on the propagation of plasma beams parallel to magnetic fields were made in the 1960's, to investigate the possibility of filling mirror or cusp fusion machines with plasma by injecting it through the open ends [*Tuck*, 1959; *Gilco*, 1961; *Scott and Voorhes*, 1961; *Jensen*, 1968]. A more recent series of experiments, concentrating on the physics of the interaction between the plasma and the field, was carried out by *Robertson* [1981, 1983], who showed that high-beta beams can be guided, focussed, and compressed by axial magnetic fields. In general, the behavior of a plasma beam close to its source is easier to investigate in the laboratory than in space, and this is particularly true of beams injected parallel to the field, since, unlike perpendicularly injected beams, they do not result in the production of field aligned currents; these, when they encounter the walls of the experimental device, might cause the beam to behave differently than it would in space.

#### 5.4. Possible Future Experiments

Some suggestions are made below for future ionospheric modification experiments that could be performed using either rockets, or a Space Shuttle, or the future Space Station, whichever is available and is the most appropriate. The experiments have been divided into two categories, low-beta and high-beta. As mentioned above, the plasma beams used in all previous experiments of this kind have had  $\beta \ll 1$ , except

very close to the source. There have been many such experiments, so it is less easy to suggest new ones at low beta than at high beta; the latter, however, would require the development of new and powerful plasma sources.

#### 5.4.1. *Low-beta experiments*

Let us begin by examining the possibility of using plasma beams to produce new ionization in the lower ionosphere, especially artificial plasma density structures like those that can be created by energetic electron beams, as described in Section 3. New ionization would be produced by collisions between ions in the beam and neutral atmospheric particles. In terms of new ionization produced per joule of energy expended, energetic ions are no more and no less efficient than energetic electrons: in either case, the energetic particle loses about 35 eV per electron-ion pair created [Banks and Kockarts, 1983]. Moreover, the ionization cross-sections for energetic electrons and positive ions are more or less the same if particles of the two species are compared at the same velocities. These statements, however, refer to electrons with energies above about 300 eV, in comparison with protons above about 0.5 MeV, or with heavier ions above even higher energy thresholds, proportional to their masses.

There is a dearth of information in the literature about the production of ionization by ions with lower energies. However, *Ishimoto et al.* [1986] have considered the possible ionospheric effects, including ionization, that may be produced by energetic  $O^+$  ions precipitated from the ring current, and having energies in the range 0.7–20 keV; such energies could be attained by artificial plasma sources. These authors find that over 80% of the energy of the precipitated ions is lost as heat in the neutral atmosphere, and that the proportion of the energy that actually goes into producing new ionization is 4.6% at 20 keV but only 2.3% at 2 keV; the ionization rate peaks at about 200 km altitude.

At still lower energies, positive ions from a plasma source are even less efficient at producing new ionization, but on the other hand the injected plasma itself can constitute a significant ionospheric perturbation. In the Soviet Aelita experiments, for instance, the density of the injected plasma cloud was at least an order of magnitude

greater than that of the ionospheric plasma at the same altitude, so it was readily observable by radar (see §5.3.1). Conceivably, a pulsed plasma beam could be used to produce periodic plasma density structures, similar to those that *Banks and Gilchrist* [1985] have suggested might be produced by means of pulsed electron beams. This procedure would enable such structures to be produced at higher altitudes; assuming plasma injection parallel to the magnetic field, they would extend from the altitude of injection to a distance of the order of the ionic mean free path.

We turn now to possible future experiments in the lineage of the Porcupine, ARCS, and SEPAC experiments described in §5.3. Among the many effects that plasma beam injections were observed to produce in these experiments, the following are by no means well understood: charging of the vehicle carrying the source; charge-neutralization and depolarization of the beam; instabilities of the beam-ionosphere interface, and erosion of the flanks of the beam; generation of whistler-mode and high-frequency waves. These particular effects cannot, perhaps, be classed as 'ionospheric modification', but others related to them, and equally in need of clarification, certainly come under this heading. Examples are the creation of a system of field-aligned electron currents, and modification of the spectrum of low-energy ( $< 1$  keV) electrons precipitating into the auroral ionosphere; from §5.3.2, it will be recalled that anomalous resistivity due to beam-induced plasma turbulence has been suggested as the cause of the electron energy spectrum modifications, and this plasma resistivity enhancement, if it exists, could also be considered as an ionospheric modification.

In considering the possible directions for future ionospheric modification experiments using low-beta plasma beams, there is, perhaps, a lesson to be learned from experiments with electron beams. Though very many such experiments had been performed previously with rockets (many more than are listed in Table 1, which refers only to experiments at energies from 10 keV upwards), the Spacelab-2 experiment, in which the Shuttle carrying the electron gun circled around the free-flying Plasma Diagnostic Package (PDP), produced numerous original results, particularly concerning the mechanisms of wave generation [*Gurnett et al.*, 1986]. This consideration suggests that a similar experiment using the Shuttle and the PDP, but with a plasma

beam source in place of the electron gun, might be equally helpful in clarifying the ionospheric effects of plasma injections.

In this connection, a need exists for the development of new diagnostic instruments, capable of measuring plasma properties that are not presently accessible. One example is the local field-aligned current density, which should be measured in support of the study of beam neutralization processes, and also for evaluating perpendicularly-injected plasma beams as potential sources of Alfvén wave radiation (see §5.3.1). Another is the resistivity of the plasma, measurements of which are needed in order to test one theory of the origin of beam-induced enhancements of low-energy auroral electron precipitation (see §5.3.2). Instruments for measuring field-aligned current density [Storey and Thiel, 1978; Illiano and Pottelette, 1979] and plasma resistivity [Storey and Malingre, 1976] have been designed, and preliminary tests of them have been made in space with encouraging results [Storey and Cairo, 1983; Storey and Thiel, 1984], but further development is needed before they can be considered as operational; the sensor system required for the resistivity measurement is little more than a pair of crossed double-sphere dipoles, with which the existing PDP is already equipped.

The experiments proposed above could be performed from the future Space Station as well as from the Shuttle, and indeed better because of the higher power available. The ingenious proposal by Stenzel [1985], mentioned at the end of §5.2.6, should also be borne in mind. Some of these experiments would require a free-flying PDP to measure the resulting ionospheric modifications; clearly, for use with the Station, the PDP would have to be maneuverable.

#### 5.4.2. High-beta experiments

The experiments to be proposed in this category are, for the most part, novel, at least in the sense that none like them has been performed before in low Earth orbit. Indeed, the means to perform them have not been available. Natural plasma has  $\beta < 0.5\%$  in the ionosphere. Artificial plasma beams have  $\beta < 1$ , except within a few metres of the source, for presently available sources and for the magnetic field

strengths that exist in the ionosphere. On the other hand, a few high-beta plasma experiments have been performed most successfully in space, notably the AMPTE series mentioned in §5.2.6 and §5.3.1., but for this it was necessary to go much further away from the Earth, where the natural magnetic fields are very much weaker. Our suggestion is that, with the aid of new plasma sources, equivalent experiments could be performed in the ionosphere from the Space Shuttle or, preferably, the Space Station.

The need for new plasma sources follows from considerations of scaling, which we can illustrate by examining the possibility of scaling the AMPTE artificial comet experiment [Valenzuela *et al.*, 1986] down from the solar wind to the ionosphere. In this experiment, the plasma source was a barium canister, which released about 2 kg of neutral Ba atoms. This neutral Ba vapor cloud expanded at a velocity estimated as 1.35 km/s, while becoming ionized by solar radiation on a time scale of  $\sim 30$  s. The resulting plasma cloud, containing about  $10^{25}$  Ba<sup>+</sup> ions, then continued to expand, pushing away the interplanetary magnetic field before it. On the sunward side and on the flanks of the cloud, the magnetic field was compressed as a result of 'draping' of the field lines, which occurred because the speed of the solar wind was faster than the Alfvén speed. The cloud attained its maximum diameter of  $\sim 100$  km after  $\sim 60$  s, when there was approximate balance between the kinetic pressure of the Ba<sup>+</sup> ions and the magnetic pressure of the compressed interplanetary field, which was measured as 120–130 nT [Lühr *et al.*, 1986]; prior to the barium release, its unperturbed value was 10 nT. From then on, the magnetic field penetrated back into the cloud at a speed of  $\sim 4.5$  km/s, which is much faster than it could have done by classical diffusion. Though the mechanism of fast penetration is not yet understood, Hacrendel *et al.* [1986] have assumed that it is related to the so-called 'snow-plow' process [Krall and Trivelpiece, 1973], for which the velocity would be

$$v_{SP} = \frac{2B_c}{\sqrt{\mu_0 \rho_c}}, \quad (5.8)$$

where  $B$  is the magnetic field strength,  $\rho$  is the mass density in the cloud, and the subscript 'c' refers to the compressed values. This formula yields a value in good

agreement with the observed one, so we shall adopt it as a basis for our scaling.

For the sake of argument, let us assume that, in low Earth orbit, a manageable value for the final diameter of the cloud would be 100 m, instead of the 100 km attained in the solar wind. Provisionally, however, we shall leave all the other aspects of the experiment unchanged, so as to see what conclusions this leads us to. Thus we take the plasma cloud to be formed of barium ions, expanding initially at 1.35 km/s, in which case it would attain its assumed full size after 37 ms. In the ionosphere, satellite orbital velocities are sub-Alfvénic (the minimum value of the Alfvén velocity, which occurs at the level of maximum density in the F region, is about 130 km/s), so the magnetic field at the surface of the cloud would not be compressed by more than a factor of 2; we take the compressed field to be  $B_c = 5 \times 10^{-5}$  T. Assuming that, momentarily, the magnetic field is wholly expelled from the volume occupied by the cloud, the energy required to create this diamagnetic cavity is 520 joules. Using the formula on p. 701 of the paper by *Valenzuela et al.* [1986], the total mass of barium in the cloud is estimated as  $2.85 \times 10^{-4}$  kg, and correspondingly the total number of barium ions is  $1.25 \times 10^{21}$ ; the mass density is  $\rho_c = 5.5 \times 10^{-10}$  kg/m<sup>3</sup>, and the number density  $2.4 \times 10^{15}$  m<sup>-3</sup>. As soon as the cloud had been formed, the compressed magnetic field would start to return. According to (5.8), the field would penetrate into the cloud at a velocity  $v_{SP} = 3.8$  km/s, so it would reach the center in 13 ms. Since this penetration time is less, by a factor of  $\sim 3$ , than the expansion time, it is questionable whether indeed a diamagnetic cavity would be formed, though the figures certainly imply that the magnetic field would be reduced significantly at the center of the cloud; however, since we are unsure of the mechanism of penetration and even more so of its scaling laws, we should regard all these figures as provisional and leave the question open.

This scaled-down version of the AMPTE artificial comet experiment would require only quite reasonable amounts of matter and energy, but in one crucial respect it is clearly infeasible: the material from which the plasma cloud is formed cannot be neutral barium vapor, since the time required for barium atoms to become photoionized in sunlight (see above) is much longer than the time of expansion of the cloud.



The AMPTE experiment itself was marginal in this respect, which worsens as the spatial scale is reduced. Hence the key to scaling the experiment down is to replace the impulsive source of ionizable neutral vapor by an impulsive source of fully ionized plasma.

Unfortunately, however, none of the plasma sources described in §5.2 has the spherical symmetry that the experiment requires. Two courses of action are therefore open to us: either we envisage the use of a completely new type of plasma source, or we change the design of the experiment so that one of the previously described types of source could be used. We shall now consider these two possibilities in turn.

Laboratory experimenters have already devised at least one way of creating, almost instantaneously, a spherically symmetrical cloud of fully ionized plasma. This is the method used in experimental research on inertial confinement fusion, and it consists of ionizing a pellet of some suitable material by irradiating it with an intense burst of electromagnetic energy from a powerful laser. By this means, but with less intense laser beams than are required for fusion research, some experimenters have already demonstrated the formation of diamagnetic cavities in magnetic fields [Kitsunetzaki *et al.*, 1974; Pechacek *et al.*, 1980]. In both of these sets of experiments, the pellet was made of solid deuterium, which is the material favored in fusion research, and fully diamagnetic ( $\beta \gg 1$ ) cavities were formed. In the more recent of the two sets, the pellet was a cylinder of D<sub>2</sub> ice, 1 mm long and 1 mm in diameter, and the plasma was formed from it by two-stage laser irradiation. First it was vaporized by a pulse from a 100 joule (J) neodymium-glass laser, and then, 2  $\mu$ s later, it was ionized and heated by another pulse from a 1 kJ gain-switched CO<sub>2</sub> laser. Holographic interferometry showed that the resulting plasma contained about  $2 \times 10^{19}$  electrons, which corresponded closely to the number of atoms originally in the pellet, and confirmed that the ionization was almost 100%; the velocity of expansion of the plasma was about  $7 \times 10^4$  m/s. The applied magnetic field was about 0.2 T, but it was non-uniform, being designed so as to confine the plasma and prevent it from reaching the walls of the vacuum chamber; the expanding plasma cloud attained its maximum diameter of about 30 cm after about 2  $\mu$ s. The number of ions in this laboratory

plasma cloud, and the energy required to create it, were similar to those for the cloud created in space by the MPD arcjet in the SEPAC Spacelab-1 experiment (see §5.1).

Accordingly, it is interesting to see what sized cloud would be produced if this laboratory experiment were to be transposed to space as it stands. By inserting the figures from the last paragraph into the argument developed earlier, in the next paragraph after the equation (5.8), we find that the plasma cloud would expand to a maximum diameter of 86 m in 0.6 ms; the plasma density would then be  $6 \times 10^{13} \text{ m}^{-3}$ , corresponding to a plasma frequency of about 70 MHz, so this artificial plasma cloud would constitute a major ionospheric modification. Its size would be much the same as we had envisaged for our scaled-down version of the AMPTE experiment: increasing the diameter to our nominal 100 m would require the mass of the pellet and the energy of the laser pulses to be increased by 60%. On the other hand, the expansion of the deuterium plasma cloud would be much faster than that of the barium cloud that we were considering earlier, which is partly because the deuterium ions are lighter, but mainly because the laser-produced plasma is hotter. The rapidity of the expansion ensures that a true diamagnetic cavity would be formed, and even 0.6 ms is a sufficient time to allow good measurements to be made by a PDP inside the cloud.

Thus, using laser-produced plasma clouds, it seems entirely feasible to perform AMPTE-type experiments in low Earth orbit. A typical experiment might proceed as follows. A pellet of ionizable material is ejected from the main spacecraft, and its subsequent motion tracked by lidar. When the pellet has reached a suitable position in relation to a free-flying PDP, it is vaporized and ionized by pulses from a high-power laser system. The PDP then measures the dynamic phenomena associated with the evolution of the plasma cloud, and relays the data back to the main spacecraft. A low-power radar mounted on this spacecraft measures the radius of the cloud versus time after firing the lasers. Such an experiment could be performed either from the Shuttle or from Space Station.

A preliminary design study, including some laboratory research, would be required in order to determine the best conditions for this experiment. The laboratory effort

would be aimed at finding the best combination of laser and pellet, and the question of how to eject the pellet should also be addressed. Devices have been built that accelerate pellets of solid hydrogen or deuterium to speeds of up to 2 km/s; they are intended for fueling magnetic confinement fusion reactors such as tokamaks [Combs *et al.*, 1986; Honig *et al.*, 1986; Schuresko, 1986]. However, these materials would be inconvenient to manipulate in orbit, and should be avoided unless hydrogen or deuterium plasmas are specifically required, so thought should be given to the choice of an alternate material for the pellet. With plasmas formed from heavy atoms, the expansion of the cloud would be slower, so there would be more time to perform the diagnostics; moreover, with a suitable choice of pellet material the cloud might be visible, either by scattered sunlight, or at night by illumination from the spacecraft.

The scientific objectives of such an experiment would be similar to those of AMPTE itself, namely to investigate the phenomena that occur when a high-beta plasma cloud is created within a pre-existing magnetoplasma. These include the motion, deformation, and dispersion of the cloud, the formation of a diamagnetic cavity, and the non-classical penetration of the magnetic field back into this cavity. They are relevant to cometary physics, and have other applications as well.

Now, however, we shall address the question of whether some of these objectives, and in particular the clarification of the mechanism of magnetic field penetration into a high-beta plasma, could not be achieved in differently designed experiments, using plasma sources of more conventional kinds such as those described in §5.2.

The difficulty about studying magnetic field penetration is that it is often a transient process, taking place so rapidly that there is insufficient time for making detailed diagnostics. Now, one general experimental approach to transient phenomena (much used, for instance, in measuring the rates of rapid chemical reactions) is to study them in a flow. By this means, rapid temporal variations are transformed into spatial variations along the flow. In the present instance, this means that we should study magnetic field penetration by examining the question of how a field penetrates into a flowing plasma, i.e., a beam. Of course, such experiments would have to be performed under high-beta conditions, meaning that the beam, as it emerges from its source,

must be sufficiently dense and sufficiently energetic to exclude the field altogether. Such conditions were indeed created in the Aelita and Porcupine rocket experiments (see §5.3.1). In those experiments, however, the beams were injected into the ionosphere perpendicularly to the magnetic field, and the penetration was so rapid as to be complete within a few metres of the source. In the Aelita experiments, no provision appears to have been made for measurements in this region of space, while in the Porcupine experiments, the plasma source was on a sub-payload ejected from the main payload at  $\sim 3.5$  m/s, so there was very little time for such measurements. It would be worthwhile to perform similar experiments with better diagnostics in the region close to the source, and even more so, to perform some new experiments with beams injected parallel to the field.

Assuming a Shuttle-borne experiment, with a high-beta plasma beam source mounted on a pallet and directed perpendicularly to the Earth's magnetic field, the best way to investigate the penetration of the field into the beam would certainly be by means of an instrument package on the end of the Remote Manipulator System (RMS). One of the lessons learned from the electron beam experiment on Spacelab-2 is that a free-flying PDP, while an excellent device for making measurements a few hundred metres from the Shuttle, is unhelpful for investigating phenomena such as BPD that may occur within a few metres of the source. Of course, the PDP itself was mounted on the RMS during the Shuttle STS 3 mission in March 1982, and was indeed used for just this purpose [Shawhan *et al.*, 1984]. However, its instrumentation was not entirely suitable; for instance, the electric field antennas were larger than the wavelengths of some of the electrostatic waves that are thought to be a feature of BPD. Accordingly, plans for the future Space Plasma Laboratory mission call for an instrument package dedicated to this investigation [Emanuel, 1986]; it will be picked up from the pallet by the RMS, which is 15 m long, and thereby maneuvered through and in proximity to the electron beam. We are now suggesting that a similar dedicated package should be used, in conjunction with the RMS, for experiments on magnetic field penetration into a high-beta plasma beam propagating perpendicularly to the field; the fact that the orbital velocity of the Shuttle is not negligible compared with

the velocity of the beam places constraints on the choice of Shuttle orbit, in order for it to be possible to satisfy the perpendicularity condition simultaneously for the direction of the axis of the beam and for the direction of motion of the plasma within it, which requires that the Shuttle itself be moving perpendicularly to the field.

Needless to say, such experiments also could and should be performed with the beam directed parallel to the magnetic field; here the considerations just evoked imply that the Shuttle would have to be in an orbit of high inclination, and the experiments performed at low latitudes, at places where orbital motion is parallel to the field. With parallel injection, however, the magnetic field is likely to penetrate the beam more slowly than it does for perpendicular injection, and its penetration may be accompanied by filamentation of the beam at long distances. Hence the phenomena of interest would extend further from the source, and should be explored by a free-flying PDP as well as by an instrument package on the RMS.

In the foregoing paragraphs, we have focused our attention on magnetic field penetration, but clearly all the other phenomena associated with plasma beam propagation in the ionosphere, as described in §5.3, need to be investigated for high-beta beams as well as for low-beta ones.

A *sine qua non* for all the proposed experiments with high-beta plasma beams is the availability of suitable plasma sources. Such sources can be and have been built (see Table 2), but not in the USA, where the effort has been directed more towards the development of plasma thrusters for spacecraft propulsion, with some work also on plasma contactors for spacecraft neutralization. Sources developed for these purposes are not necessarily appropriate for space experiments on high-beta plasma beams, so there is an urgent need for research and development on space-qualified, high-power, high-beta plasma sources.

An investment in high-beta plasma research in low Earth orbit might yield unexpected dividends. It is a commonplace that over 99% of the matter in the universe is in the form of plasma, but perhaps it is less widely appreciated that almost all of this plasma has  $\beta > 1$ : natural low-beta plasmas such as exist in Earth's ionosphere are relatively rare. The solar wind plasma in interplanetary space has  $\beta \simeq 1$ , but

since its flow velocity is so much higher than the ion thermal velocity, it behaves as a high-beta plasma in all phenomena engendered by its encounters with the planets (such as bow shocks and magnetopauses, or the ionopause in the case of Venus, which lacks a magnetosphere since it has no intrinsic magnetic field, but has a high-beta ionosphere instead), with comets (bow shocks, plasma tails), and ultimately with the interstellar gas (heliopause). In interstellar clouds, such as those in H-I and H-II regions,  $\beta \simeq 10$  is typical. There are even natural examples of narrow beams of high-beta plasma, some emerging from compact stars within our own galaxy, others from the nuclei of remote, more active galaxies [Blandford, 1986]. While it is doubtful whether such large-scale phenomena could be modeled realistically in low Earth orbit, it is conceivable that some aspects of them could be, and, more generally, any deeper understanding of high-beta plasma physics that could be gained from experimental research in low Earth orbit might well prove to have wider applications.

## 5.5. Summary of Proposed Experiments

### 5.5.1. Artificial Plasma Density Structures

The use of a plasma beam, instead of the electron beam proposed by Banks and Gilchrist [1985], should enable such structures to be created at higher altitudes.

This experiment, and most of the others summarized below, need prior laboratory work to develop a suitable high-power plasma source.

### 5.5.2. Low-Beta Plasma Beam Dynamics

The broad objective of these experiments would be to investigate the phenomena associated with plasma beam propagation through the ionospheric magnetoplasma, which include:

- Penetration of the Earth's magnetic field into the initial high-beta beam;
- Acceleration of the beam electrons to suprathermal energies, and their diversion into field aligned currents;

- Neutralization of the beam ions by ionospheric thermal electrons;
- Generation of electrostatic and electromagnetic waves (Alfvén, ion cyclotron, lower hybrid, whistler-mode, high-frequency);
- Creation of anomalous plasma resistivity.

For the sake of continuity with the majority of the previous rocket experiments, the initial Shuttle experiments now proposed should emphasize beam propagation perpendicular to the magnetic field.

The method of investigation would consist essentially of repeating the Shuttle Spacelab-2 electron-beam experiment, but with a plasma source in place of the electron gun, and with improved diagnostics. The latter would include a small RMS-mounted instrument package, designed for measuring the properties of the beam near to its source. The instrumentation of the free-flying PDP should include devices for measuring plasma resistivity and field-aligned current density; these require further development, which may call for some rocket experiments as well as for laboratory work.

#### *5.5.3. Two-Stream Instabilities*

This proposal is due to *Stenzel* [1985]. Its objective is to create, in a large volume (many tens of  $\text{m}^3$ ) of uniform space plasma, well controlled conditions favoring the excitation of ion-ion interstreaming instabilities, and to measure the properties of the resulting plasma turbulence.

This experiment is proposed for Space Station. It would involve erecting a large flat multi-grid electrostatic probe facing into the ram direction, and biasing the grids in such a way as to reflect a known proportion of the oncoming ionospheric plasma. Diagnostics would be performed by an instrument package mounted on an RMS, plus eventually an instrumented free-flyer.

#### 5.5.4. *High-Beta Plasmoid Dynamics*

These experiments would be low-altitude analogs of the AMPTE artificial comet experiments, and would have the same scientific objectives, especially the study of the non-classical penetration of a magnetic field into a high-beta plasma.

The basis of the experimental method is the sudden formation of a fully-ionized plasma cloud by laser irradiation of a pellet ejected from the Shuttle or from the Space Station. A preliminary study, including laboratory experiments, is needed to identify the most suitable combination of laser and of pellet material, and to develop the pellet ejection system. Diagnostics would be accomplished by a free-flying PDP, and by a radar mounted on the main spacecraft.

#### 5.5.5. *High-Beta Plasma Beam Dynamics*

These experiments would be similar in design to those proposed in §5.5.2, with the difference that they would require the use of a plasma source of much higher power, which has yet to be developed in the USA. Their scientific objectives overlap those of §5.5.4, inasmuch as the main one is to clarify the mechanism of magnetic field penetration into a flowing high-beta plasma. For this reason, the initial experiments should emphasize beam propagation parallel to the magnetic field, a situation in which field penetration is probably a simpler and slower process than it is for perpendicular propagation.

### 5.6. References

- Alexandrov, V.A., *et al.*, Energetic electron fluxes stimulated with pulsed injection of plasma in the ionosphere, *Adv. Space Res.*, 1(2), 141-145, 1981a.
- Alexandrov, V.A. *et al.*, Structure of plasma blobs injected into the ionosphere from a rocket, *Adv. Space Res.*, 1(2), 147-151, 1981b.
- Alfvén, H., *On the Origin of the Solar System*, Clarendon, Oxford, 1954.
- Artsimovich, A.V., *et al.*, Development of a steady plasma engine (SPE) and its use on a 'Meteor' artificial satellite, *Cosmic Res. Engl. Transl.*, 12, 414-429, 1974.



- Askhabov, S.N., *et al.*, Plasma jet from a steady-state Hall electron accelerator, *Sov. J. Plasma Phys.*, *1*, 125-128, 1981.
- Baker, D.A., and J.E. Hammel, Experimental studies of the penetration of a plasma stream into a transverse magnetic field, *Phys. Fluids*, *8*, 713-722, 1965.
- Banks, P.M., and G. Kockarts, *Aeronomy*, Part A, Academic, New York, 1973.
- Banks, P.M., and B.E. Gilchrist, Artificial plasma density structures produced by energetic electron beams from rockets and spacecraft, *Geophys. Res. Lett.*, *12*, 175-178, 1985.
- Bishaev, A.M., and V. Kim, Local plasma properties in a Hall-current accelerator with an extended acceleration zone, *Sov. Phys. Tech. Phys. Engl. Transl.*, *23*, 1055-1057, 1978.
- Blandford, R., Hydromagnetic aspects of active galactic nuclei, in *Magnetospheric Phenomena in Astrophysics*, edited by R.I. Epstein and W.C. Feldman, American Institute of Physics, New York, pp. 24-44, 1986.
- Bostick, W.H., Experimental study of ionized matter projected across a magnetic field, *Phys. Rev.*, *104*, 292-299, 1956.
- Bostick, W.H., Experimental study of plasmoids, *Phys. Rev.*, *106*, 404-412, 1957.
- Boswell, R.W., Very efficient plasma generation by whistler waves near the lower hybrid frequency, *Plasma Phys.*, *26*, 1147-1162, 1984.
- Brown, C.O., and E.A. Pinsley, Further experimental investigations of a cesium Hall-current accelerator, *AIAA J.*, *3*, 853-859, 1965.
- Buneman, O., J.G. Siambis, and L.R.O. Storey, *Plasmoid Equilibrium and Propagation in the Exoatmospheric Environment*, Proposal submitted to the Innovative Science and Technology Office, Strategic Defense Initiative Organization, July 1986.
- Byers, R.C., Private communication to L.R.O. Storey, 1986.
- Cann, G.L., and G.L. Marlotte, Hall current plasma accelerator, *AIAA J.*, *2*, 1234-1241, 1964.

- Cambou, F., *et al.*, General description of the Araks experiments, *Ann. Géophys.*, **36**, 271-283, 1980.
- Chen, F.F., *Introduction to Plasma Physics and Controlled Fusion -- Volume 1: Plasma Physics*, Plenum, New York, 1984.
- Cheng, A.F., Transverse deflection and dissipation of small plasma beams and clouds in magnetized media, *J. Geophys. Res.*, **92**, 55-63, 1987.
- Combs, S.K., *et al.*, Operation of a repeating pneumatic hydrogen pellet injector on the Tokamak Fusion Test Reactor, *J. Vac. Sci. Tech.*, **A4**, 1113-1117, 1986.
- Crow, J.T., A.T. Forrester, and D.M. Goebel, Ion beam propagation across magnetic fields, in *Low Energy Ion Beams 1977*, edited by K.G. Stephens and J.L. Moruzzi, p. 228, American Institute of Physics, New York, 1978.
- Curtis, S.A., and J.M. Grebowsky, Energetic ion beam injection and solar power satellite transport, *J. Geophys. Res.*, **85**, 1729-1735, 1980.
- Dolan, T.J., *Fusion Research*, pp. 501-515, Pergamon, New York, 1982.
- Dorodnov, A.M., Technical applications of plasma accelerators, *Sov. Phys. Tech. Phys.*, **23**, 1058-1065, 1978.
- Emanuel, W., Space Plasma Laboratory configuration assessment, Oral presentation at the SPL Investigators' Working Group Meeting, NASA Marshall Space Flight Center, 22-23 September, 1986.
- Erlandson, R.E., *et al.*, Argon ions injected parallel and perpendicular to the magnetic field, in *Ion Acceleration in the Magnetosphere and Ionosphere*, edited by T. Chang, pp. 201-205, American Geophysical Union, Washington, Geophysical Monograph No. 38, 1986.
- Erlandson, R.E., *et al.*, Initial results from the operation of two argon ion generators in the auroral ionosphere, *J. Geophys. Res.*, **92**, 4601-4616, 1987.
- Eubank, H.P., and T.D. Wilkerson, Plasma motion in a curved magnetic field, *Phys. Fluids*, **4**, 1107-1111, 1961.

- Ferraro, V.C.A., On the theory of the first phase of a geomagnetic storm: a new illustrative calculation based on an idealised (plane not cylindrical) model field distribution, *J. Geophys. Res.*, **57**, 15-49, 1952.
- Fiala, V., A diamagnetic cylindrical equilibrium of ions injected into a magnetized plasma, simulating controlled space experiments, *Plasma Phys.*, **23**, 347-356, 1981.
- Finke, R.C., (Ed.), *Electric Propulsion and its Applications to Space Missions*, published as *Progress in Aeronautics and Astronautics*, **79**, American Institute of Aeronautics and Astronautics, New York, 1981.
- Gilleo, M.A., Flow of low-density high-speed plasma through a magnetic barrier, *Phys. Fluids*, **4**, 1399-1406, 1961.
- Grebnev, I.A., *et al.*, The study of a plasma jet injected by an on board plasma thruster, *Adv. Space Res.*, **1(2)**, 153-158, 1981.
- Green, T.S., Intense ion beams, *Rep. Prog. Phys.*, **37**, 1257-1344, 1974.
- Grossman, W., R.V. Hess, and H.A. Hassan, Experiments with coaxial Hall current plasma accelerator, *ALAA J.*, **3**, 1034-1039, 1965.
- Gussenhoven, M.S., and E.G. Mullen, Geosynchronous environment for severe spacecraft charging, *J. Spacecraft and Rockets*, **20**, 26-34, 1983.
- Gurnett, D.A., *et al.*, Plasma waves associated with the AMPTE artificial comet, *Geophys. Res. Lett.*, **12**, 851-854, 1985.
- Gurnett, D.A., *et al.*, Whistler-mode radiation from the Spacelab 2 electron beam, *Geophys. Res. Lett.*, **13**, 225-228, 1986.
- Haerendel, G., and R.Z. Sagdeev, Artificial plasma jet in the ionosphere, *Adv. Space Res.*, **1(2)**, 29-46, 1981.
- Haerendel, G., *et al.*, First observations of the acceleration of barium ions into the magnetosphere, in *European Programs on Sounding Rocket and Balloon Research in the Auroral Zone*, pp. 203-211, European Space Agency, Neuilly, Special Publication No. 115, 1976.

- Haerendel, G., *et al.*, Dynamics of the AMPTE artificial comet, *Nature*, **320**, 719-722, 1986.
- Hammer, J.H., Reconnection in spheromak formation and containment, in *Magnetic Reconnection in Space and Laboratory Plasmas*, edited by E.W. Hones, pp. 319-331. American Geophysical Union, Washington, Geophysical Monograph 30, 1984.
- Häusler, B., *et al.*, Observations of the artificially injected Porcupine xenon ion beam in the ionosphere, *J. Geophys. Res.*, **91**, 287-303, 1986a.
- Häusler, B., *et al.*, Plasma waves observed by the IRM and UKS spacecraft during the AMPTE solar wind lithium releases: Overview, *J. Geophys. Res.*, **91**, 1283-1299, 1986b.
- Hellinger, L., S. Ridgeway, and A. Schaffer, Transverse traveling wave plasma engine, *AAJ*, **3**, 1028-1033, 1965.
- Heppner, J.P., *et al.*, The Cameo barium releases:  $E_{\parallel}$  fields over the polar cap, *J. Geophys. Res.*, **86**, 3519-3542, 1981.
- Honig, J., K. Kim, and S.W. Wedge, Hydrogen pellet acceleration with a two-stage system consisting of a gas gun and a fuseless electromagnetic railgun, *J. Vac. Sci. Tech.*, **A4**, 1106-1112, 1986.
- Hudson, M.K., and I. Roth, Thermal fluctuations from an artificial ion beam injection into the ionosphere, *J. Geophys. Res.*, **89**, 9812-9822, 1984.
- Ijichi, K., H. Harada, and K. Kuriki, MPD arcjet system for space experiment with particle accelerator (SEPAC), in *Electric Propulsion and its Applications to Space Missions*, edited by R.C. Finke, published as *Progress in Aeronautics and Astronautics*, **79**, pp. 616-630, American Institute of Aeronautics and Astronautics, New York, 1981.
- Illiano, J.M., and R. Pottelle, Measurement of the collective motion of the electrons deduced from the shift of the lower oblique resonance frequency, *Phys. Lett.*, **70A**, 315-316, 1979.

- Ishimoto, M., *et al.*, The role of energetic  $O^+$  precipitation in a mid-latitude aurora, *J. Geophys. Res.*, *91*, 5793-5802, 1986.
- Jahn, R.G., *Physics of Electric Propulsion*, McGraw-Hill, New York, 1968.
- Janes, G.S., and R.S. Lowder, Anomalous electron diffusion and ion acceleration in a low-density plasma, *Phys. Fluids*, *9*, 1115-1123, 1966.
- Jensen, V.O., Experimental investigation of axial plasma injection into a magnetic dipole field, *Phys. Fluids*, *11*, 240-245, 1968.
- Jones, D.,  $Xe^+$ -induced ion-cyclotron harmonic waves, *Adv. Space Res.*, *1(2)*, 103-106, 1981.
- Katz, I., *et al.*, Polarization of spacecraft generated plasma clouds, *Geophys. Res. Lett.*, *11*, 1115-1116, 1984.
- Kaufmann, R.L., *et al.*, Heavy ion beam-ionosphere interactions: electron acceleration, *J. Geophys. Res.*, *90*, 9595-9614, 1985.
- Kintner, P.M., and M.C. Kelley, Ion beam produced plasma waves observed by the  $\delta n/n$  plasma wave receiver during the Porcupine experiment, *Adv. Space Res.*, *1(2)*, 107-115, 1981.
- Kintner, P.M., and M.C. Kelley, A perpendicular ion beam instability: solutions to the linear dispersion relation, *J. Geophys. Res.*, *88*, 357-364, 1983.
- Kintner, P.M., *et al.*, A comparison of plasma waves produced by ion accelerators in the F-region ionosphere, in *Ion Acceleration in the Magnetosphere and Ionosphere*, edited by T. Chang, pp. 206-208, American Geophysical Union, Washington, Geophysical Monograph No. 38, 1986.
- Kitsunezaki, A., M. Tanimoto, and T. Sekiguchi, Cusp confinement of high-beta plasmas produced by a laser pulse from a freely-falling deuterium ice pellet, *Phys. Fluids*, *17*, 1895-1902, 1974.
- Krall, N.A., and A.W. Trivelpiece, *Principles of Plasma Physics*, pp. 123-128, McGraw-Hill, New York, 1973.

- Lary, E.C., R.G. Meyerand, and F. Salz, Ion acceleration in a gyro-dominated neutral plasma -- theory and experiment (Abstract only), *Bull. Amer. Phys. Soc., Ser. III*, 7, 441, 1962.
- Li, R., *et al.*, Propagation of neutralized ion beam in a transverse magnetic field (Abstract only), *Bull. Amer. Phys. Soc., Ser. II*, 31, 1480, 1986.
- Lindberg, L., Plasma flow in a curved magnetic field, *Astrophys. Space Sci.*, 55, 203-225, 1978.
- Lockner, T.R., R.J. Lipinski, and R.B. Miller, Plasmoid propagation, Sandia National Laboratories, Albuquerque, Report No. SAND-85-0917, 1985.
- Lühr, H., *et al.*, *In situ* magnetic field observations of the AMPTE artificial comet, *Nature*, 320, 708-711, 1986.
- Malingre, M., and R. Pottelette, Excitation of broadband electrostatic noise and of hydrogen cyclotron waves by a perpendicular ion beam in a multi-ion plasma, *Geophys. Res. Lett.*, 12, 275-278, 1985.
- Marshall, J., Performance of a hydromagnetic plasma gun, *Phys. Fluids*, 3, 134-135, 1960.
- Menon, M.M., *et al.*, Quasi-steady-state multimewatt ion source for neutral beam injection, *Rev. Sci. Instrum.*, 56, 242-249, 1985.
- Miller, R.B., *An Introduction to the Physics of Intense Charged Particle Beams*, Plenum, New York, 1982.
- Mishin, E.V., V.Y. Kapitanov, and R.A. Treumann, Anomalous diffusion across the magnetic field-plasma boundary: the Porcupine artificial plasma jet, Max-Planck-Institut für Extraterrestrische Physik, Garching, Preprint No. 47, 1986a.
- Mishin, E.V., *et al.*, The influence of a magnetized background plasma and collective effects on the dynamics of a bounded quasineutral ion beam, *J. Geophys. Res.*, Submitted, 1986b.
- Moore, T.E., *et al.*, Anomalous electron distributions due to an artificial ion beam in the ionosphere, *J. Geophys. Res.*, 87, 7569-7579, 1982.

- Moore, T.E., *et al.*, Plasma jet effects on the ionospheric plasma, in *Active Experiments in Space*, edited by W.R. Burke, pp. 207-212, European Space Agency, Noordwijk, Special Publication No. 195, 1983.
- Morozov, A.I., *et al.*, Plasma accelerator with closed electron drift and extended acceleration zone, *Sov. Phys. Tech. Phys. Engl. Transl.*, **17**, 38-45, 1972.
- Morozov, A.I., *et al.*, Caesium plasma source for the Araks experiment, *Space Sci. Instrum.*, **4**, 139-141, 1978.
- Obayashi, T., *et al.*, Initial results of SEPAC scientific achievement, *Earth-Orient. Applic. Space Technol.*, **5**, 37-45, 1985.
- Okabayashi, M., *et al.*, The spheromak, in *Unconventional Approaches to Fusion*, edited by B. Brunelli and G.G. Leotta, pp. 95-134, Plenum, New York, 1982.
- Ott, E., and W. Mannheimer, Cross-field injection, propagation, and energy deposition by intense ion beams, with applications to tokamak plasma heating, *Nucl. Fusion*, **17**, 1057-1065, 1977.
- Papadopoulos, K., On the shuttle glow (the plasma alternative), *Radio Sci.*, **19**, 571-577, 1984.
- Pechacek, R.E., *et al.*, Measurement of the plasma width in a ring cusp, *Phys. Rev. Lett.*, **45**, 256-259, 1980.
- Peter, W., and N. Rostoker, Theory of plasma injection into a magnetic field, *Phys. Fluids*, **25**, 730-735, 1982.
- Pottelette, R., *et al.*, Observations of high-frequency turbulence induced by an artificial ion beam in the ionosphere, *J. Geophys. Res.*, **89**, 2324-2334, 1984.
- Purvis, C.K., and R.O. Bartlett, Active control of spacecraft charging, in *Space Systems and their Interactions with Earth's Space Environment*, edited by H.B. Garrett and C.P. Pike, *Prog. Astronaut. Aeronaut.*, **71**, 299-317, 1980.
- Robertson, S., Compression of an intense space-charge-neutral ion beam by an axial magnetic field, *Phys. Fluids*, 883-884, 1981.

- Robertson, S., Magnetic guiding, focussing, and compression of an intense charge-neutral ion beam, *Phys. Fluids* 26, 1129-1138, 1983.
- Robertson, S., *et al.*, Propagation of an intense ion beam transverse to a magnetic field, *Phys. Rev. Lett.*, 47, 508-511, 1981.
- Roth, I., *et al.*, Simulations of beam excited minor species gyroharmonics in the Porcupine experiment, *J. Geophys. Res.*, 88, 8115-8122, 1983.
- Sagdeev, R.Z., *et al.*, Experiments with injection of powerful plasma jet into the ionosphere, *Adv. Space Res.*, 1(2), 129-140, 1981.
- Sagdeev, R.Z. *et al.*, The current system generated by the Porcupine artificial ion beam in the ionospheric background plasma, Max-Planck-Institut für Extraterrestrische Physik, Garching, Preprint No. 49, 1986.
- Sasaki, S., *et al.*, Gas ionization induced by a high speed plasma injection in space, *Geophys. Res. Lett.*, 13, 434-437, 1986.
- Schmidt, G., Plasma motion across magnetic fields, *Phys. Fluids*, 3, 961-965, 1960.
- Schuresko, D.D., Accelerating hydrogenic pellets to high velocities (Abstract only), *Bull. Amer. Phys. Soc.*, 31, 1441, 1986.
- Scott, F.R., and H.G. Voorhes, Plasma injection into a vacuum magnetic field, *Phys. Fluids*, 4, 600-606, 1961.
- Shawhan, S.D., *et al.*, Wave emissions from dc and modulated electron beams on STS 3, *Radio Sci.*, 19, 471-486, 1984.
- Stenzel, R.L., Oral presentation at the Workshop on Plasma Physics and Fusion Scientific Activity for the Space Station, Rogersville, Alabama, 19-22 May 1985.
- Storey, L.R.O., and M. Malingre, A proposed method for the direct measurement of enhanced resistivity, in *European Programmes on Sounding-Rocket and Balloon Research in the Auroral Zone*, pp. 387-409, European Space Agency, Neuilly, 1976.
- Storey, L.R.O., and J. Thiel, Thermal and field-aligned-drift effects near the lower oblique resonance, *Phys. Fluids*, 21, 2325-2335, 1978.



- Storey, L.R.O., and L. Cairo, An attempt to measure enhanced resistivity in the auroral ionosphere, Private communication, 1983.
- Storey, L.R.O., and J. Thiel, An attempt to measure the field-aligned drift velocity of thermal electrons in the auroral ionosphere, *J. Geophys. Res.*, **89**, 969-975, 1984.
- Thiel, J., *et al.*, Excitation of the lower oblique resonance by an artificial plasma jet in the ionosphere, *J. Geophys. Res.*, **89**, 2385-2387, 1984.
- Treumann, R.A., *et al.*, Dynamics of quasineutral beams, in *Active Experiments in Space*, edited by W.R. Burke, European Space Agency, Noordwijk, Special Publication No. 195, pp. 197-206, 1983.
- Treumann, R.A., and B. Häusler, On the propagation of a dense quasineutral ion beam across a magnetized plasma, *Astrophys. Space Sci.*, **110**, 371-378, 1985.
- Tuck, J.L., Plasma jet piercing of magnetic fields and entropy trapping into a conservative system, *Phys. Rev. Lett.*, **3**, 313-315, 1959.
- Tuczek, H., Acceleration of plasma by electromagnetic fields, in *Plasmas in Space and in the Laboratory*, edited by H.L. Jordan and K. Schindler, pp. 531-557, European Space Research Organisation, Paris, Special Publication No. 20, 1967.
- Valenzuela, A., *et al.*, The AMPTE artificial comet experiments, *Nature*, **320**, 700-723, 1986.
- Wessel, F., and S. Robertson, Polarization of an intense space-charge-neutral ion beam incident upon a magnetic field, *Phys. Fluids*, **24**, 739-745, 1981.

### Addendum

As this report was going to print, the authors' attention was called to the following paper, which describes a rocket experiment with a positive ion beam not neutralized by electrons. The purpose of the experiment was to study spacecraft charging, and the ionospheric effects of the beam were not investigated.

Cohen, H. A., *et al.*, Spacecraft charging due to positive ion emission: An experimental study, *Geophys. Res. Lett.*, 6, 515-518, 1979.

The abstract is reproduced below:

"Results have been obtained from the flight of a sounding rocket payload instrumented to determine the cause and extent of charging of vehicles in the ionosphere during the ejection of energetic charged particles. Vehicle potential was measured using several independent probes while beams of positive ions or electrons were ejected. Positive and negative potentials were created by the ejection of electrons and positive ions respectively. For constant ion currents of 8 microamperes and energies of 1 keV, vehicle potentials ranged from volts to hundreds of volts, depending on ambient plasma density but independent of neutral density and vehicle pitch angle. A maximum vehicle potential greater than 1 keV was obtained during an emission of 400 microamperes of 2 keV positive xenon ions."

## 6. IONOSPHERIC MODIFICATION BY X-RAYS AND EUV RADIATION

### 6.1. Introduction

In this chapter we consider two new methods of ionospheric modification by means of X-rays, or more generally by means of a combination of X-rays and extreme ultraviolet (EUV) radiation. The methods differ in their source of X-rays and in the presence or absence of collimation of the X-ray beam. One of the methods makes use of an infrared laser beam to generate X-ray/EUV radiation. The beam is focussed on a tantalum (or other heavy metal) target, with the X-ray/EUV radiation so generated being collimated into a narrow beam by means of reflection at grazing incidence from a metal paraboloid. The other method makes use of the high-energy electron beam ( $E_e \approx 5$  MeV) considered in Chapter 4: metal targets are scattered into the beam and X-ray radiation produced by the electrons impinging upon the targets. The X-ray radiation generated by this second method is not collimated. Some variations of these basic methods are feasible. For example, the collimation step in the first method could be omitted and the uncollimated X-ray/EUV radiation used for modification. However, we will not discuss these variations in detail. Further, of the two methods proposed here, we will only consider the infrared laser/collimated X-ray beam method in depth, since the technology, although new, has been tested in the laboratory and appears to have immediate promise for application in space. The relativistic electron beam method exploits developing technology, has certain distinctive features in the form of the ionospheric modification that it produces, and appears to be feasible, but it will require more development before it can be considered to be practicable.

It will be seen that one of our X-ray sources involves the use of a laser, but it is not an X-ray laser. It is well known that the United States has considered the development of a space-based X-ray laser that is energized by a nuclear explosion and whose purpose is to incapacitate ballistic missiles. The X-rays from such a laser could well create significant modification effects in the ionosphere, or upper atmosphere

sphere generally. However, in this report we do not consider such an X-ray source, since its application to upper atmosphere research does not appear to be feasible and our purpose is to investigate sources that will have their primary application in such research. We might point out at this time, however, that Stanford University has helped pioneer the development of short wavelength lasers and currently has an ultraviolet laser in operation. Such a laser could be used on a rocket or other spacecraft for modification of the ionospheric plasma, but its use will not be considered further here.

The lower ionosphere is largely created by X-rays from the sun, with some assistance from solar ultraviolet radiation and, at the lowest altitudes (D-region), from cosmic rays. The E-region is believed to be generated mainly by soft solar X-rays (wavelengths in the range 10-100 Å; the X-ray designations are defined in Table 1), and hard solar X-rays are an important source of ionization in the D-region during periods of high solar activity [Whitten and Poppoff, 1965]. Man-made X-rays therefore have a very natural application to ionospheric modification and a controlled source of X-rays in the upper atmosphere would enable features of the naturally-occurring ionospheric generation process to be studied experimentally for the first time. Solar ultraviolet light also contributes significantly to the formation of the ionosphere, particularly the intense Lyman- $\alpha$  line (1216 Å), which penetrates deeply and contributes significantly to D-region ionization, and the Lyman- $\beta$  line (1025 Å), which contributes to E-region ionization. A man-made source of UV radiation in the ionosphere would have many basic science applications as well as having an obvious application to ionospheric modification.

Table 1 defines the soft and hard categories of X-rays, and gives the wavelength range for extreme ultraviolet (EUV). The various designations vary between authors and, in the present competitive environment for the production of shorter wavelength lasers, and for the development of X-ray lasers in particular, it is not unusual to find the wavelength limit for X-rays being moved up into what is defined as the EUV range in Table 1. The wavelength ranges in the table are those most commonly given, and we will generally adhere to its terminology. The data in Tables 2a and

**Table 1.** X-ray and Extreme Ultraviolet (EUV) wavelength ranges (where  $1 \text{ \AA} = 10^{-10} \text{ m} = 0.1 \text{ nm}$ ).

| Description | Wavelengths ( $\text{\AA}$ ) | Wavelengths (nm) |
|-------------|------------------------------|------------------|
| Hard X-rays | 0.1 - 1                      | 0.01 - 0.1       |
|             | 1 - 10                       | 0.1 - 1          |
| Soft X-rays | 10 - 100                     | 1 - 10           |
| EUV         | 100 - 1,000                  | 10 - 100         |

2b supplement the wavelength ranges given in Table 1. They show, respectively, the photon energies for electromagnetic waves with wavelengths in the range 0.01–1000  $\text{\AA}$ , and the wavelength ranges for photon energies in the range 10 eV to 1.0 MeV. The energies are given in electron volts, the conversion factor for joules is  $1 \text{ eV} = 1.6022 \times 10^{-19} \text{ J}$ , and  $E(\text{eV}) = 12,399/\lambda(\text{\AA})$ .

## 6.2. Absorption of X-Rays

Several different physical processes contribute to X-ray absorption in matter; they differ in relative importance depending on the photon energy  $h\nu$ , where  $h$  is Planck's constant and  $\nu$  is frequency, and on the atomic number of the particular atoms involved. The following three processes are the most important for the absorption of X-rays in the upper atmosphere [Culhane and Sanford, 1981]:

(1) *The Photoelectric Effect.* This effect is responsible for the most important absorption process for the X-rays considered in this report. In the photoelectric effect, the X-ray photons remove bound electrons from the atoms of the absorbing material and the electrons released from the atoms acquire and carry off the photon energy. The photoelectric absorption cross-section decreases with photon energy for a given absorber, and increases with atomic number for a fixed photon energy. Light, low atomic number elements like hydrogen and carbon are therefore much less effective absorbers than are the heavy elements. However, it is the total number of atoms in the path of the X-rays that determines the overall reduction in their intensity. As a

**Table 2a.** A table relating wavelength  $\lambda$  measured in Angstrom units ( $\text{\AA}$ ) to photon energy  $E$  in electron volts (eV).

| $\lambda$ ( $\text{\AA}$ ) | $E$      |
|----------------------------|----------|
| 0.01                       | 1.24 MeV |
| 0.1                        | 124 keV  |
| 1.0                        | 12.4 keV |
| 10                         | 1.24 keV |
| 100                        | 124 eV   |
| 1000                       | 12.4 eV  |

**Table 2b.** A table relating photon energy  $E$  in electron volts (eV) to wavelength  $\lambda$  measured in Angstrom units ( $\text{\AA}$ ).

| $E$     | $\lambda$ ( $\text{\AA}$ ) |
|---------|----------------------------|
| 1.0 MeV | 0.0124                     |
| 100 keV | 0.124                      |
| 10 keV  | 1.24                       |
| 1 keV   | 12.4                       |
| 100 eV  | 124                        |
| 10 eV   | 1240                       |

result, although a gas has many fewer atoms per unit volume than a solid, an X-ray beam can be absorbed quite effectively in a gas if the beam traverses a long path.

(2) *The Compton Effect.* Compared with the photoelectric effect, the Compton effect becomes significant at higher photon energies ( $h\nu > 50$  keV). These photon energies are much greater than the energy that binds the electrons in atoms and the target electrons may be thought of as being virtually free. The effect can be regarded simply as the collision of a photon with an electron: the incoming photon collides with and gives up some of its energy to one of the atomic electrons and leaves the interaction site at some angle to its original direction. The recoiling electron leaves in a direction that makes an angle with the original photon path and carries away momentum equal to the momentum difference between the original and outgoing photon. For a given element, the Compton effect takes over increasingly from the photoelectric effect as the photon energy increases. The process does not totally stop the incoming photons, but redirects or scatters them and reduces their energy. However, the total cross section for the interaction gives a valid measure of the likelihood of an X-ray being removed from the beam direction.

(3) *Pair Production.* At even higher photon energies ( $h\nu > 1$  Mev) than those involved in the photoelectric and Compton effects, it is possible for a photon to interact with matter in such a way that it disappears and is replaced by an electron-positron pair. This third process is known as *pair production*, and it takes place in the region of electric field around an atomic nucleus. The cross section increases with the square of the atomic number ( $Z$ ) of the material in which the interaction takes place. This may be attributed to the size of the region of strong electric field around the nucleus also increasing with  $Z^2$ . A roughly equal division of photon energy between the electron and the positron is the most likely outcome.

The X-ray photons of primary interest in this report are those generated by an infrared laser beam and their energies are currently on the order of a few keV or less. As a consequence, X-ray absorption due to the Compton effect or pair production will not be considered further. It is possible that the X-ray photon energies resulting from the infrared laser generation process could begin to approach 50 keV in the

future, in which case absorption via the Compton effect would begin to assume some relevance. However, our present view is that such an increase in photon energy will not be achieved easily. On the other hand, for the relativistic electron beam method of generation of X-rays, which is considered briefly in a later section, it is likely that the photon energies will exceed 50 keV and absorption via the Compton effect will be important.

### 6.3. X-ray Absorption Cross Sections

It will be noted that the X-ray wavelength range covers three decades, whereas in the visible range the wavelengths vary only by a factor of  $\sim 2$ . It should therefore be no surprise that there is a substantial difference between the physical properties of the hardest and softest X-rays. Perhaps the most important difference for our purpose is the wide variation of the absorption cross section of the various atomic and molecular species in air. The largest cross sections, typically  $10^{-18}$ – $10^{-19}$   $\text{cm}^2$  occur in the soft X-ray band, where the K limits for carbon, nitrogen, and oxygen are located (see Chapter 6 of *Banks and Kocharts*, [1973]). This is of course the primary reason for the close association between X-ray absorption and the formation of the E-region of the ionosphere: unit optical depth for the wavelength range 10–100 Å is concentrated in a layer about 20 km thick centered near 110 km. The absorption cross sections for the same atomic species lie in the range  $10^{-24}$ – $10^{-22}$   $\text{cm}^2$  for  $0.1 \leq \lambda \leq 1.0$  Å and in the range  $10^{-23}$ – $10^{-19}$  for  $1 \leq \lambda \leq 10$  Å.

Specific K limit ionization thresholds for oxygen, nitrogen, and carbon are 23.3 Å (0.533 keV), 31.0 Å (0.397 keV), and 44.0 Å (0.282 keV), respectively. For those altitudes with which we are most concerned (ionospheric altitudes less than 200 km) the predominant gas is molecular nitrogen, with molecular oxygen the next most common constituent. *Banks and Kocharts* [1973] divide the spectral range into two parts, depending on whether the wavelength is greater or less than 31 Å, and they divide each of the ranges 10–31 Å and 31–100 Å into three parts for each of which they provide a mean value of cross section. These values can be used to simplify the calculation of absorption of an X-ray beam with a wavelength, or wavelengths, in the



range 10–100 Å.

## 6.4. X-ray Beam Generation by Infrared Laser

### 6.4.1. Description of System

In the following we will describe a general procedure for the generation of X-rays by means of an infrared laser, and we will illustrate its practical application by reference to an experimental system that is currently in operation in the Ginzton Laboratory at Stanford (research directed by Professors S.E. Harris and J.F. Young). The numbers quoted for the experimental system are illustrative, but they should be treated with great care when projecting a possible application of the system in space. As we will show, the present experimental system would be capable of producing columns of substantially enhanced ionization if it could be operated in its present configuration in the ionosphere. However, many improvements and variations of the present configuration are possible, which have the potential for greatly improving both its efficiency as an X-ray generator and its ability to produce ionospheric ionization.

The general procedure we will consider for the generation of X-rays by means of an infrared laser is illustrated in Figure 1. The generation process has the following two steps. First, the infrared beam from a Nd:YAG laser (wavelength approximately 1.06  $\mu\text{m}$ ) is focussed on a piece of metal with a high atomic number such as tantalum, where it generates a small, intensely hot spot that is a strong source of soft X-rays and EUV radiation. The radiation is predominantly blackbody radiation and the wavelength  $\lambda_{\text{max}}$  for maximum spectral emittance is inversely proportional to the temperature  $T$  (in degrees Kelvin), according to Wien's displacement law:

$$\lambda_{\text{max}}T = 2.8978 \times 10^{-3} \text{ m deg K.} \quad (6.1)$$

For the illustrative Stanford system, starting with a compact laser generating  $\sim 1$  nsec, 1 J infrared pulses, the temperature of the heated spot lies in the range  $10^5$ – $10^6$  degK, and the resulting X-ray radiation is confined largely to the band 30–300 Å. Higher powered and therefore larger lasers can be used to generate shorter

wavelength X-ray radiation (e.g. Mallozzi *et al.* [1973]). The efficiency of the infrared to X-ray conversion process is about 10% in the illustrative system, but efficiencies of 50% or more have been achieved in other systems by going to higher frequency lasers (ultraviolet lasers have been used) and shorter pulses [e.g., Nishimura *et al.*, 1983].

The X-rays from the heated spot spread out isotropically and thus could be used to produce a roughly spherical region of ionization in the ionosphere surrounding the metal target, if desired. This possible method of ionospheric modification could have application in space research, but it will not be considered further here because of the greater interest of the X-ray beam method. To generate a beam of X-rays, we introduce a second step. The spot where these X-rays is generated on the tantalum target is located at the focus of a gold-plated stainless steel paraboloid. Through reflection at grazing incidence, the paraboloid forms the X-rays into a beam that can be quite narrow (1-10 cm in diameter) and which will maintain this narrowness over comparatively large distances in the absence of scatterers. As is to be expected, there is a loss of X-rays in the conversion from a largely isotropic distribution to a beam. For the Stanford system, the efficiency of the grazing incidence reflection process of beam formation is roughly 10%.

The spreading of the beam depends on many different factors. For example, the heated spot radiating the X-rays is not a geometrical point but has a finite width of the order of 100-500  $\mu\text{m}$ . As a result, there is an intrinsic spread to the X-rays associated with their source. The reflector will not be a perfect paraboloid or ellipsoid, and its surface will also have certain irregularities. These imperfections will further spread the beam. Then, finally, there is diffraction associated with the finite aperture of the reflector. The spreading caused by the latter can be estimated and it is very small: on the order of centimeters at distances in the range 10-100 km. Spreading due to the finite size of the source appears to be the major factor, since the reflectors in present use have small dimensions and a small angular spread in the radiation from the source can translate into significant spreading at distances in the range 10-100 km. Rough estimates based on the reflectors currently in use at Stanford, which have an aperture width of about 10 cm, and a similar length, give a beam width of about

50 m at 10 km distance for the largest heated spot size (500  $\mu\text{m}$ ), as compared with a width of 10 cm for the idealized system.

The reflecting surface for the Stanford system shown in Figure 1 is an ellipsoid instead of a paraboloid, and the X-ray beam is focussed instead of being formed into a parallel beam. However, it is a trivial change to substitute a paraboloid and thus form a parallel beam. Furthermore, a hyperbolic surface could also be used, if a spreading beam was desired. No further reference will be made here to the focussing of X-rays, but it could be an important capability if a particularly intense flux of X-rays was required at a specific location in the ionosphere.

Now consider the following order-of-magnitude computation, which illustrates a possible experimental situation. We start with a laser generating 1 J pulses of infrared radiation, which convert to roughly 0.1 J of X-rays radiated from the heated spot and to roughly 0.01 J in the X-ray pulses in the beam produced by the tantalum target/reflector assembly. We now use the following relationship, which follows from the conservation of optical étendue [Welford and Winston, 1978], to convert between the beam width at the target to the width at another location:

$$A_1\Omega_1 = A_2\Omega_2, \quad (6.2)$$

where  $A_1$  and  $A_2$  are the initial and final areas of the beam, and  $\Omega_1$  and  $\Omega_2$  are the initial and final solid angles associated with the beam. For our 'final' beam location we take the focal plane (Figure 1). Typical initial values are  $A_1 = 10^{-4} \text{ cm}^2$  and  $\Omega_1 = \pi$ . Possible choices of the area  $A_2$  depend on the characteristics of the reflector assembly; we will take  $A_2 = 400 \text{ cm}^2$  as a typical figure. For  $A_2 = 400 \text{ cm}^2$ , i.e., a focal area 23 cm in diameter, (1) gives  $\pi 10^{-4} = \pi \theta_2^2 \times 400$ , where  $\Omega_2 = \pi \theta_2^2$ . Thus  $\theta_2 = 5 \times 10^{-4}$  radians. If we now take a distance  $L = 10 \text{ km}$  along the beam, its diameter will be roughly  $L\theta_2$ , or 5 m. For a distance of 50 km the beam diameter will be about 25 m. These estimates do not take scattering of the beam into account.

#### 6.4.2. Effect of the Geomagnetic Field

In the other sections of this report we consider the variety of ionospheric modification effects that can be produced by beams of charged particles, including plasma

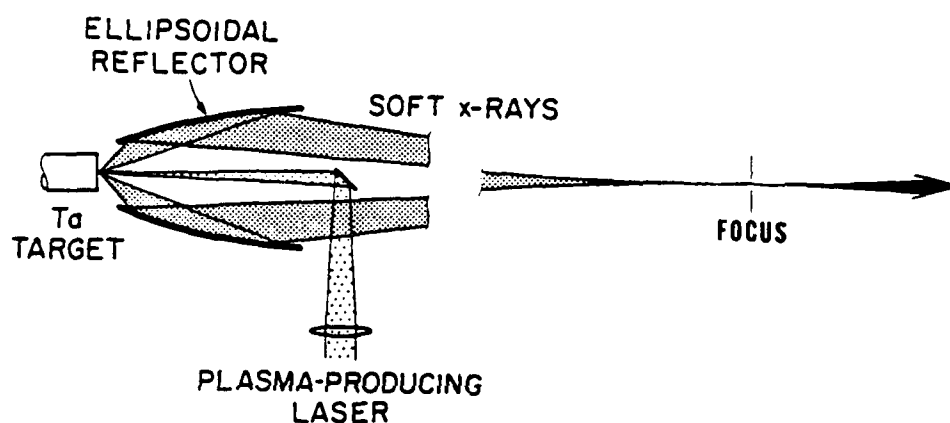


**Figure 1.** Schematic of the X-ray generation process. A Nd:YAG laser at the bottom of the figure is used to produce an intense infrared beam that is focussed on a tantalum target (left), producing an intensely hot spot --actually a plasma--whose blackbody radiation lies predominantly in the soft X-ray range. The spot is located at one focus of an ellipsoidal reflector and the X-rays are focussed by reflection at grazing incidence from the ellipsoid. The focal point, the other focus of the ellipsoid, is shown to the right in the figure, which is an adaption of Figure 1 in *Young et al.* [1987].

(neutral) beams. In all except one possible case (where a relativistic electron beam propagates through an ionization channel), the earth's magnetic field plays a major role, since the charged particles in the beams, no matter how energetic, are deflected by the field. A special case is the one where the charged particles are moving in the direction of the magnetic field. However, even in this latter case the magnetic field plays a crucial role, since the charged particle beam must be directed along the field and therefore the choice of its direction is severely constrained. In addition, the earth's field is not generally very uniform except in the equatorial region, and a particle beam originally directed along the magnetic field will soon be exposed to the curvature of the field if it is to travel to any significant distance.

The propagation of an X-ray beam is not directly influenced by the earth's magnetic field. There may be small, second-order effects in the beam absorption, for example, that we have not investigated, but in general the beam can be directed at any angle to the earth's field without concern for its deflection. This is an important distinction between the 'photon' method of modification and those involving charged particles.

#### 6.4.3. Penetration Distance

Let us now consider the depth of penetration and ionization production of the X-ray beam. As a first case, let us assume that both the density of absorbers/scatterers and their cross sections are constant. This is an idealization, but it applies quite closely to the situation where the X-ray beam is directed horizontally. Assume the horizontal distance variable is  $x$ , the initial intensity of radiation is  $I_0$  and that the intensity at any subsequent position is  $I$ . The cross section will be denoted by  $\sigma$  and the number density of absorbers/scatterers by  $n$ . We then use a standard procedure (e.g., *Liou [1980]*) to derive  $I$  in terms of  $\sigma$ ,  $n$ , and  $x$  as follows.

The loss in intensity  $\Delta I$  in a distance  $\Delta x$  can be written  $\Delta I = I\sigma n\Delta x$ . This gives  $\Delta I/I = \sigma n\Delta x$  and integrating both sides we obtain

$$I = I_0 \exp\left(-\int_0^x \sigma n dx\right), \quad (6.3)$$

where the quantity  $\int_0^x \sigma n dx$  is the *optical depth*. Until this stage we have made no explicit assumption about the spatial variations of the cross section  $\sigma$  or absorber density  $n$ . We now assume both are constant and obtain

$$I = I_0 \exp(-\sigma n x). \quad (6.4)$$

This last equation shows that the X-ray beam is attenuated exponentially, and that its intensity is reduced to  $1/e$  of its initial value in a distance  $1/\sigma n$ . Since this latter quantity depends only on the properties of the absorbing medium, and tells us something significant about the rate of absorption with distance, we will refer to it as the *characteristic penetration distance* and give it the symbol  $d_c$ . Thus the optical depth  $\sigma n x$  implied by (6.4) becomes unity when  $x = d_c$ .

At an altitude of 100 km, the predominant atmospheric constituent is neutral molecular nitrogen ( $N_2$ ) with a density of  $\sim 10^{13} \text{ cm}^{-3}$  [Banks and Kockarts, 1973]. Taking a wavelength of 100 Å, for which the molecular nitrogen cross section is  $\sim 1.3 \times 10^{-18} \text{ cm}^2$ , we obtain  $d_c \sim 0.8 \text{ km}$ , and it is clear that an X-ray beam will not penetrate to any great distance. However, if the wavelength is changed to 10 Å, the nitrogen cross section drops to  $\sim 8 \times 10^{-20} \text{ cm}^2$  and  $d_c \sim 13 \text{ km}$ , and we could expect the beam to penetrate for some tens of kilometers. The increase of penetration distance with decreasing wavelength continues as the wavelength is reduced below 10 Å, and the distances can become quite large. At 1 Å, for example, the  $N_2$  absorption cross section is  $\sim 10^{-22} \text{ cm}^2$  and  $d_c \sim 13,000 \text{ km}$ .

Table 3 shows the variation of  $d_c$  for a selection of wavelengths in the range 1–500 Å and altitudes in the range 80–140 km. It can be seen that there is a very rapid increase of  $d_c$  with increasing altitude. Taking a general view, an X-ray/EUV beam with wavelengths in the band 30–300 Å will not penetrate horizontally through the atmosphere to any great distance for altitudes below 100 km. However, for altitudes above 110 km the longest wavelength components of the beam can penetrate for at least some tens of kilometers, and the shortest wavelength components to much greater distances. These results also have clear implications for the X-ray/EUV beam

if it is directed downwards from some altitude in the range 110–500 km: it will penetrate down to an altitude of about 90–100 km, but it will not penetrate significantly below that level. Wavelengths less than  $10 \text{ \AA}$  will be required if deep penetration below 100 km is desired.

Figure 2 illustrates the latter point. It shows a plot of the depth of penetration of X-radiation into the earth's atmosphere from sources external to the earth [Culhane and Sanford, 1981]. Specifically, the curve in the figure shows the altitude at which 50% of the X-rays incident on the earth's atmosphere are absorbed. In accordance with our conclusion above, it can be seen that it is only X-rays with photon energies greater than 1 keV (wavelengths less than  $10 \text{ \AA}$ ) that penetrate significantly below 100 km.

#### 6.4.4. Ionization Production

Let us now consider the ionization produced by our X-ray beam. From the discussion in the previous subsection we might expect this ionization to be comparatively small for altitudes above 140 km, since there will be a roughly inverse relation between penetration distance and the ionization produced per unit volume of the ionosphere illuminated by the X-ray beam. Similarly, we would expect to see substantial ionization produced below 100 km and little penetration.

Once again we will assume initially that the X-ray beam is directed horizontally through the ionosphere, so that the number densities and cross-sections are constant. This approach gives us enough information to generalize to the case of an arbitrarily directed beam. The beam will be assumed to be cylindrical, with uniform intensity  $I$  across the circular cross section (radius  $r$ ). Suppose that a pulse of X-rays of total energy  $E$  and duration  $\tau$  is radiated. We can then write

$$I_0 = \frac{E}{\pi r^2 \tau}, \quad (6.5)$$

which, from (6.4), gives

$$I = \frac{E}{\pi r^2 \tau} \exp(-\sigma n x). \quad (6.6)$$

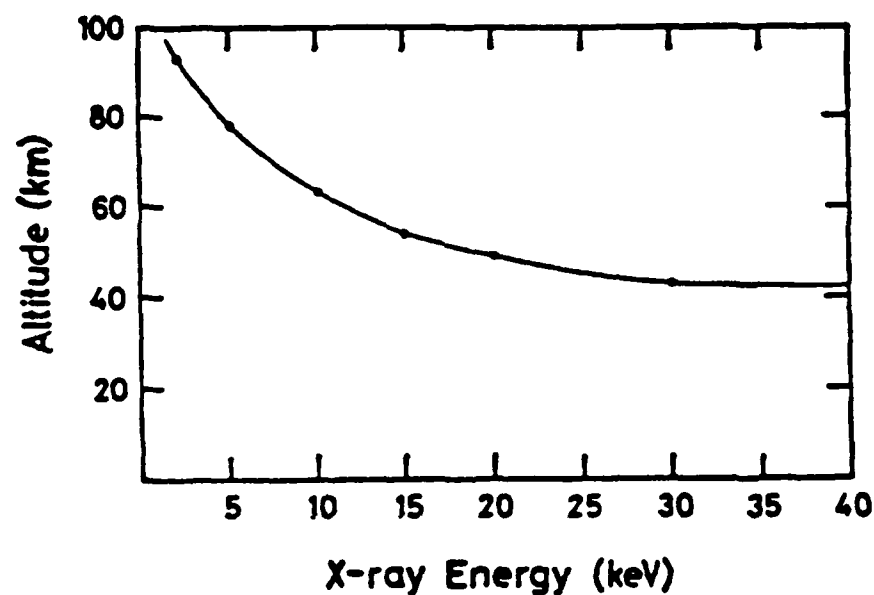


**Figure 2.** Curve showing the penetration of X-rays down into the earth's atmosphere from sources outside the atmosphere [Culhane and Sanford, 1981]. The points plotted show the altitudes at which 50% of the X-rays incident vertically on the earth's atmosphere are absorbed. X-rays with energies less than 1 keV are absorbed at higher altitudes.



**Table 3.** Some representative characteristic penetration distances  $d_c$  at four different altitudes  $h$  for some wavelengths in the X-ray and EUV bands. The distances are in kilometers and an asterisk indicates a distance greater than 10,000 km.

| $\lambda$ (Å) | $h = 80$ km | $h = 100$ km | $h = 120$ km | $h = 140$ km |
|---------------|-------------|--------------|--------------|--------------|
| 1             | 300         | *            | *            | *            |
| 5             | 3           | 100          | *            | *            |
| 10            | 0.4         | 13           | 236          | 1790         |
| 50            | 0.1         | 4.3          | 82           | 621          |
| 100           | 0.02        | 0.8          | 14           | 110          |
| 500           | 0.001       | 0.04         | 0.8          | 6.2          |

This last equation gives the intensity at any point along the cylindrical beam. To compute the ionization produced, consider a thin cross sectional slice of the beam, of thickness  $dx$ . The volume of the element is  $\pi r^2 dx$  and the energy deposited per unit time from the X-ray beam is

$$I(\pi r^2 dx) \sigma n. \quad (6.7)$$

We now estimate the number of electrons produced by assuming an energy utilization of 35 eV per ion pair [Banks and Kockarts, 1973, Part A, p. 83]. Writing  $n_x$  for the number density of the electrons produced by the X-rays, and making the appropriate substitutions, we obtain the following from (6.6) and (6.7)

$$n_x = \frac{E \sigma n}{35 \pi r^2} \exp(-\sigma n x), \quad (6.8)$$

where it is assumed that  $E$  is measured in eV.

#### 6.4.5. Illustrative Computation

In Section 6.4.1 we quoted an X-ray pulse energy of roughly 0.01 J for the system currently operating at Stanford. Assuming a pulse energy of 0.1 J, for a modestly

upgraded system, we can write (6.8) in the form

$$n_x = 5.68 \times 10^{15} \left( \frac{\sigma n}{r^2} \right) \exp(-\sigma n x). \quad (6.9)$$

It will now be assumed that  $\sigma \approx 3 \times 10^{-23} \text{ m}^2$  and that the radius  $r$  is 0.1 m. The cross section is for molecular nitrogen and is typical for wavelengths in the range 10–100 Å [Banks and Kockarts, 1973], and the radius is representative of the aperture of grazing incidence reflectors currently in use at Stanford. This latter assumption is idealistic: it implies that the heated spot is a geometric point located at the focus of the paraboloid producing the cylindrical beam. The numerical values of the two quantities, and the radius in particular, can be varied substantially from those just chosen, but our purpose here is to illustrate general behavior, not to provide exact numerical results, and the chosen values are adequate for this illustrative purpose. Equation (6.9) now becomes

$$n_x = 1.7 \times 10^{-5} n \exp(-3 \times 10^{-23} n x), \quad (6.10)$$

where  $n$  and  $n_x$  are measured in  $\text{m}^{-3}$ .

It is now necessary for us to adopt representative values for the number density of molecular nitrogen. These values will be taken from altitude profiles published by Banks and Kockarts [1973] (see Part A, p. 4) and Whitten and Poppoff [1965] (see p. 70) and they are tabulated in Table 4. Also tabulated are typical ambient daytime ion densities [Banks and Kockarts, 1973, Part A, p. 14].

The data in Table 4 show that the X-ray beam can produce substantial ionization in the vicinity of the generator. For example, at an altitude of 90 km, the ionization density produced by the beam for  $x \approx 0$  is about  $10^5$  times greater than the ambient ionization density. This is during the daytime; during the night the ionization produced by the beam should be roughly the same, but the ambient density will be less, giving an even greater contrast between the two levels of ionization. The contrast between the local ionization caused by the beam and the ambient ionization grows less as the altitude increases. As shown by Table 4, the local beam ionization is only

**Table 4.** Representative number densities  $n$  for neutral molecular nitrogen and the corresponding expressions for  $n_x$  (from Equation 6.10) at six different E-region altitudes  $h$ . Also shown are typical ambient daytime ion densities  $n_i$  and the approximate length  $D$  of the ionized path produced by the beam.

| $h$ (km) | $n$ ( $\text{m}^{-3}$ ) | $n_i$ ( $\text{m}^{-3}$ ) | $n_x$ ( $\text{m}^{-3}$ )                   | $D$ (m) |
|----------|-------------------------|---------------------------|---|---------|
| 90       | $10^{20}$               | $2 \times 10^{10}$        | $2 \times 10^{15} \exp(-3 \times 10^{-3}x)$ | 3.8     |
| 100      | $10^{19}$               | $4 \times 10^{10}$        | $2 \times 10^{14} \exp(-3 \times 10^{-4}x)$ | 28      |
| 110      | $2 \times 10^{18}$      | $9 \times 10^{10}$        | $3 \times 10^{13} \exp(-6 \times 10^{-5}x)$ | 95      |
| 120      | $6 \times 10^{17}$      | $10^{11}$                 | $1 \times 10^{13} \exp(-2 \times 10^{-5}x)$ | 250     |
| 130      | $2 \times 10^{17}$      | $10^{11}$                 | $3 \times 10^{12} \exp(-6 \times 10^{-6}x)$ | 566     |
| 140      | $7 \times 10^{16}$      | $10^{11}$                 | $1 \times 10^{12} \exp(-2 \times 10^{-6}x)$ | 1240    |

an order of magnitude above the ambient ionization at 140 km and around 160 km there is little difference.

When the expressions for  $n_x$  in Table 4 are evaluated and the resulting ionization densities plotted against distance  $x$ , a distance  $D$  can be derived beyond which the X-ray ionization densities are less than the ambient density (we are still considering horizontally directed X-ray beams). This distance  $D$  is representative of the length of ionized path that might be measured by a ground-based radar or other detector during operation of the X-ray beam generator. As might be expected from the previous discussion of penetration distances,  $D$  is small at low altitudes and increases with increasing altitude. The values of  $D$  are tabulated in Table 4 and can be seen to vary from around 4 km at  $h = 90$  km to greater than 1200 km at  $h = 140$  km (these two cases are further illustrated in Figure 3). Once again, as we saw with the penetration distance, the altitude range 90–140 km demarcates two regions: (1) an upper region,  $h > 140$  km, in which the X-ray beam penetrates to large distances, but, as we now see, a region in which the beam produces little change in ionization, and (2) a lower region,  $h < 90$  km, in which the beam penetrates only to small distances, but, as we

now see, a region in which the beam can produce substantial changes in ionization.

The above computations of the ionization are based on the assumption of a beam of X-rays only 0.1 m in radius. As we have seen, the finite size of the heated spot generating the X-rays is more likely to lead to beam radii of around 5 m at a distance of 10 km from the generator. Since the number density of the electrons produced by the beam varies as (radius)<sup>-2</sup>, it is crucial that the radius be kept small if the additional electrons are to be observable above the normal background level. The four most obvious methods for ensuring this condition are (1) sharp focussing of the initial laser beam on the heavy metal target, (2) accurate location of the heated spot at the focus of the reflector, (3) use of very short pulses of incident infrared radiation, and (4) the use of some active method, such as the application of a strong magnetic field, to reduce the expansion of the plasma created at the heated spot.

The above results apply to a horizontally directed X-ray beam, but, taken in conjunction with the work in the preceding sub-sections, they have obvious implications for non-horizontally directed beams. For example, if we suppose the X-ray beam generator is located at  $h = 140$  km and the beam is directed vertically downwards, we would expect to see a moderate increase of ionization (to roughly ten times the ambient level) within the path of the beam down to  $h \approx 120$  km. The increase of ionization, and attenuation of the X-ray beam, will then become more substantial, with the beam becoming totally absorbed somewhere in the range  $90 < h < 100$ .

#### 6.4.6. *Recombination*

The subject of recombination arises several times in this report. In the present case the initial ionization produced by the X-ray beam consists predominantly of the positive atmospheric ions  $N_2^+$  and  $O_2^+$  and free electrons, just as was the case with the ionization produced by relativistic electron beams (Section 4), and much of the discussion of plasma chemistry contained in that section pertains to the ionization produced in the X-ray case. There is a substantial difference, however, in the relevant altitudes. As we have seen above, the X-rays are absorbed primarily in the altitude range 90-120 km, whereas the relativistic electron beam can penetrate much lower in

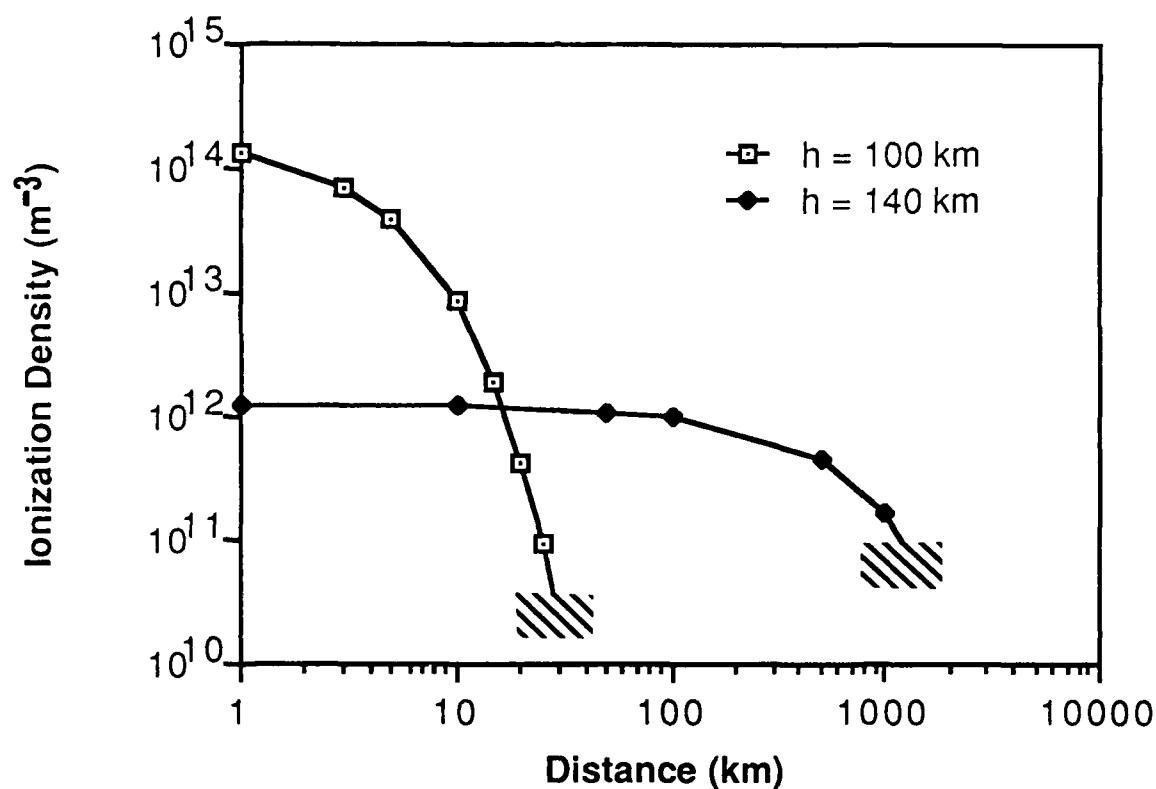


**Figure 3.** Two curves showing examples of the ionization produced by a single 0.1 J beamed pulse of X-rays as it propagates horizontally at altitudes of 90 km and 140 km. The shading at the ends of the curves indicates that the the ionization produced by the beam has declined to the level of the ambient ionization and will be less than the ambient level for distances greater than those indicated by the start of shading. The ionization levels produced by the X-rays at 140 km are much less that those produced at 90 km, but the radiation penetrates much further.

the atmosphere, to where the chemistry is very different.

We would expect a dissociative recombination process of the form



where the asterisks indicate that the atoms may be internally excited, to be the principal process leading to loss of the molecular ions and free electrons produced by the X-ray beam. These processes are known to be rapid and to be the principal means of ion recombination in the ionosphere.

The lifetime of the ionization produced by the X-rays can be estimated by using the formula

$$\tau_D \approx \frac{1}{\alpha_D n_e}, \quad (6.12)$$

where  $\tau_D$  is the time constant (or decay time) for the process,  $\alpha_D$  is the recombination rate, and  $n_e$  is the electron density (this formula has already appeared in subsections 2.1.1 and 4.2.2). The recombination rate depends on the electron temperature (see Equation 4.4), which for our altitudes of interest can be taken to be about 300deg K. The corresponding recombination rate is  $\alpha_D \approx 3 \times 10^{-7} \text{ cm}^3 \text{ sec}^{-1}$  or  $\alpha_D \approx 3 \times 10^{-13} \text{ m}^3 \text{ sec}^{-1}$  [Banks and Kockarts, 1973, Part A, p. 255]. Thus

$$\tau_D \approx \frac{3 \times 10^{12}}{n_e}, \quad (6.13)$$

where it is assumed that  $n_e$  is measured in units of  $\text{m}^{-3}$ . Referring to Table 4, we find  $n_e = n_x$  (in the beam) varying in the range  $10^{10} - 10^{15} \text{ m}^{-3}$ , with the implication from (6.13) that the lifetime of the ionization produced by the X-ray beam will probably only amount, at most, to some tens of seconds under the assumed daylight conditions.

Because the ionization produced by the X-ray beam involves the neutral component of the ionosphere, which does not vary much on a diurnal basis, we would expect the ionization produced by the beam to remain roughly the same from day to night. The ambient ionization, on the other hand, will vary significantly, with the nighttime electron density down by 1-2 orders of magnitude from the daytime density in the altitude range 90-140 km [Cormier *et al.*, 1965]. There may therefore

be some advantage to using a more diffuse or lower-powered X-ray beam at night to produce a more weakly ionized column than those discussed above, but still with enough ionization for it to stand out from the surrounding nighttime ionosphere. As noted above, ambient daytime electron densities typically vary from  $10^{10} - 10^{11} \text{ m}^{-3}$  for altitudes in the range 90–140 km. During the night, an ionized column with electron densities in the range  $10^{10} - 10^{11} \text{ m}^{-3}$  would be 10–1000 times more highly ionized than the surrounding ionosphere, and so should be easily measurable, and yet the level of ionization would be such that the column might have a lifetime measured in minutes or tens of minutes.

### 6.5. X-Ray Generation by Energetic Electron Beams

This method of generation will only be briefly discussed. It is relevant because it could be combined with the relativistic electron beam method of ionospheric modification discussed in Section 4.

Starting with a beam of relativistic electrons in the ionosphere, hard X-rays could be produced by scattering heavy metal targets into the beam. The electrons impinging on the targets will produce X-rays in exactly the same way that X-rays are normally produced in X-ray tubes. Without specifying the shape of the metal targets in any manner, we would expect this method of X-ray generation to produce a largely spherical distribution of X-ray intensity and consequent region of ionization.

### 6.6. Discussion

Two new methods for modifying the ionosphere by means of X-rays have been described. One of the methods, and a version of the other, produce uncollimated X-rays and thus their product is a more-or-less localized region of enhanced ionization around the source of the X-rays. The techniques involved in these latter generation processes have only been briefly discussed, but they could be effective in producing heavily ionized regions in the upper atmosphere. The second method, which gives a beam of soft X-rays and EUV radiation, has been analyzed in some detail because of the number of new experiments on ionospheric modification that it would make

possible. It uses an infrared laser beam focussed on a heavy metal target to generate the X-rays, but it makes use of reflection at grazing incidence from a metal paraboloid to form the X-rays into a beam.

The X-ray beam generation process is relatively efficient and it has already been developed and tested in the laboratory. Our computations indicate that an X-ray beam with the same characteristics as those already being produced in the laboratory can penetrate to considerable distances in the ionosphere with limited spreading (largely due to the finite size of the heated spot that is the source of X-rays) and that it can produce substantial ionization when it is absorbed. Ordinarily, penetration and ionization production are conflicting requirements, since high ionization implies low penetration, but there are circumstances where advantage can be taken of both characteristics. For example, an X-ray beam can be directed downwards from a platform at an altitude well above 100 km; it will propagate down with little initial loss (ionization) until it reaches an altitude in the range 90–100 km, where it will be rapidly absorbed and produce its maximum ionization. Once again we note the independence of the X-ray beam propagation from the earth's magnetic field. In the example just cited, the beam can be directed downwards without concern for the angle it makes with the earth's field, unlike a beam of charged particles. Another advantage of using an X-ray beam for ionospheric modification, as compared with a charged particle beam, is its elimination of vehicle charging problems.

There are constraints on the X-ray beam technique of ionospheric modification. First, it will have been noted in our computations above that the altitude range 90–140 km frequently arises when illustrative data are derived. This is due to the remarkable change in beam absorption that takes place over the range: at 90 km the beam is quite rapidly absorbed and below 90 km it will not propagate to any substantial distance, whereas at 140 km and above the beam will propagate to large distances with little loss. Thus the altitude range 90–140 km is a transition region, separating a lower region of high absorption from an upper region of low absorption. For ionospheric modification at altitudes above 140 km, our X-ray beam method will probably not be greatly effective.



A second constraint on the beam technique relates to the altitude constraint. We have specified a wavelength range of approximately 30–300 Å for the laser technique of X-ray generation. The wavelength range depends directly on temperature of the spot heated by the laser: the higher the temperature, the shorter the wavelengths of the X-rays that are produced. Shorter wavelength X-rays would mean greater penetration of an X-ray beam at altitudes below 90 km and, returning to the possible experimental situation described above, deeper penetration of a beam from a source on a platform above 100 km. In this latter case, ionospheric modification could be produced at lower altitudes than 80–90 km. Unfortunately, it does not seem feasible at this time to shorten the wavelengths of the X-rays substantially below about 10 Å, for reasons relating to the confinement of the extraordinarily hot plasma that is created (and which is the source of the X-rays that are radiated) when the infrared beam strikes the heavy metal target. Further research is needed to remove this limitation.

We have restricted consideration to an infrared laser producing 1–10 J pulses, or more specifically to a system configured around the one currently in operation at Stanford. Much more powerful infrared lasers are available and could be used for X-ray generation. However, we question whether this would be a reasonable step to take at this time. As we have shown, a 10 J system, if flown, could produce substantial ionization changes in the lower ionosphere. Further, while a more powerful laser could conceivably lead immediately to higher target temperatures and thus shorter X-ray wavelengths, it is not clear at this time that the greater energy can be used effectively due to the confinement problem mentioned above.

As we have repeatedly pointed out, there is a tradeoff between beam penetration and ionization production. There is a further tradeoff between the ionization level that is produced and its lifetime: large ionization densities have a short lifetime. It is interesting in this context to note that there may be an advantage at night to produce only a moderate increase of ionization—to a level only moderately greater than the ambient level. This might be done by deliberately increasing the width of the X-ray beam, thus producing a larger column of ionization, or by otherwise reducing the intensity of the X-rays in the beam. A high-powered X-ray beam is not necessarily

an advantage under all conditions.

We have not dwelled on the ease with which the X-ray beam could be focussed on a point in the ionospheric plasma. A roughly spherical region of highly ionized plasma could be produced by this technique that could have interesting properties: an extreme case of ionospheric modification.

### 6.7. Suggestions for Further Work

The infrared laser method of generating an X-ray/EUV beam described in this chapter has obvious potential for interesting new experiments on ionospheric modification, which could help illuminate the basic processes of formation of the ionosphere. Before such experiments can be carried out, however, there must be a transition of the X-ray/EUV beam generator from its present laboratory bench setup to a well-tested and rugged generator that can be flown on a rocket (a balloon flight does not appear likely to take the generator to a high enough altitude for the beam to penetrate significantly far from the platform, although it would otherwise have many advantages for an initial experiment). Thus, if it was desired to conduct an X-ray beam in the ionosphere, one of the first tasks would be construction of a flight-ready beam generator and its testing in a vacuum chamber. The possibility of a balloon flight should be investigated further, despite our opinion at this time that it would not lead to a useful beam experiment: it would still be possible to produce substantial ionization in the vicinity of the generator, and the experience gained in operating the X-ray/EUV generator as part of a balloon payload would be an invaluable preliminary to a rocket experiment. An extension of the present feasibility study to include a more rigorous analysis of the beam generation and propagation of the beam in the ionosphere and possibly also neutral atmosphere (in support of a balloon experiment) would also be desirable.

A key experimental study that should be made is one of the various techniques (some of which are detailed in this report) for reducing the size of the spot on the heavy metal target that is heated by the infrared beam. Spreading of the X-ray beam depends primarily on the size of the heated spot, and there is a direct relation between

the spot size and the spreading of the beam. The more closely the spot size can be controlled, and, in particular, the smaller it can be made, the better the spreading can be controlled. Such a study can be most effectively conducted in the laboratory.

Assuming the completion of the preliminary studies and construction of a flight-ready generator, the next step would be a rocket experiment. There is no doubt, even at this early stage, that an X-ray beam generator can be constructed to conform to the weight, size, and other payload limitations of a rocket flight. Thus the decision on whether to conduct a rocket experiment would need to be based on the new information that would be provided by the experiment, on the usefulness of the new technology that would result from the experiment, on the relevance of such an experiment to other interests of the Air Force and the Department of Defence generally, and on the cost of the experiment. Scientifically, a rocket experiment could produce much new information on the properties of the ionosphere.

## 6.8. References

- Banks, P.M., and G. Kockarts, *Aeronomy*, 2 Volumes, 421 pp. and 429 pp., Academic Press, N.Y., 1973.
- Cormier, R.J., J.C. Ulwick, J.A. Klobuchar, W. Pfister, and T.J. Keneshea, Ionospheric Physics, Ch. 12 in *Handbook of Geophysics and Space Environments*, Ed. S.L. Valley, Air Force Cambridge Res. Labs., Hanscom Field, Massachusetts, 1965. (ADA056800)
- Culhane, J.L., and P.W. Sanford, *X-ray Astronomy*, 192 pp., Faber and Faber, London, 1981.
- Liou, K.-N., *An Introduction to Atmospheric Radiation*, 19-21, Academic Press, N.Y., 1980.
- Mallozzi, P.J., H.M. Epstein, R.G. Jung, D.C. Applebaum, B.P. Fairand, and W.J. Gallagher, X-ray emission from laser generated plasmas, pp. 165-220 in *Fundamental and Applied Laser Physics*, Ed. M.S. Feld, A. Javan, and N.A. Kurnit, Wiley, New York, 1973.

- Nishimura, H., F. Matsuoka, M. Yagi, K. Yamada, S. Nakai, G.H. McCall, and C. Yamanaka, Radiation conversion and related ablation behavior of a gold-foil target irradiated by 0.35, 0.53, 1.06, and 10.6  $\mu\text{m}$  lasers, *Phys. Fluids*, **26**, 1688-1692, 1986.
- Welford, W.T., and R. Winston, *The Optics of Nonimaging Concentrators*, 200 pp., Academic, New York, 1978.
- Whitten, R.C., and I.G. Poppoff, *Physics of the Lower Ionosphere*, 232 pp., Prentice-Hall, N.J., 1965.
- Young, J.F., J.J. Macklin, and S.E. Harris, Grazing incidence ellipsoidal reflector for longitudinally pumping short-wavelength lasers, *Optics Letts.*, **12**, 90-92, 1987.

## 7. NEUTRAL GAS RELEASES

### 7.1. Introduction

In this section we discuss the possible consequences which follow from the release of a cloud of neutral gas from an orbiting or other high speed platform in the ionosphere. Interest in this type of experiment has evolved during the past decade as a consequence of the Critical Ionization Velocity (CIV) concept. From laboratory observations and some space experiments, it is known that neutral gases, when injected into an magnetized plasma at a velocity which is greater than that corresponding to the ionization energy of the gas, will undergo rapid ionization. This phenomenon is attributed to a complicated sequence of compounding events. First, a few of the fast moving neutrals are assumed to be ionized by some process. These few streaming ions then interact with the background plasma to generate intense ion electrostatic waves which, in turn, heat the electron component of the ambient plasma. If the energy transfer rate is rapid so the electrons become sufficiently hot, they can further ionize the neutral gas, thereby permitting an even more rapid conversion of the original neutral gas kinetic energy into plasma heating. Eventually, a rapid cascade of ionization may result, totally converting the neutral gas to plasma. Both laboratory experiments and computer simulations [*Machida and Goertz, 1986*] demonstrate the CIV effect.

Experiments to verify the validity of the CIV concept to the conditions of space plasma have been undertaken, but the results are not uniformly positive. Consequently, extensive efforts supported by NASA, the DOD, and international agencies are underway to develop understanding of all of the complex factors involved in CIV.

Here we wish to describe another interesting, less well known process which occurs when neutral gases are released at high speeds in the ionosphere, but, for various reasons, the heating of the plasma is insufficient to yield the CIV effect. The basic idea is as follows: Imagine that a cloud of neutral gas is released within the ionosphere from an orbiting platform. As this injected gas cloud moves along the orbital path (and expands with respect to its original volume), it will undergo two distinct interactions

with the upper atmosphere. First, elastic scattering will occur with the ambient atmospheric gases. These collisions will gradually dissipate the directed kinetic energy of orbital motion, slightly heating the atmosphere and strongly heating the injected neutral gas. Second, and most important for the present idea, for certain conditions there will be charge exchange between the neutral gas and the ambient ions (primarily  $O^+$ ) of the ionosphere. The new ions can no longer continue to follow the neutral orbital trajectory but immediately gyrate around the magnetic field at their points of origin. This gyration, which is circular in the local frame of the local ionosphere, has a radius set by the mass of the new ion and its initial velocity perpendicular to the magnetic field. As shown in the discussion below, because these new ions have different gyroradii than the ambient ions of the ionosphere, there will be an immediate electrodynamic effect which leads to the generation of ELF/VLF waves and other electron density fluctuations that can significantly disturb the local ionosphere.

## 7.2 Basic Processes

The geometry of the situation is shown in Figure 7.1. A spherically expanding cloud of neutral gas, composed of particles identified by the symbol  $X$  and having molecular mass  $M_x$ , is shown at an instant of time when the cloud has a radius  $R$ . At this moment, the cloud is traveling at a velocity  $\mathbf{V}$  relative to the ambient magnetic field,  $\mathbf{B}$ , through an ionospheric plasma composed primarily of  $O^+$  and electrons. For this discussion, we will assume that the  $X$ -type neutral particles (and subsequent ions) are much more massive than the  $O^+$  ions.

The effect we wish to investigate follows from charge exchange, represented by the reaction



where  $X$  represents an atom or molecule of the injected gas and  $O^+$  is assumed to be the dominant ion of the ionosphere.

The charge exchange reaction given by Eqn.(7.1) proceeds very rapidly when the ionization potentials of the two neutral gases ( $X$  and  $O$ ) are the same. In this

situation, called resonant charge exchange, cross sections as large as  $10^{-14}$  cm<sup>2</sup> obtain. However, when there is a difference between the ionization potentials of the two gases (called the energy defect), charge exchange can occur only if the kinetic energy of relative motion is adequate to make up the difference of ionization potentials. Thus, charge exchange between unlike ions and neutral particles in the ionosphere is generally very slow at the mean thermal energies of the ionosphere ( $\sim 0.1$  to  $0.3$  eV).

With respect to the present circumstances, the orbital energy of the injected neutral gas particles enters into the energetics of the charge exchange process and it can be expected that charge exchange will proceed at a rapid rate ( $\sigma \sim 5 \times 10^{-15}$  cm<sup>2</sup>) as long as the injected gas particles continue to move at high speeds relative to the background atmosphere. Thus, charge exchange will occur easily for a newly injected neutral particle (and for its ion still having the same kinetic energy), but as the energy of this particle (and its gyrating ion) degrades as a consequence of collisions with atmospheric gases, the cross section for charge exchange will quickly become small.

With this background information, there are important consequences which follow from the release of a cloud of neutral gases from an orbiting vehicle. If, as was hypothesized earlier, we have relatively heavy neutral particles, so that the kinetic energy of relative motion overcomes the energy defect of charge exchange with  $O^+$ , we can expect the rapid conversions of  $X$  atoms or molecules into  $X^+$  ions. As each rapidly moving neutral gas particle is converted into an ion, it retains its original directed velocity,  $\mathbf{V}$ . However, owing to the local magnetic field, the ion immediately experiences a  $\mathbf{V} \times \mathbf{B}$  deflection. This situation is shown in Figure 7.2 from the coordinate frame of the local ionosphere. Because the  $X^+$  ions are more massive than the  $O^+$  ions, and because of their directed velocity of motion, the gyroradii of the  $X^+$  ions will be much larger than the  $O^+$  gyroradii, perhaps by a factor of 10 or more, and very much greater than the gyroradii of the ambient electrons.

The consequence of this generation of new ions with large gyroradii is a sideways deflection of all newly created  $X^+$ , which will immediately create a lateral shift of positive charge with a net electrical charge imbalance at the edges of the neutral

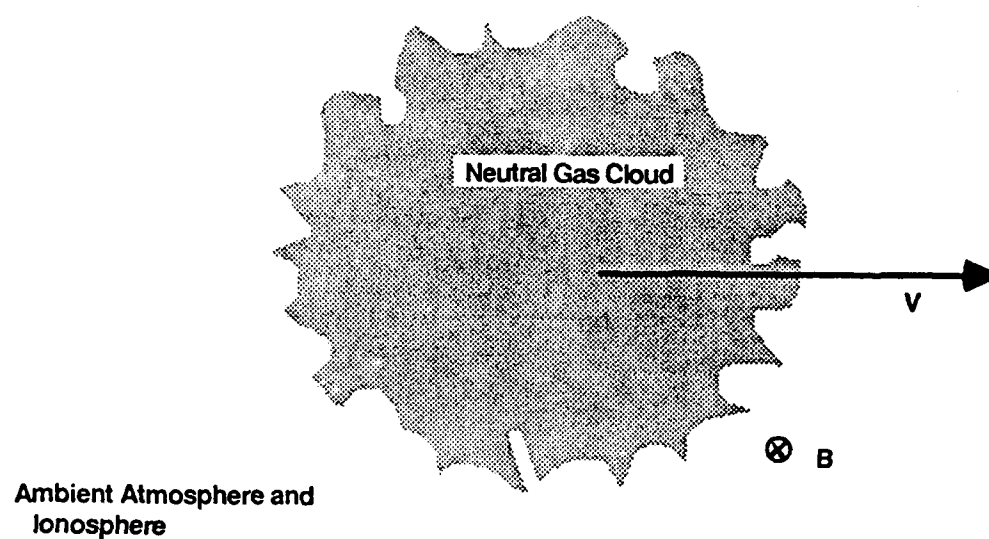


**Figure 7.1.** Showing a cloud of X-type neutral particles expanding radially outward while moving through the ionosphere with a velocity  $V$  relative to the magnetic field  $B$ . The background ionosphere is assumed to be composed of  $O^+$  ions and electrons.



gas cloud. (This occurs because the ambient electrons and  $O^+$  have relatively small gyroradii compared with that of the high speed, heavy  $X^+$  ion.) This effect occurs only at the edges of the trace of the neutral cloud in a zone which is approximately an  $X^+$  gyrodiometer thick. Elsewhere, the larger gyroradius of the  $X^+$  ion doesn't make any difference since the trajectory of the ion will be through a uniform electron/ $O^+$  plasma. This situation is shown in Figure 7.3.

The principal consequence of the charge exchange process is thus to create a polarization electric field in a region defined by the outer edge of the passing cloud. This electric field is not static, but strongly fluctuating: Owing to the random nature of the charge exchange reactions and the fact that the trajectories of the  $X^+$  ions are circular around the local magnetic field, it can be expected that strong incoherent electric fields at the cyclotron frequency of the  $X^+$  ion will occur. In addition, ion-ion plasma micro-instabilities may also be stimulated. The consequent fluctuating electric fields will have an impact on the ambient electron motions, with the effect that energy will be transferred from the  $X^+$  ions to plasma waves involving the electron gas. Heating of the electrons is an inevitable consequence, with the production of strong electron gas irregularity structures.

In some ways, the above description is parallel to the sequence of events thought to occur in the critical ionization velocity phenomenon. However, the strict CIV conditions necessary for subsequent neutral gas ionization are not required to establish the wave effects desired here, nor do we need to consider the consequences of ion-ion microinstabilities: The principal effects are macroscopic in nature and arise from finite gyroradii effects in the finite geometry of the orbiting cloud.

The foregoing description treats the neutral cloud at a fixed time. In fact, the cloud itself will continually expand as it travels along (See Figure 7.4). In this situation, it can be expected that the region of active wave generation will follow the outer boundary of the neutral cloud, remaining about a gyrodiometer thick and continuing to result in plasma disturbances and low frequency wave generation. This outward propagating disturbance will reach its eventual limit as a consequence of scattering and energy loss in the neutral atmosphere: The average  $X$  particle energy will be

Background ionosphere and  
atmosphere

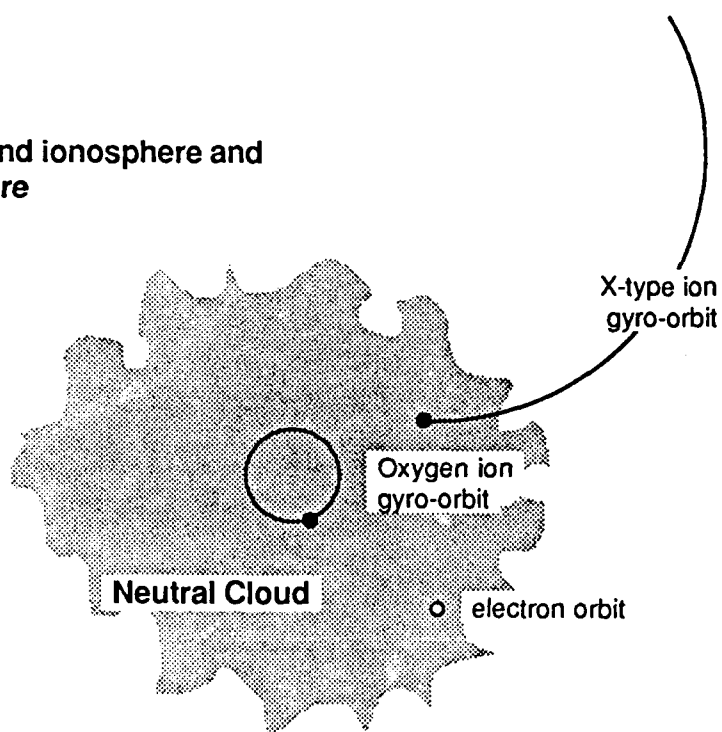


**Figure 7.2.** Illustrating the trajectory of a new, massive charge exchange-produced  $X^+$  ion. The gyrotrajectory of a typical  $O^+$  ion and a thermal electron are also shown. The magnetic field is directed into the page, and the initial neutral gas velocity is to the right.

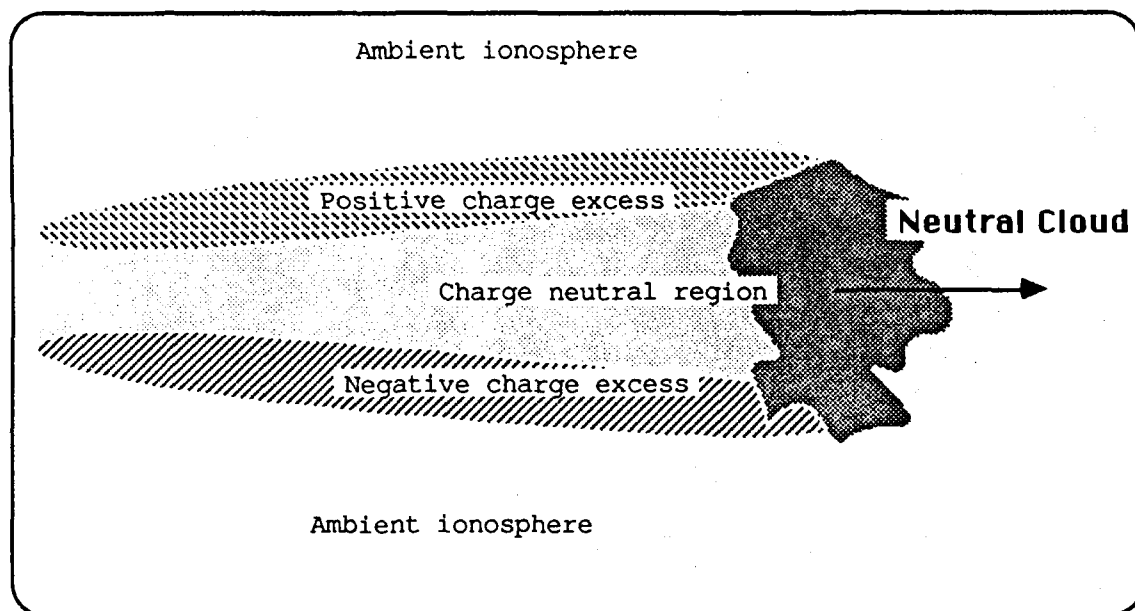


**Figure 7.3.** Illustrating the behavior of a collection of  $X^+$  ions produced from the moving cloud. Owing to their greater gyroradii relative to  $O^+$ , there is a net upwards displacement of electric charge. Within the main body of the cloud this is neutralized by the ambient electrons, but at the upper and lower edges, there is a real displacement current which fluctuates in space and time with a characteristic frequency originally set by the  $X^+$  ions.

reduced below that required to initiate charge exchange and the basic interaction will quickly disappear.

The lifetime of the effect at a given point in space will depend on the rate at which the  $X^+$  ions dissipate their energy. The transfer of energy to plasma waves is one important channel, while charge exchange with the neutral gases of the atmosphere is another. In this last situation, the  $X^+$  ions will undergo the reverse resonance charge exchange process represented by eqn.(1) and leave hot  $X$  neutrals moving away from the source in random directions, and cold  $O^+$  tied again to the local magnetic field lines.

Finally, the transformation of  $O^+$  into  $X^+$  can have an effect upon the ionospheric composition if the ionic loss process for  $X^+$  is substantially different than for  $O^+$ . This would be equivalent to a real change in ionization density and might be important for some applications, but is not pursued here owing to its similarity to water vapor injection experiments, the results of which are well known [e.g. *Bernhardt*, 1982].

### 7.3. Discussion

The charge exchange process is a new concept with respect to initiating disturbances in the ionosphere. Unlike the critical ionization phenomenon, it does not increase the total ionization present but, rather, acts through electrodynamics to change the ion composition (to  $X^+$ ) and to transform the initial kinetic energy of motion to plasma heating and plasma waves.

Although there have been many previous neutral gas release experiments in the upper atmosphere, it appears only a few would have been adequate to produce the disturbances described here. Barium cloud releases from rockets, for example, depend upon photoionization of slowly moving neutral vapors to create ion clouds. The subsequent plasma processes, although of great interest and importance, are not those which would occur as a consequence of charge exchange. Barium shaped-charge releases possess higher initial velocities but the choice of direction for the gas is generally parallel to the local magnetic field, a circumstance that greatly reduces the gyroradius effect.

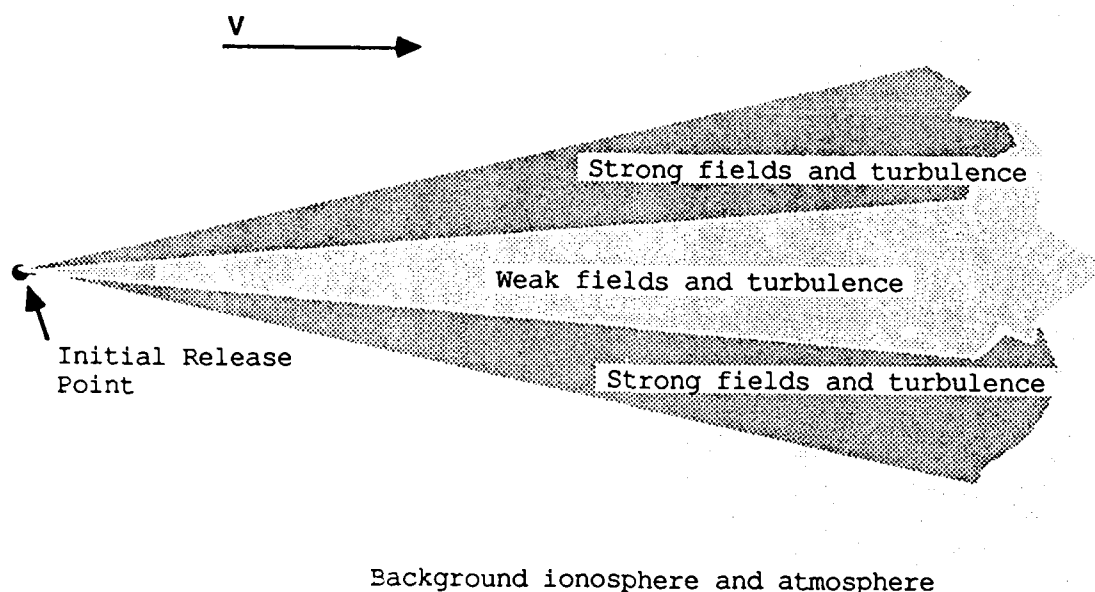


**Figure 7.4.** Showing the regions of plasma disturbance set by the expanding neutral cloud as they occur in the ionospheric frame of reference. The expansion angle of the effect is set by the magnitudes of the orbital velocity ( $\sim 7.7 \text{ km sec}^{-1}$ ) and the thermal speed of the cloud (which depends on the mass of the neutral particles and their temperature (typical expansion speeds may be  $100 \text{ to } 300 \text{ m sec}^{-1}$ )).

The recent Cameo experiments [Heppner *et al.*, 1981] involving the release of barium from an orbiting platform could have demonstrated some of the charge exchange effects, had the release been made at lower altitudes. As it was, however, the release was made from a high altitude spacecraft in a region where charge exchange with  $O^+$  was a very slow process compared with photoionization.

It is likely that the best indication of charge exchange effects can be found in thruster firing data acquired from experiments on STS-3 (1982) and Spacelab-2 (1985). In these flights, small gas releases were observed by various plasma diagnostic instruments carried by the University of Iowa PDP and VCAP instrument packages. cursory examination of the data shows that broad band ELF and VLF noise accompanies each thruster firing and that this continues for an extended period of time after the firing has stopped (See Figure 7.5). Unfortunately, samples of most of the plasma diagnostic instruments are available only at 1.6 second time intervals. Nevertheless, the fact that such gas releases produce consistent plasma signatures is a good indication that there is an anomalous interaction between the predominantly neutral thruster clouds and the surrounding plasma medium.

#### 7.4. Future Work

Both theoretical and experimental work are needed to explore the full range of processes associated with the charge exchange neutral cloud idea. With respect to theory, it would be possible to conduct plasma simulations with a 3-dimensional plasma code (developed by Prof. O. Buneman at Stanford) now available on both Livermore and Los Alamos computers. The results would give a good indication of the different types of plasma waves created in such a release and some indication of the subsequent electron density irregularity structures. In addition, basic calculations of the consequences of a gas release need to be done, taking into account various possible charge exchange rates for different gases and the effects of cloud expansion.

With respect to future experiments, observations could be made using the space shuttle and a simple plasma diagnostics payload that would be able to capture the fast time response of the various neutral gas phenomena. Such a payload would be

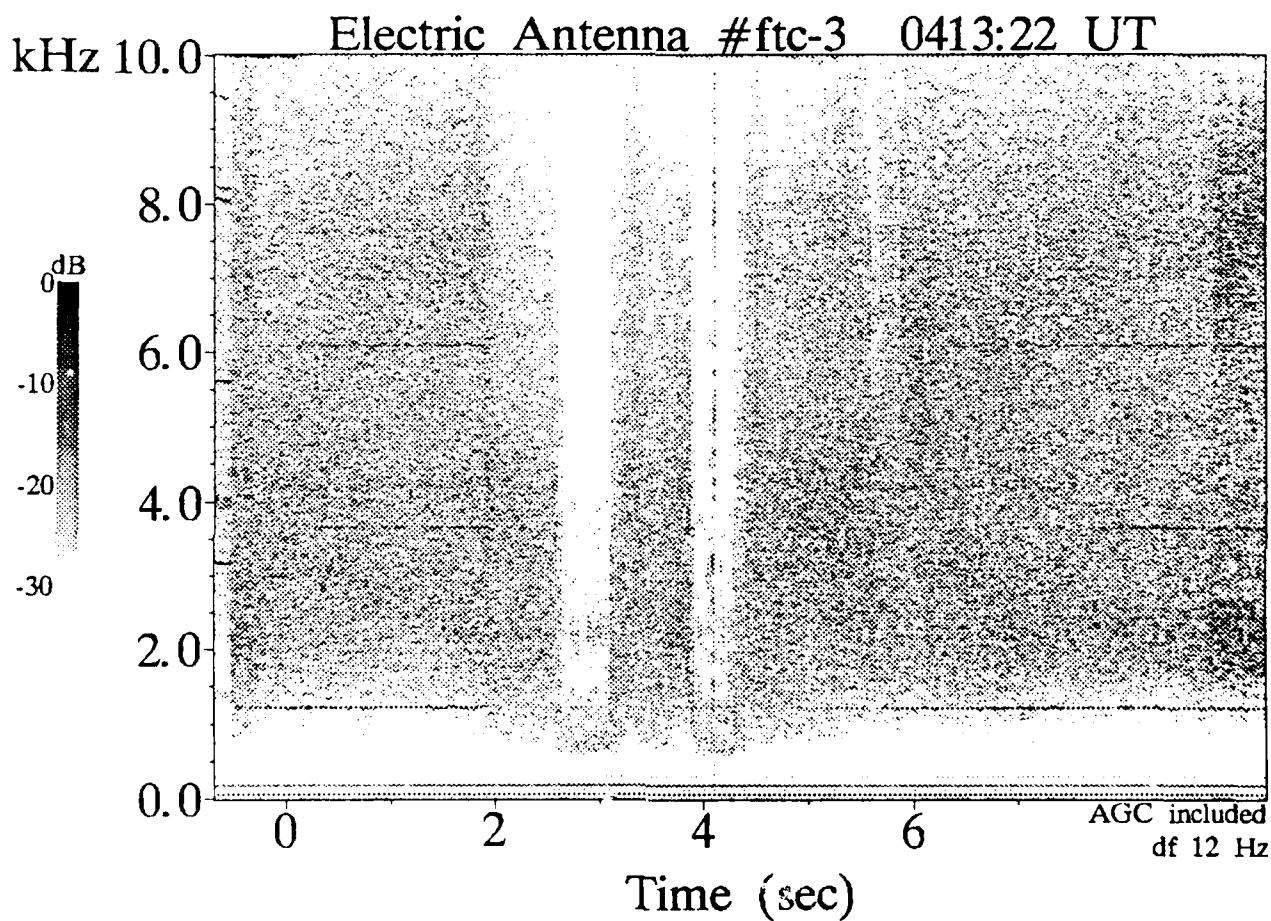


Figure 7.5. The VLF spectrum of a STS Orbiter thruster firing as acquired from experiments on the OSS-1 mission of STS-3. The display shows the intensity of electric fields as a function of frequency (vertical scale) and time (horizontal scale). A short (a few milliseconds) thruster firing produces a multi-second long pulse of a.c. electric field noise. This typical thruster signature may be the results of a strong, charge exchange mediated interaction with the ionosphere.

far less complicated (and much less costly) than the anticipated CRESS experiment, which incorporates various violent explosives to produce traceable vapors. In fact, it would be more than adequate to use a collection of pressurized, inert gases to investigate the charge exchange processes: He, Ne, and Xe would give a variety of masses and ionization potentials needed to explore the physical processes involved. In addition, experiments could be conducted near ground-based facilities, permitting realtime radio, radar, and optical mappings of the neutral gas disturbance zone.

Finally, study of existing thruster data from STS-3 and Spacelab-2 experiments could provide important information about gas release phenomena. Both optical and plasma data are available for study, and great progress might be possible in a relatively short period of time, relative to mounting new experiments on the space shuttle or other orbiting platforms.

### 7.5. References

- Machinda, S., and C. K. Goertz, A simulation study of the critical ionization velocity process, *J. Geophys. Res.*, *91*(11), 965, 1986
- Bernhardt, P.A., Plasma fluid instabilities in ionospheric holes, *J. Geophys. Res.*, *87*, 7539, 1982.
- Heppner, J. P., M. L. Miller, M. B. Pongratz, G. M. Smith, L. L. Smith, S. B. Mende, and N. R. Nath, The CAMEO barium releases: Parallel electric fields over the polar cap, *J. Geophys. Res.*, *86*, 3519, 1981.



## 8. CONCLUSION

As was pointed out in the Introduction, the study detailed in this report was primarily a search for new concepts in ionospheric modification, with our Laboratory's previous work on ionospheric modification with low energy electron beams taken as a starting point. The topics that were considered in some detail included ionospheric modification by three different classes of electron beams: low energy (Chapter 2), medium energy (Chapter 3), and high energy, or relativistic, beams (Chapter 4). In addition, consideration was given to ionospheric modification by means of neutral, or plasma, beams (Chapter 5), by X-rays and EUV radiation (Chapter 6), and by releases of neutral gas from an orbiting vehicle (Chapter 7).

The results of the study are summarized in Chapter 1, and more specific summaries for each method of ionospheric modification are given at the end of the corresponding chapter. Several detailed suggestions for new experiments are made in addition to suggestions for applications of our current low energy electron beam experiments to ionospheric modification. Most of the recommendations involve particle or photon beams, but an experiment to investigate a new charge exchange mechanism in a cloud of neutral gas released from a rapidly moving vehicle in the ionosphere is also described and is recommended. Two of the suggested new experiments, one involving relativistic electron beams and the other beams of soft X-rays/EUV radiation, utilize new technologies that have only recently been developed and which have a potentially large payoff in terms of new effects that can be produced in the ionosphere and in the new knowledge that will be gained of the ionosphere.